VOLUME 45, NUMBER 4, DECEMBER 2022

HADRONIC JOURNAL Volume 45, Number 4, December 2022

HADRONIC JOURNAL

Founded in 1978 by Prof. R. M. Santilli at Harvard University. Some of the past Editors include Professors S. L. Adler, A. 0. Barut, L. C. Biedenharn, N. N. Bogoliubov, M. Froissart, J.Lohmus, S. Okubo, Nobel Laureate Ilya Prigogine, M. L. Tomber, J. P.Vigier, J. Wess, Nobel Laureate Chen Ning Yang.

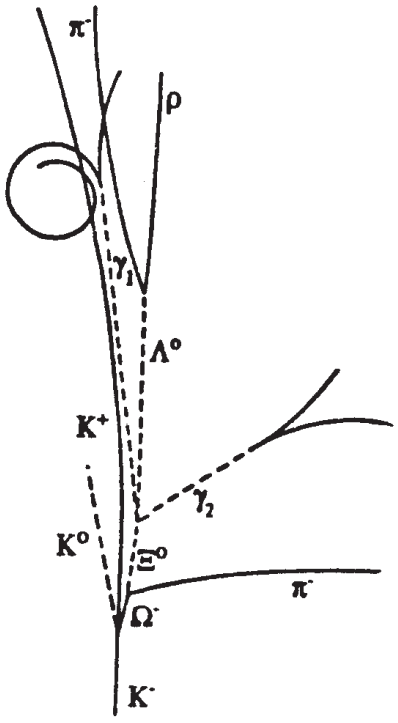

EDITORIAL BOARD

A.O.ANIMALU
A. K. ARINGAZIN
A. A. BHALEKAR
S. J. DHOBLE
J. DUNNING-DAVIES T.
L. GILL
L. P. HORWITZ
S. L. KALLA
S. I. KRUGLOV
M. NISHIOKA
R. F. O'CONNELL
Z. OZIEWICZ*
E. RECAMI
M. SALEEM
B. G. SIDHARTH
S. SILVESTROV
H. M. SRIVASTAVA
E. TRELL
R.I. TSONCHEV
QI-REN ZHANG
C.A.WOLF
YI-ZHONG ZHUO

*In memoriam

FOUNDER and Editor In Chief
R. M. SANTILLI

HADRONIC PRESS, INC.

HADRONIC JOURNAL

Established in 1978 by Prof. R. M. Santilli at Harvard University Hadronic Journal and Algebras, Groups and Geometries have been regularly published since 1978 without publication charges and are among the few remaining independent refereed journals.

This Journal publishes advances research papers and Ph. D. theses in any field of mathematics without publication charges.

For subscription, format and any other information please visit the website
http://www.hadronicpress.com

HADRONIC PRESS INC.
35246 U. S. 19 North Suite 215
Palm Harbor, FL 34684, U.S.A.
http://www.hadronicpress.com
Email: info@hadronicpress.com
Phone: +1-727-946-0427

HADRONIC JOURNAL

Founder and Editor in Chief
RUGGERO MARIA SANTILLI
The Institute for Basic Research
35246 U. S. 19 North Suite 215, Palm Harbor, FL 34684, U.S.A.
Email: resarch@i-b-r.org; TEL: +1-727-688-3992

A. O. ANIMALU, University of Nigeria, Department of Physics, Nsukka, Nigeria animalu@nmc.edu.ng
A.K. ARINGAZIN Department of Theoretical Physics, Institute for Basic Research Eurasian National University Astana 010008, Kazakhstan aringazin@mail.kz
A.A. BHALEKAR Department of Chemistry, R.T.M. Nagpur University, Nagpur, 440033 India anabha@hotmail.com
S.J. DHOBLE Department of Physics R.T.M. Nagpur University Nagpur, 440033 India sjdhoble@rediffmail.com
J. DUNNING-DAVIES, Department of Physics (Retired) University of Hull Hull, HU6 7RX England j.dunning-davies@hull.ac.uk
T. L. GILL Howard University Research Center ComSERC Washington, DC 20059, USA tgill@howard.edu
L. P. HORWITZ, Department of Physics Tel Aviv Univ., Ramat Aviv, Israel horwitz@taunivm.tau.ac.il
S. L. KALLA, Department of Mathematics Vyas Institute of Higher Education Jodhpur, 342008, India shyamkalla@gmail.com
S.I. KRUGLOV University of Toronto at Scarborough, Physical and Environmental Sciences Dept., 1265 Military Trail, Toronto, Ontario, Canada M1C 1A4 skrouglo@utm.utoronto.ca
M. NISHIOKA, Yamaguchi University Department of Physics, Yamaguchi 753, Japan
R. F. O'CONNELL, Louisiana State University Department of Physics, Baton Rouge, LA 70803
Z.OZIEWICZ,* Universidad National Autonoma de Mexico, Faculdad de Estudios Superiores C.P. 54714, Cuautitlan Izcalli Aparto Postal # 25, Mexico **** In memoriam***
E. RECAMI, Universita' de Bergamo, Facolta' di Ingeneria, Viale Marconi 5, 1-24044 Dalmine (BG) Italy recami@mi.ifn.it
M. SALEEM, University of the Punjab Center for High Energy Phys., Lahore, Pakistan dms@lhr.paknet.com.pk
B.G. SIDHARTH International Institute for Applicable Mathematics &b Information Sciences, B.M. Birla Science Center, Adarshnagar, Hyderabad 500063 (India) iimisbgs@yahoo.com.in
S. SILVESTROV School of Education, Culture and Communication (UKK) Malardalen University Box 883, 71610 Västerås, Sweden sergei.silvestrov@mdh.se
H. M. SRIVASTAVA, Department of Mathematics and Statistics, University of Victoria, Victoria, B. C. V8W 3P4, Canada, hmsri@uvvm.uvic.ca
E. TRELL Faculty of Health Sciences, University of Linkoping, Se-581 83, Linkoping, Sweden erik.trell@gmail.com
R.I. TSONCHEV Facultad de Fisica, Universidad Autonoma de Zacatecas, P. O. C-580, Zacatecas 98068, zac, Mexico rumen@ahobon.reduaz.ms
QI-REN ZHANG, Peking University, Department of Technical Phys., Beijing 100871, China zhangqr@sun.ihep.ac.cn
C.A. WOLF Department of Physics, Massachusetts College of Liberal Arts, North Adams, Ma 01247 cwolf@mcla.mass.edu
YI-ZHONG ZHUO, Institute of Atomic Energy P.O. Box 275 (18) Beijing 102413, China zhuoyz@mipsa.ciae.ac.cn

ISSN: 0162-5519

Established in 1978 by Prof. R. M. Santilli at Harvard University Hadronic Journal and Algebras, Groups and Geometries have been regularly published since 1978 without publication charges and are among the few remaining independent refereed journals.

This Journal publishes advances research papers and Ph. D. theses in any field of mathematics without publication charges.

For subscription, format and any other information please visit the website http://www.hadronicpress.com

HADRONIC PRESS INC.
35246 U. S. 19 North Suite 215
Palm Harbor, FL 34684, U.S.A.
http://www.hadronicpress.com
Email: info@hadronicpress.com
Phone: +1-727-946-0427

HADRONIC JOURNAL Volume 45, Number 4, December 2022

H/P HADRONIC PRESS, INC.

HADRONIC JOURNAL

VOLUME 45, NUMBER 4, DECEMBER 2022

ON THE POSSIBILTY OF FUSING HYDROGEN WITH HIGH LEVEL NUCLEAR RADIOACTIVE WASTE VIA COLD NUCLEAR FUSION, 357

U.V.S. Seshavatharam
Honorary faculty, I-SERVE, Survey no-42, Hitech City
Hyderabad-84, Telangana, India
S. Lakshminarayana
Department of Nuclear Physics, Andhra University
Visakhapatnam-03, Andhra Pradesh, India

ON RELATIVISTIC HARMONIC OSCILLATOR, 369

A. I. Arbab
Department of Physics, College of Science, Qassim University
P.O. Box 6644, Buraidah 51452, Saudi Arabia

NEUTRINO EXCHANGING POTENTIAL WITH BESSEL FUNCTION OF LOW ORDER, 383

Bibek Koirala[1,2], Saddam Husain Dhobi[1,2,3], Prakash Subedi[1,2], Milan Gurung[4]
[1]Department of Physics, Patan Multiple Campus, Tribhuvan University, Lalitpur-44700, Nepal
[2]Innovative Ghar Nepal, Laitpur-44700, Nepal
[3]Robotics Academy of Nepal, Lalitpur-44700, Nepal
[4]Central Department of Physics, Tribhuvan University
Kirtipur, 44618, Nepal

NEW THERMODYNAMICS: HOW MANKIND'S USE OF ENERGY INFLUENCES CLIMATE CHANGE, 399

Kent Mayhew
68 Pineglen Cres.
Ottawa, Ontario, Canada K2G 0G8

ON THE INDUCTION OF A LOW-ENERGY NUCLEAR REACTION IN A SUPERSONIC PLASMA VORTEX, 423

Igor Bayak
Belarus, 230025, Grodno Av., Kosmonavtov 4V 45

ANALYSIS OF THE ORIGIN, STRUCTURE AND PROPAGATION OF TRANSVERSE ELECTROMAGNETIC WAVES USING BIPOLARS, 431
Farzad Haghmoradi-Kermanshahi
Electrical Engineering Department
Faculty of Engineering, Razi University
Kermanshah 67149, Iran
PROBING THE ELECTROMAGNETIC STRUCTURE OF NUCLEONS, 443
M Y Hussein
Department of Physics, University of Bahrain
P.O. Box 32038, Kingdom of Bahrain
And
Search Center, Shaikh Ebrahim Bin Mohammed Al Khalifa
Center for Culture and Research, P.O. Box 13725
Muharraq, Kingdom of Bahrain
STUDIES ON THE NONLINEARITY OF WAVE-PARTICLE DUALITY, 445
Yi-Fang Chang
Department of Physics
Yunnan University
Kunming, 650091, China

INDEX VOL 45, 2022.....469

HADRONIC JOURNAL 45, 357 - 368 (2022)
DOI 10.29083/HJ.45.04.2022/SC357

ON THE POSSIBILTY OF FUSING HYDROGEN WITH HIGH LEVEL NUCLEAR RADIOACTIVE WASTE VIA COLD NUCLEAR FUSION

U.V.S. Seshavatharam
Honorary faculty, I-SERVE, Survey no-42, Hitech City
Hyderabad-84, Telangana, India
seshavatharam.uvs@gmail.com
Orcid number 0000-0002-1695-6037
S. Lakshminarayana
Department of Nuclear Physics, Andhra University
Visakhapatnam-03, Andhra Pradesh, India
lnsrirama@gmail.com
Orcid number 0000-0002-8923-772X

Received July 15, 2022
Revised August 30, 2022

Abstract

Considering our very recent paper on production of gold from tungsten- like heavy metals via cold nuclear fusion, in this paper, we are showing a simple theoretical procedure for cold nuclear transmutation of high level radioactive nuclear waste (produced from recycling of spent nuclear fuel) into stable and non-radioactive atomic nuclides. It may help in saving mother earth, its environment and mankind. The basic idea is - under vacuum conditions, moderate pressure and temperature, fusing hydrogen with liquid form of high level radioactive nuclear waste. Our proposal can be given a chance for its possible workability. It may be noted that, based on strong and electroweak interactions, recently, we have proposed a very simple nuclear binding energy formula having four terms and one energy coefficient. It eliminates the need of considering Coulombic repulsion scheme. Proceeding further, we have proposed a simple mechanism for understanding 'hydrated cold nuclear fusion' and its energy liberation mechanism via the difference of maximum binding energy per nucleon and the difference of binding energy of final and base atomic nuclides.

Keywords: high level nuclear radioactive waste; strong and weak interactions; nuclear binding energy; cold nuclear fusion;

Copyright © 2022 by Hadronic Press, Inc., Palm Harbor, FL 34684, USA

1. Introduction

Even though it is a very fruitful technology for mankind, 'nuclear fission' is facing many challenges in disposing the high level radioactive nuclear waste (HLW) produced from recycled spent nuclear fuel [1]. HLW accounts for over 95% of the total radioactivity produced in the nuclear power process. The basic problem is that, these waste radioactive nuclides are having inherently hidden beta and gamma radiations and for million years of coming future, there is a chance of their decay resulting in the death of human beings via radiation sickness, various genetic disorders and several cancers. The standard industrial process for HLW solidification is conversion of the HLW aqueous nitrate solution into borosilicate or phosphate glass at around 1150 deg. C. Mixture of radioactive waste solution and molten glass are poured into steel canisters [2,3].In future, it is planned to bury these containers at remote and unmanned locations under a depth of 0.5 to 0.6 km [4,5].It is very unfortunate to say that, due to natural degrading and erosion processes, human made engineering structures cannot survive for more than 10,000 years. If this point is a guess, there is no issue. If it is really true, it is very dangerous to run atomic reactors that produce high level radioactive atomic nuclides having mega years of half life and it is absolutely illogical to store and to bury them in deep earth. In this critical situation, considering cold nuclear fusion technology [6-10], we make a theoretical attempt to transform the radioactive nuclear waste to next stage stable atomic nuclides. It may help in running nuclear power plants with ease, comfort and without any harm to mankind. We have presented our views in 45th Indian Social Science Congress, Chennai, India [11].

2. A review on cold nuclear fusion and nuclear binding energy

Since 1989, many scientists and engineers are seriously working on cold nuclear fusion experiments that produce 'excess' heat with no hazardous nuclear radiation [12-15]. Here it is very important to emphasize that, energy liberated in cold nuclear fusion is approximately one million times higher than the energy released in burning of ordinary fossil fuels. It clearly indicates less consumption rate of cold fusion fuel in milligram/sec compared with more consumption of fossil fuels in liter/sec. Point to be noted is that, as the name

itself suggests, 'cold nuclear fusion' can be visualized as a peculiar exothermic nuclear physical phenomenon associated with fusion of a heavy atom with one hydrogen atom at low temperatures of the order 2000 degree Kelvin against currently believed fusion of atoms associated with a temperature of the order of million degree Kelvin.

Cold nuclear fusion experiments can be classified into two categories. First one is 'Electrolytic or Alkaline Cold Fusion' associated with 'Electrolysis of Deuterium' and second one is 'Hydrated Cold Fusion' associated with 'preheating of hydrated metals in a pressurized reactor'. In a theoretical perceptive, for any scientist, it is imperative to explain the possibility of low temperature nuclear fusion of atoms against hot fusion and the dominating nuclear Coulombic repulsive forces. In this context, important point to be noted is that, increasing mass number of nucleus can be considered as a representation of increasing strong nuclear attraction. Based on this point, it can be understood as - fusion of two hydrogen ions/atoms at million deg. C seems to be different from fusion of a heavy atom that constitutes (50 to 200) nucleons (having a density of the order of 10^{23} nucleons/cm^3) and one hydrogen atom at 3000 deg. C. Fusing Hydrogen with metals in liquid state seems to be more interesting.

It is currently believed that, nuclear Coulombic repulsion phenomenon plays a vital role in stopping or breaking the cold nuclear fusion of hydro-protons with heavy nuclear atomic nuclides. In this context, NASA team developed a mechanism called 'lattice confinement'[16,17]. In this new mechanism, Titanium or Erbium metal lattices are loaded with deuterium at a density of the order of 10^{23} ions/cm^3. This density is roughly 10^{10} times greater than the hot fusion reactor density. Photons coming from an electron accelerator trigger the reaction and dissociate some of the lattice deuterons into protons and neutrons. Interactions between Erbium/Titanium, positively charged lattice deuterons, neutrons and protons generate fusion energy with the production of new atoms like Thulium. Interesting point to be noted is that, the lattice atoms' negative electrons 'screen' and reduce the repulsion between the positively charged deuteron ions and help in enhancing the nuclear reaction rates. In this context, we would like to appeal that, independent of Coulombic

repulsion, and considering strong and electroweak interactions, nuclear binding energy can be understood with the following four term unified relation [9,10]. For Z= 3 to 118 where $N \geq Z$,

$$BE \cong \left\{A-\left[1+\left(0.0016\left(\frac{Z^2+A^2}{2}\right)\right)\right]-A^{1/3}-\frac{(A_s-A)^2}{A_s}\right\}(B_0 \cong 10.1\ \text{MeV}) \quad (1)$$
$$\cong \left\{A-\left[1+\left(0.0008\left(Z^2+A^2\right)\right)\right]-A^{1/3}-\frac{(A_s-A)^2}{A_s}\right\}(B_0 \cong 10.1\ \text{MeV})$$

where
1) A = Mass number and Z = Proton number.
2) $\dfrac{\text{Mean mass of Pions}}{\text{Mean mass of Weak bosons}} \cong \dfrac{\sqrt{\left(m_\pi c^2\right)^0\left(m_\pi c^2\right)^\pm}}{\sqrt{\left(m_z c^2\right)^0\left(m_w c^2\right)^\pm}} \cong 0.0016$
3) $A_s \cong 2Z+0.0016(2Z)^2 \cong 2Z+0.0064Z^2$
   $\cong$ Estimtaed Mass number close to stability zone.
4) $B_0 \cong \dfrac{1}{2}\left[\left(2m_u c^2+m_d c^2\right)+\left(m_u c^2+2m_d c^2\right)\right] \approx 10.1$ MeV
   where (m_u, m_d) reprsent Up and Down quark masses.

In this relation,

1) First term can be considered as a consequence of nuclear volume.
2) Second term can be considered as a consequence of non-participating nucleons associated with electroweak interaction and minimum number of non-participating nucleons is defined as 1.
3) Third term can be considered as a consequence of surface and radial effects.
4) Fourth term can be considered as a consequence of asymmetry about the mean stable mass number.

3. Progress and mega project funding on cold nuclear fusion

As the main objective of cold nuclear fusion is to produce clean thermal energy, from 2015 onwards, 'Google' team put lot of efforts in understanding and generating excess heat via all known experimental cold nuclear techniques

with advanced and more sophisticated measuring tools. Even though it was a failure, in 2019-20, Google team members published a seminal paper in the prestigious journal 'Nature' and expressed their strong encouragement for conducting future experiments [18,19]. Another interesting point to be noted is that, right from the beginning, NASA team has shown lot of interest in cold fusion techniques and in 2020, published two very important papers in the prestigious journal 'Physical Review C' paving a way for accomplishment of cold nuclear fusion with 'deuterated' Erbium atoms by a new technique called 'lattice confinement'. Following these points and considering the main objective of generating clean energy, in 2020 last quarter, European Union funded 10 million Euros for two cold nuclear fusion projects for a period of 4 years.

4. Basic mechanism of Hydrated cold nuclear fusion

At fundamental level, concept of 'cold nuclear fusion' (CNF) is highly attractive and mostly speculative. Considering the complicated issues related with hot nuclear fusion associated million deg. C and understanding the environmental friendly applications of CNF associated with ambient temperatures, many world class scientists and engineers are being attracted towards CNF experiments and theory. Readers are encouraged to refer Wikipedia, NASA publications [16,17], Google publications [18,19] and grant reports of European funding agencies.

The basic idea of CNF is to observe the generation of excess heat by fusing metals with Hydrogen atoms at room temperature or temperatures around 1000 to 2000 deg. C. Generally, CNF experiments are taking place in the form of Electrolytic equipments having Palladium electrodes and heavy water [12,13] and Pressurized steel chambers filled with metallic powders and hydrogen [20,21]. As nuclear reactions of CNF are assumed to be taking place at low energies compared to hot fusion energies, in most of the cases, CNF can also be called as 'Low energy nuclear reactions' (LENR). For advanced information readers are encouraged to refer [22,23]. The most confusing point of CNF is – after fusion, whether base metal is in the form of 'Metallic Hydride' or 'heavy

isotope of base metal' or 'changed proton number of base metal'. With reference to the current low energy room temperature nuclear reactions, 'isotopic shift' seems to be a notable aspect of CNF [20]. In our recent paper [6], we have proposed a simple explanation for understanding the energy liberation mechanism of CNF with the difference of nuclear binding energy of final and initial metallic nuclides. Considering 'Hydrated cold nuclear fusion' experiments pertaining to Nickel powder [21], we proposed the following points [6].

1) Evacuated and sealed reactor is loaded with small quantity of very fine Nickel- like powder and large quantity of hydrogen gas under certain pressure.
2) As the reactor is slowly heated by external electric power, both reactor temperature and pressure, slowly increase and hydrogen atoms start making too and fro forced oscillations in the reactor.
3) At certain controllable temperature and pressure conditions, hydrogen atoms, start entering the nuclear core of the Nickel atoms triggering nuclear fusion reactions.
4) Within the nuclear core of Nickel atom, due to weak nuclear interaction [7], hydrogen atom immediately transforms to a neutron and by strong attractive nuclear force, new neutron combines with nuclear core and increases Nickel mass by one unit.
5) Due to increasing heaviness in mass and due to weak nuclear force, newly formed neutron transforms to proton, electron and neutrino.
6) Due to strong nuclear attractive force, new proton joins with Nickel's nuclear core and increases the nuclear proton number by one unit.
7) New electron joins with Nickel's electronic orbits and increases Nickel's electron number by one unit.
8) In this way, within the nuclear reactor, as time progresses, Nickel mass number increases slowly and some times, Nickel transforms to its next level new atoms. This concept can be compared with the observed cold fusion nuclear transmutations.
9) Based on the currently believed nuclear binding energy scheme, maximum binding energy per nucleon is around 8.8 MeV.

10) Considering the fusion of one hydrogen atom in hydrated cold fusion, energy acquired by the final nucleus during the fusion of hydrogen atom seems to be 8.8 MeV. This can be considered as the origin of 'missing energy' or 'excess energy' in cold nuclear fusion.
11) In the absence of increase in internal kinetic energy, there is a scope for liberation of excess energy in the form of safe thermal energy. This can be considered as the basic information missing in mainstream nuclear physics.
12) Due to Coulombic repulsion, asymmetry effect, pairing effect and other nuclear effects, final atom is forced to choose a little bit of binding energy less than 8.8 MeV and thus it is able to release left over binding energy in the form of internal kinetic energy or external thermal energy. Thus, in hydrated cold fusion, heat release to occur, binding energy difference of final atomic nuclide and base atomic nuclide seems to be less than 8.8 MeV.
13) Qualitatively, energy released during hydrated cold fusion seems to be approximately equal to 8.8 MeV minus the difference of binding energy of final and base atomic nuclides.
14) Based on this idea, under normal conditions, for the case of $_2He^4$, fusion of four protons can liberate (35.2-28.3)=6.9 MeV and it is 3.5 times less than the current estimates.
15) Point to be understood is that, lesser the binding energy of final atomic nuclide, higher is the liberated thermal energy and vice versa.
16) Reactor input charge can be chosen to constitute, less abundant, stable and heavy mass numbers of light Z in large proportion so that, after fusing with hydrogen, output becomes more abundant, light and stable mass numbers of Z+1.Thus difference in binding energy of (Z+1, A+1) and (Z, A) is on lower side and less than 8.8 MeV.
17) Considering $_{28}Ni^{62}$ and $_{29}Cu^{63}$ isotopes, liberated thermal energy can be around {8.8–(550.0–544.4)}= 3.2 MeV.
18) Considering the case of fusion of two Deuterium atoms, liberated thermal energy can be around, {(4*8.8)–[28.3–(2*2.22)]}=11.3 MeV. Clearly speaking, fusion of two deuterium atoms can be considered as a representation of fusion of 4 nucleons. Binding energy of $_2He^4$ is 28.3 MeV and binding energy of deuterium is 2.22 MeV.
19) With a suitable catalyst and sufficient hydrogen under suitable pressure, if reactor's temperature is maintained at (1000 to 1500) ^{0}C, there seems a lot of scope for a chain reaction of cold fusion in which light isotopes

transform to their next stage with increased proton number or mass number and liberate safe and clean heat energy continuously.

20) By arranging 4 to 6 reactors and charging them periodically in tandem, required thermal energy can be produced continuously. In this new direction, by carefully selecting the base isotope and its corresponding catalyst, experiments can be conducted and ground reality of cold fusion can be understood at various temperature and pressure conditions.

21) It may be noted that, part of nuclear binding energy difference of final and base atomic nuclides can be seen in the form of safe and controllable thermal energy with an order of (1 to 3) MeV per atom against 200 MeV pertaining to the dangerous and unsafe nuclear fission of one Uranium atom.

5. CNF – the next stage of metallic hydrides

It is very clear to say that, modern science and technology is aiming in understanding and developing metallic hydrides to store Hydrogen in large quantities at various pressure and temperature conditions. Other notable applications include heat pumps, heat refrigerators and heat storage [24]. In this context, considering the basic concept of CNF, we are moving one step further. Clearly speaking, at reasonable pressure and temperature conditions,

1) Process of adding Hydrogen to metals can be called as CNF Hydration.
2) Hydrogen fuses with metals and help in developing heavy isotopes of respective metals.
3) Hydrogen fuses with metals and help in developing next stage metals having a change in proton number.
4) During the above two nuclear reactions, part of nuclear binding energy difference comes out in the form of safe thermal energy.

Following the above concepts, advancing the current scientific approach and developing new engineering techniques, it is certainly possible to thoroughly study the implications and validation of CNF.

6. Processing of high level radioactive waste with cold nuclear fusion

Following the above paragraphs, it seems possible to fuse radioactive nuclides with hydrogen at moderate pressures and temperatures. In our recently presented and published paper, we have made an attempt to produce Iridium, Platinum and Gold- like metals by considering Tungsten- like heavy metals [10]. Key point of study is that, at around 3500 deg. C, Hydrogen transforms to hydro-proton and hydro-electron [25]. Coming to our subject title, we express our views in the following way.

1) See Table-1 for long lived and medium lived high level radioactive nuclides.

Table-1: Long lived and Medium lived HLW nuclides

Long lived HLW nuclides		**Medium lived HLW nuclides**	
HLW nuclide	**Half life in 10^6 Years**	**HLW nuclide**	**Half lifein Years**
43-Technetium-99	0.211	63-Europium-155	4.76
50-Tin-126	0.23	36-Kripton-85	10.76
34-Selenium-79	0.33	48-Cadmium-113	14.1
40-Zirconium-93	1.53	38-Strontium-90	28.9
55-Caesium-135	2.3	55-Caesium-137	30.23
46-Palladium-107	6.5	50-Tin-121	43.9
53-Iodine-129	15.7	62-Samerium-151	88.8

2) Fill the evacuated nuclear reactor (NR) with 100 grams of HLW and load the whole volume of nuclear reactor with hydrogen gas to the possible extent.
3) Gradually heat the nuclear reactor and observe for emission of beta and gamma radiations. If there is no radiation, continue the heating process.
4) As temperature of the nuclear reactor is increasing, hot hydrogen gas starts fusing with liquid radioactive nuclides with increasing kinetic energy.
5) As a result, mass number of the respective radioactive nuclide increases and moves away from the stability line. It may be noted that, as per the proposed binding energy formula, estimated mean stable mass number can be expressed as, $A_s \cong 2Z + 0.0016(2Z)^2 \cong 2Z + 0.0064Z^2$. Based on this

relation, mass numbers presented in Table-1 are above the mean stable line.

6) Increased mass number results in addition of extra neutron. As mass number is moving away from stability line, at one stage, by emitting a beta particle, extra neutron transforms to extra proton and the radioactive nuclide transforms to stable non-radioactive atomic nuclide. Emitted beta particle joins with existing electronic orbits.
7) For example, Cs-137 gains one neutron and transforms to stable Ba-138. To confirm this, in an alternative approach, radioactive nuclear waste can be bombarded with free neutrons coming from other nuclear sources.
8) Run the experiment for two to three hours and allow the reactor to cool.
9) Observe and analyze the reactor contents for a possible transformation of radioactive nuclides to non-radioactive stable nuclides.
10) Repeat the process and re-analyze.

7. Conclusion

In this paper, we have made a simple review on cold nuclear fusion and tried to apply the concept to high level radioactive waste based on adding a neutron and converting to a proton via weak decay. By adding a neutron, half life of the radioactive nuclide is getting shortened and emitted beta particle seems to be confined to the nuclide with an increased proton number. In this way, we are providing a theoretical mechanism for conducting experiments to convert highly radioactive nuclear waste to non-radioactive stable nuclides. If it is successful, it will be a boon for the mankind and fission based atomic reactors. Point to be noted is that, without considering neutron sources and by considering only hydrogen as a bombarding particle, artificial nuclear transmutation can be carried out. It needs further study and research. Really, if 'cold nuclear fusion' is having any notable significance in current science and technology, as it seems to be endowed with nuclear isotopic changes, apart from energy liberation mechanisms, it can be studied and validated in this way also.

Acknowledgements

Authors are greatly inspired by the dedicated works of cold fusion experimentalists and theoreticians. Author Seshavatharam is indebted to professors Shri M. Nagaphani Sarma, Chairman, Shri K.V. Krishna Murthy, founder Chairman, Institute of Scientific Research in Vedas (I-SERVE), Hyderabad, India and Shri K.V.R.S. Murthy, former scientist IICT (CSIR), Govt. of India, Director, Research and Development, I-SERVE, for their valuable guidance and great support in developing this subject.

References

[1] A. Andrews. Nuclear Fuel Reprocessing: U.S. Policy Development. CRS Report for Congress, RS22542, 2008.

[2] Geological Disposal of Radioactive Wastes Produced by Nuclear Power, European Commission, EUR 21224, 2004.

[3] Disposition of High-Level Waste and Spent Nuclear Fuel: The Continuing Technical and Societal Challenges. National Academies Press, 2001.

[4] I. Pegg. Turning nuclear waste into glass. Phys. Today, 68, 33-39,2015.

[5] Ashutosh Goel et al. Challenges with vitrification of Hanford High-Level Waste (HLW) to borosilicate glass – An overview. Journal of Non-Crystalline Solids: X. 4,100033, 2019.

[6] Seshavatharam U.V.S, Lakshminarayana S. On the Role of Nuclear Binding Energy in Understanding Cold Nuclear Fusion. Mapana Journal of Sciences, 20(3), 29-42,2021.

[7] Seshavatharam U.V.S, Lakshminarayana S. On the Combined Role of Strong and Electroweak Interactions in Understanding Nuclear Binding Energy Scheme. Mapana Journal of Sciences, 20(1),1-18, 2021.

[8] Seshavatharam U.V.S, Lakshminarayana S. Implications and applications of fermi scale quantum gravity. International Astronomy and Astrophysics Research Journal. 2(1):13-30, 2020.

[9] Seshavatharam U.V.S, Lakshminarayana S. H. K. Cherop and K.M. Khanna. Three Unified Nuclear Binding Energy Formulae. World Scientific News, 163, 30-77, 2022.

[10] Seshavatharam U.V.S, Lakshminarayana S. Small scale production of gold with tungsten like heavy and cheap metals via cold nuclear fusion associated with safe and secured hydration. Materials Today: Proceedings. 57, Part-2, 603-606, 2022. Doi: 10.1016/j.matpr.2022.01.468, 2022.

[11] Seshavatharam U.V.S, Lakshminarayana S. On the possibility of fusing hydrogen with high level nuclear radioactive waste via cold nuclear fusion. 45th Indian Social Science Congress, 28 March -1 Apri1, 2022, B.S. Abdur Rahman Crescent Institute of Science and Technology , Chennai, India. https://crescent.education/45issc-csd/

[12] M. Fleischmann and S. Pons. Electrochemically induced nuclear fusion of deuterium, J. Electroanal. Chem. 261, 301-308, 1989.

[13] Cohen, J.S., & Davies, J.D. Is cold fusion hot? Nature 338, 705-706, 1989.

[14] Frodl, P., et al. Possible participation of Lithium in Fleischman Pons reaction is testable. Zeitschrift fur Natur forschung 45a, 757-758, 1990.

[15] S. Focardi, V. Gabbani, V. Montalbano, F. Piantelli, and S. Veronesi. Large excess heat production in Ni-H systems, Nuovo Cimento A, 111, 1233-1242, 1998.

[16] Vladimir Pines et al. Nuclear fusion reactions in deuterated metals. Phys. Rev. C, 101(4), 044609, 2020.

[17] Steinetz Bruce M et al. Novel nuclear reactions observed in bremsstrahlung-irradiated deuterated metals. Phys. Rev. C. 101(4), 044610, 2020.

[18] Berlinguette, C.P., Chiang, YM., Munday, J.N. et al. Revisiting the cold case of cold fusion. Nature 570, 45–51, 2019.

[19] Philip Ball. Lessons from cold fusion, 30 years on. NATURE, 569, 601, 2020.

[20] Tadahiko Mizuno and Jed Rothwell. Excess Heat from Palladium Deposited on Nickel. J. Condensed Matter Nucl. Sci. 29, 1–12, 2019.

[21] Parkhomov A et al. Nickel-hydrogen reactors: Heat generation, isotopic and elemental composition of fuel. Radioelectronics. Nanosystems. Information Technologies. 9. 74-93 2017.

[22] Jean-Paul Biberian. Cold Fusion: Advances in Condensed Matter Nuclear Science. Elsevier. ISBN:0128159456, 9780128159453, 2020.

[23] Freire, Luciano Ondir, and Delvonei Alves de Andrade. Preliminary survey on cold fusion: It's not pathological science and may require revision of nuclear theory. Journal of Electroanalytical Chemistry 903: 115871, 2021.

[24] M. Lototskyy et al. Niche applications of metal hydrides and related thermal management issues. Journal of Alloys and Compounds, 645(1), S117-S122, 2015.

[25] Peebles P. J. E. Recombination of the Primeval Plasma. Astrophysical Journal.153,1-11, 1968.

HADRONIC JOURNAL 45, 369 - 381 (2022)
DOI 10.29083/HJ.45.04.2022/SC369

ON RELATIVISTIC HARMONIC OSCILLATOR

A. I. Arbab
Department of Physics, College of Science, Qassim University
P.O. Box 6644, Buraidah 51452, Saudi Arabia
arbab.ibrahim@gmail.com

Received August 30, 2022
Revised September 1, 2022

Abstract

A relativistic quantum harmonic oscillator in 3+1 dimensions is derived from a quaternionic non-relativistic quantum harmonic oscillator. This quaternionic equation also yields the Klein-Gordon wave equation with a covariant (space-time dependent) mass. This mass is quantized and is given by $m_{*n}^2 = m_\omega^2 \left(n_r^2 - 1 - \beta \left(n+1\right)\right)$, where $m_\omega = \frac{\hbar\omega}{c^2}$, $\beta = \frac{2mc^2}{\hbar\omega}$, n, is the oscillator index, and n_r is the refractive index in which the oscillator travels. The harmonic oscillator in 3+1 dimensions is found to have a total energy of $E_{*n} = (n+1)\,\hbar\omega$, where ω is the oscillator frequency. A Lorentz invariant solution for the oscillator is also obtained. The time coordinate is found to contribute a term $-\frac{1}{2}\hbar\omega$ to the total energy. The squared interval of a massive oscillator (wave) depends on the medium in which it travels. Massless oscillators have a null light cone. The interval of a quantum oscillator is found to be determined by the equation, $c^2t^2 - r^2 = \lambda_c^2(1 - n_r^2)$, where λ_c is the Compton wavelength. The space-time inside a medium appears to be curved for a massive wave (field) propagating in it. The extra 4-dimension for the harmonic oscillator is tantamount to the magnetic field (z-direction) in the Landau model of a charge moving in magnetic field.

Keywords: Quaternionic quantum mechanics; Schrodinger equation; Relativistic dynamics; Mass spectrum; Relativistic harmonic oscillator; Quarks.

Copyright © 2022 by Hadronic Press, Inc., Palm Harbor, FL 34684, USA

1 Introduction

Shrödinger equation is very successful in identifying the physics of a quantum simple harmonic oscillator. Simple harmonic motion is of prime importance in the physical world. It finds a lot of applications in physics. For instance, atoms in a crystal lattice execute the simple harmonic motion. While a classical harmonic motion is determined by Newton's laws, a quantum analog reveals the quantization of the oscillator energy that was left unrestricted in the classical regime.

While Shrödinger equation can describe a non-relativistic harmonic oscillator, a relativistic one is left to be described by a relativistic quantum equation. This possibility may allow us to envisage an alternative method to quantize the field of a relativistic quantum boson particle. Note that the electromagnetic field has been quantized as consisting of a collection of an infinitely large number of harmonic oscillators. A relativistic oscillator picture can help quantize a massive field. It can be applied to any confined system where relativistic quantum effects become dominant, e.g., nuclear and quark models of matter.

The total energy of the oscillator reflects the degree of freedom the oscillator has. A harmonic oscillator in 3 - dimensions is described by its total energy, $E_n = (n + \frac{3}{2})\,\hbar\omega$ where $n = 0, 1, 2, \cdots$, and ω is the oscillator frequency [1]. In quantum mechanics, we deal with probability in identifying the position and momentum of a particle. For instance, the position of the oscillator is not well determined a priori. Owing to the theory of relativity, a particle in space-time follows a path, world- line, that is defined by the squared interval, $s^2 = c^2t^2 - r^2$. Massless particles move along a null world line, $s^2 = 0$, with a velocity equal to that of light in a vacuum, while massive particles are described by a time-like interval, $s^2 > 0$, and so their velocity is less than that of light in vacuum. However, when the medium is not free, such an interval will be altered and depends on the refractive index of the medium present. This situation could be present when we think of light propagation in curved space.

The harmonic oscillator model is very successful in describing the crystal lattice of a solid that gives a correct thermodynamic description of the specific heat capacity of the solid. However, a field-theoretic model is based

on treating the field as an infinitely large number of harmonic oscillators. It is thus instructive to consider an extension of a non-relativistic harmonic oscillator to a quantum relativistic one where relativistic effects are blended with quantum one. Therefore, one may suggest the use of a relativistic quantum oscillator in describing the gravitational field, when the effect of curvature and quantum mechanics becomes imminent.

The harmonic oscillator studied by Shrödinger is nonrelativistic and is thus valid only under certain conditions. The search for a relativistic quantum harmonic oscillator can be traced back to several authors [3, 5, 2, 4, 6, 7]. It is argued by Feynman that a covariant harmonic oscillator can explain the quark model [6]. We pose the question that how the path of a quantum particle is described by special relativity and quantum mechanics. To answer these questions, we investigate the evolution of a harmonic oscillator in 3+1 dimensions (space-time continuum).

To this aim, we introduce the quaternionic Shrödinger equation for the harmonic oscillator. In quantum field theory, the field is modeled by a collection of an infinitely large number of harmonic oscillators. In such a case a relativistic picture of the oscillator becomes inevitable. While Shrödinger equation is not a relativistic wave equation, the quaternionic Shrödinger equation, however, yields a relativistic quantum harmonic oscillator equation that is analogous to the Klein-Gordon wave equation. This urges us to employ quaternions to describe physical laws where we expect to obtain unexpected interesting results that may have been connected with other physical phenomena. This may result from the structure of the space-time in which quaternionic quantities act. It is interesting to see that a non-relativistic quaternion equation led steadily to a relativistic one. Hence, a path from one paradigm to another is thus opened.

Recall that the relativistic and quantum nature of the oscillators is not independent, they are constrained by the quantum relativistic interval, *viz.*, $r^2 - c^2t^2 = \lambda_c^2(n_r^2 - 1)$, where $\lambda_c = \frac{\hbar}{mc}$ is the Compton wavelength of the oscillator, and n_r is the refractive index of the medium in which the oscillator propagates. The total energy of the oscillator in the 3+1 dimension is found to be $E_{*n} = (n + 1)\,\hbar\omega$, where the contribution of the time coordinate in the Hamiltonian is equal to $-\frac{1}{2}\hbar\omega$.

This may suggest that time acts as an energy sink. Or equivalently,

this term may be considered as a relativistic correction to the 3 - dimensional harmonic oscillator. In d+1 dimensions, the total energy is $E^d_{*n} = (n + \frac{d-1}{2})\,\hbar\omega$. Interestingly, the ground state energy of 1+1 dimensional relativistic quantum harmonic oscillator is zero.

2 Quaternionic Shrödinger equation

A classical 3-dimensional harmonic oscillator is described by the Hamiltonian

$$H = \frac{p^2}{2m} + \frac{1}{2}\,m\omega^2 r^2\,, \tag{1}$$

where m and ω are the mass and frequency of the oscillator. In quantum mechanics, it is described by the Hamiltonian

$$H = \frac{P^2}{2m} + \frac{1}{2}\,m\omega^2 X^2\,, \tag{2}$$

where X and P are now hermitian operators, and expressed mathematically as $P = -i\hbar\vec{\nabla}$ and $X = r$. The state of the oscillator is described by Shrödinger equation

$$H\,\psi(r,t) = E\,\psi(r,t)\,, \tag{3}$$

where E is the total energy of the oscillator.

Let us now extend ψ, P and X to become quaternions, as follows

$$\tilde{\Psi} = \left(\frac{i}{c}\psi_0\,, \vec{\psi}\right)\,, \qquad \tilde{P} = \left(\frac{i}{c}\,E\,, \vec{p}\right)\,, \qquad \tilde{X} = (ict\,, \vec{r})\,. \tag{4}$$

Applying Eq.(4) in Eq.(3), using Eq.(2), yields the quaternionic (extended) Shrödinger equation for the harmonic oscillator, *viz.,*

$$\frac{1}{2m}\tilde{P}^*\tilde{P}\,\tilde{\Psi} + \frac{1}{2}m\omega^2\tilde{X}^*\tilde{X}\,\tilde{\Psi} = E\tilde{\Psi} \tag{5}$$

Upon using Eq.(4) and the product rule for two quaternions, $\tilde{A} = (a_0, \vec{a})$ and $\tilde{B} = (b_0, \vec{b})$, *i.e.,* $\tilde{A}\,\tilde{B} = (a_0 b_0 - \vec{a}\cdot\vec{b}\,\,, a_0\vec{b} + \vec{a}\,b_0 + \vec{a}\times\vec{b})$, one finds

$$\frac{1}{c^2}\frac{\partial^2\psi_0}{\partial t^2} - \nabla^2\psi_0 + \frac{2m}{\hbar^2}\left(\frac{1}{2}\,m\omega^2(r^2 - c^2t^2) - E\right)\,\psi_0 = 0\,, \tag{6}$$

after equating the scalar parts of the resulting equations. The vector part, $\vec{\psi}$, also satisfies the same differential equation in Eq.(6), *viz.*,

$$\frac{1}{c^2}\frac{\partial^2\vec{\psi}}{\partial t^2} - \nabla^2\vec{\psi} + \frac{2m}{\hbar^2}\left(\frac{1}{2}m\omega^2(r^2 - c^2t^2) - E\right)\vec{\psi} = 0\,, \tag{7}$$

Owing to this vector property, ψ_0 and $\vec{\psi}$ can be availed to study the photon dynamics and the related electromagnetic properties. Equations (6) and (7) are symmetric equations in space and time and thus are Lorentz invariant. It is thus invariant under Lorentz transformation. In a covariant form, Eq.(6) can be expressed as

$$\left(\partial_\mu\partial^\mu - \frac{2m}{\hbar^2}\left(\frac{1}{2}m\omega^2\, x_\mu x^\mu + E\right)\right)\psi_0 = 0\,.$$

Equation (7) can be seen as a Klein-Gordon wave equation with a space-time - dependent mass "effective mass" as

$$m_*^2 = m^2\left(\frac{\omega^2}{c^2}(r^2 - c^2t^2) - \frac{2E}{mc^2}\right). \tag{8}$$

It is evident from Eq.(8) that m_* is imaginary for $r^2 - c^2t^2 < 0$ (time-like interval), and is zero for $r^2 - c^2t^2 = \frac{2E}{m\omega^2}$. This equation is due to a hyperbola. Therefore, an oscillator moving along this hyperbola is massless. Equation (6) suggests that a time-independent (stationary) state along the null path with $r = \pm ct$ is described by

$$\nabla^2\psi_0 + \frac{2mE}{\hbar^2}\psi_0 = 0\,. \tag{9}$$

The solution of Eq.(9) is that of a standing wave. With some scrutiny, Eq.(6) can be seen as relativistic - Shrödinger equation for the harmonic oscillator with a space-time dependent potential energy that is given by

$$V(r,t) = \frac{1}{2}m\omega^2(r^2 - c^2t^2)\,. \tag{10}$$

It is interesting to notice that Eq.(6) is Lorentz invariant, and can be viewed as representing a 4-dimensional harmonic oscillator. The potential $V(r,t)$

is negative for time-like and positive for space-like intervals. Notice that when $m = 0$, Eq.(8) yields, $m_* = 0$ too, at any position and at any time.

We now separate the spatial and temporal components of Eq.(6) as

$$\frac{1}{c^2}\frac{\partial^2\psi_0}{\partial t^2} - \frac{m^2\omega^2c^2}{\hbar^2}\,t^2\,\psi_0 = \nabla^2\psi_0 + \frac{2m}{\hbar^2}\,(E - \frac{1}{2}\,m\omega^2r^2)\,\psi_0\,. \qquad (11)$$

Let us write $\psi_0(r,t) = \phi(r)\,\chi(t)$. Applying this in Eq.(11), and equate each part of the resulting equation to $-\lambda$, yield the two equations

$$\frac{1}{c^2}\frac{d^2\chi}{dt^2} - \frac{m^2c^2\omega^2}{\hbar^2}\,t^2\chi + \lambda\chi = 0\,, \qquad (12)$$

and

$$\nabla^2\phi + \frac{2m}{\hbar^2}\left(E + \frac{\hbar^2\lambda}{2m} - \frac{1}{2}\,m\,\omega^2r^2\right)\phi = 0\,, \qquad (13)$$

where λ is constant. Equation (13) is the ordinary equation of the 3-dimensional harmonic oscillator but with energy $E_* = E + \frac{\hbar^2\lambda}{2m}$. The solution of Eq.(13) in 1 - dimension (x-axis) is given by the normalized eigenfunction [1]

$$\phi_n(x) = \left(\frac{\sqrt{\frac{m\omega}{\pi\hbar}}}{2^n n!}\right)^{1/2} H_n\left(\sqrt{\frac{m\omega}{\hbar}}\,x\right)\,e^{-\frac{m\omega}{2\hbar}x^2}\,, \qquad (14)$$

where $n = 0, 1, 2, \cdots$, having the energy eigenvalues,

$$E_* \equiv E_n = \left(n + \frac{1}{2}\right)\hbar\omega + \frac{\hbar^2\lambda}{2m}\,, \qquad E_n = \left(n + \frac{\hbar\lambda}{2m\omega} + \frac{1}{2}\right)\hbar\omega\,, \quad (13a)$$

where H_n is the Hermite polynomial. The above energy is reminiscent of the energy due to the motion of a charged particle in a magnetic field (Landau level). The energy of the system is given by

$$E_n = \left(n + \frac{1}{2}\right)\hbar\omega_B + \frac{\hbar^2k_z^2}{2m}\,, \qquad \omega_B = \frac{qB}{m}\,, \qquad (13b)$$

where B is the applied magnetic field and k_z is the wave vector in the z-direction. But since it is unlikely for a wave to travel in the z-direction, $k_z^2 < 0$. The wave can only tunnel (decay).

Equation (13a) suggests a new quantum number, n_t, representing an oscillation of the particle in time. Accordingly, n represents the particle oscillation in space. It is defined by $n_t = \frac{\hbar\lambda}{2m\omega}$ so that $n_t \propto \omega^{-1}$. The effect of the second term in the energy equation is to shift the energy of the ordinary oscillator by the value $\frac{\hbar^2\lambda}{2m}$. The solution of Eq.(12) is

$$\chi(t) = C\, e^{\frac{m\omega}{2\hbar}\, c^2t^2}\,, \tag{15}$$

where C is constant, and $\lambda = -\frac{m\omega}{\hbar}$. Thus, comparing eqs.(13a) and (13b) yields, $k_z^2 = \lambda = -\frac{m\omega}{\hbar}$. Thus, the extra dimension (magnetic field) for a 2-dimensional system is like the 4-dimension (time) for the harmonic oscillator.

The full wavefunction in 1+1 dimension for a harmonic oscillator is thus

$$\psi_{0n}(x,t) = C\left(\frac{\sqrt{\frac{m\omega}{\pi\hbar}}}{2^n n!}\right)^{1/2} H_n\left(\sqrt{\frac{m\omega}{\hbar}}\,x\right) e^{-\frac{m\omega}{2\hbar}(x^2-c^2t^2)}\,, \tag{16}$$

with a total energy $E_* = n\,\hbar\omega$.
In 3+1 dimensions, the total energy of the oscillator is given by

$$E_* = \left(n+\frac{3}{2}\right)\hbar\omega - \frac{1}{2}\hbar\omega \qquad \text{or} \qquad E_{*n} = (n+1)\,\hbar\omega\,. \tag{17}$$

It is intriguing to state that the total energy of the harmonic oscillator in 3-dimensions was considered to emerge from the spatial coordinates and the corresponding momenta contribution. It was never argued that, as in special relativity, time is also a coordinate that should be incorporated. Hence, a relativistic harmonic oscillator (4-dimensional) should have its energy being contributed from the 4 coordinates. And since time is considered as an imaginary coordinate, its contribution to the total energy is negative and equals to $-\frac{1}{2}\,\hbar\omega$. This assertion is tantamount to the *equipartition theorem* which states that each squared coordinate (degree of freedom) in the Hamiltonian of the system contributes a value of $\frac{1}{2}\,k_BT$ to the total energy of the thermal system, where T is the absolute temperature and k_B is the Boltzman constant. We analogously state the following:

"*for a relativistic quantum harmonic oscillator each squared coordinate contributes an energy of* $\frac{1}{2}\,\hbar\omega$ *to the total energy, while a time coordinate*

contributes $-\frac{1}{2}\hbar\omega$, *and each squared momentum along a direction* i *contributes a term* $n_i\,\hbar\omega$ *to the total energy of the oscillator*".

It is found recently that a complex harmonic oscillator in 2-dimensions has an energy of $E_n = (n+1)\hbar\omega$, sharing the same energy as that of a 3+1 dimensional harmonic oscillator [8]. It is known as a vexing problem that the zero energy resulting from a minimal field has a non-zero value. However, if we consider the time coordinate besides the space one, the total energy of a one-dimensional harmonic oscillator will be zero and no vacuum energy dilemma occurs.

3 Relativistic quantum interval

In special relativity, the worldline of a particle in space-time is determined by the squared interval, $s^2 = c^2t^2 - r^2$. This interval is invariant under Lorentz transformation. The worldline of a massless particle (photon) is determined by $s^2 = 0$. This means that the photon moves with a velocity of light. Massive objects move along a worldline (time-like) that is causally connected since it moves with a velocity less than the velocity of light in a vacuum ($v < c$). However, in quantum mechanics, the particle worldline is a bit fuzzy, since the Heisenberg uncertainty relation, relating position and momentum, doesn't render the particle path to be well-defined.

Assuming that Eq.(6) satisfies a plane wave solution of the form $\psi_0(r,t) = A\,e^{-i(\omega' t - \vec{k}\cdot\vec{r})}$, where A is constant, we obtain

$$\omega^2(r^2 - c^2t^2)\,m^2 - 2E\,m + \hbar^2(k^2 - \frac{\omega'^2}{c^2}) = 0\,. \tag{18}$$

For massless oscillator (photon), Eq.(18) yields the non-dispersive relation, $\omega' = k\,c$. Equation (18) can be seen to define the mass of the oscillator. And since the mass of the oscillator is positive definite, then for a minimum mass, one finds

$$c^2t^2 - r^2 = \lambda_c^2\left(1 - \frac{k^2c^2}{\omega^2}\right), \qquad \lambda_c = \frac{\hbar}{mc}, \qquad \omega' = \omega\,. \tag{19}$$

Equation (19) defines the squared quantum interval of a massive oscillator. It is time-like for $\omega < kc$ and time-like for $\omega > kc$, and light-like (null)

when $\omega = ck$. Equation (19) relates the squared interval to the refractive index (n_r), where $n_r = kc/\omega$, as

$$c^2t^2 - r^2 = \lambda_c^2 \left(1 - n_r^2\right) . \tag{20}$$

This equation blends geometry, relativity, optic, and quantum mechanics. It is argued by Korbel that the above interval expresses the particle space-time extensions [9]. Furthermore, this space-time is related to the internal structure of the oscillator. Owing to Eq.(19), his model is applicable for stationary oscillator, *i.e.,* that with $k = 0$, where $\lambda_c = s$. Hence, the interval squared depends on the medium in which the oscillator travels. We prefer to call Eq.(20) the quantum interval. It reveals that the space-time is not flat inside a medium, and will be curved if the oscillator (*e.g.,* light) had a mass. Accordingly, light is refracted by glass because the space-time is not flat inside the glass. Equation (20) represents an equation of a hyperbola, or straight line depending on the value of n_r.

The interval is space-like ($s^2 < 0$) for $n_r > 1$, and time-like ($s^2 > 0$) when $n_r < 1$. Consequently, the mass of a particle (oscillator) reflects its interaction with the medium in which it moves. In a medium with $n_r < 1$, the role of space and time is interchanged. This situation occurs for a particle falls inside a black hole beyond the event horizon. This is tantamount to saying that time-like interval becomes space-like and vice versa. Interestingly, conductors have $n_r < 1$ for x-rays and ultra-violet (UV) radiations. This means that conductors are opaque to ordinary light (oscillator) but transparent to x-rays and UV radiations.

3.1 Mass spectrum of oscillator

Let us now apply Eq.(17) in Eq.(8), using Eq.(20), to obtain mass spectrum of the oscillator as

$$m_{*n}^2 = m_\omega^2 \left(n_r^2 - 1 - \beta\,(n+1)\right) , \qquad m_\omega = \frac{\hbar\omega}{c^2} , \qquad \beta = \frac{2mc^2}{\hbar\,\omega} . \tag{21}$$

One can suggest that m is the mass of the oscillator in 3 dimensions whereas m_* its mass in 4- dimensions. It is apparent from Eq.(21) that the mass of higher excitations becomes smaller. The parameter β signifies the number

of particle - antiparticle pair created at a given oscillation (ω), and m_ω is the equivalent mass to a given oscillation. It is emphasised by Aldaya *et al.* that the quantum dynamics of a relativistic oscillator involves an extra quantization condition that $N = \frac{mc^2}{\hbar\omega} = 1, \frac{3}{2}, 2, \cdots$ [10]. Since the minimum energy to create a single pair requires an energy of $2mc^2 = \hbar\omega$, the minimum vale of β is 1. Interestingly, Eq.(21) represents the quantization of the mass of the oscillator in 3+1 dimensions [11]. This mass quantization may reflect the mass spectrum of a bound system that is composed of harmonic oscillators (*e.g.,* hadrons) [6]. For a bound system, the interval $s^2 = \ell^2$ in Eq.(20), can express the physical size (extension) of the oscillator, $\ell = \lambda_c\sqrt{1 - n_r^2}$. For the time-like interval, ℓ is real and will be imaginary for the space-like interval. Thus, the potential energy in Eq.(10) can be written as

$$V(r,t) = \frac{(n_r^2 - 1)}{\beta}\hbar\omega\,, \qquad V(r,t) = \frac{1}{2}m(n_r^2 - 1)\lambda_c^2\omega^2\,, \tag{22}$$

upon using Eq.(21). It can be seen as representing an oscillation with an amplitude, $A = \sqrt{n_r^2 - 1}\,\lambda_c$. Eq.(22) reveals the quantum nature of the oscillator potential energy. Negative potential energy would suggest that the force between the oscillators becomes repulsive. A quantum force of the form $V/\ell \propto \hbar\omega$ can be associated with these oscillators. This may explain why no free quark can be observed, and that the quarks (if modeled by oscillators) are confined perpetually inside hadrons. The quantum potential energy in Eq.(22) can be compared with that due to spin-orbit coupling, or the one due to a magnetic dipole moment in presence of an external magnetic field (B) [1].

The motion of a charged particle (q) in a uniform magnetic field was considered by Landau who showed that the motion parallel to the field is unaffected, while that perpendicular to the field is that of a two-dimensional harmonic oscillator, the frequency of which is the cyclotron frequency [12, 13]. This is given by $\omega = qB/m$, so that Eq.(22) becomes

$$V = -\mu\, B\,, \qquad \mu = (1 - n_r^2)\frac{q\hbar}{m\beta}. \tag{23}$$

In this situation, μ defines the magnetic dipole moment of the oscillator, which depends on the medium in which the oscillator pair exists. It seems

that the effect of space and time on a harmonic oscillator is analogous to the influence of the electric and magnetic fields, respectively. A negative potential energy arises when $n_r < 1$. This indicates that the emerging force is attractive. One may associate a magnetic moment of a stationary oscillator, *i.e.*, $k = 0$ and $n_r = 0$. For $\beta = 1$, or $\hbar\omega = 2mc^2$, one has $\mu_s = \frac{q\hbar}{m}$, and for $\beta = 2$, or $\hbar\omega = mc^2$, one has $\mu_l = \frac{q\hbar}{2m}$. The former one can be related to spin and the latter to the orbital angular momentum of the oscillator.

4 Concluding Remarks

We have considered in this work a model of a quaternionic quantum harmonic oscillator using Shrödinger paradigm. This model can be applied to study the prorogation of massive photons in space-time. We obtained a relativistic quantum harmonic oscillator (in 3+1 dimension) generalizing the non-relativistic Shrödinger equation. The total energy of this oscillator is given by $E_{*n} = (n+1)\hbar\omega$. It can be seen as a time-correction to the non-relativistic oscillator, where the correction energy is $-\frac{1}{2}\hbar\omega$.

It is shown that a massless photon follows a null interval, and thus travels in a straight line. However, a massive photon follows a time-like interval in a medium and therefore bends. Hence, inherently all (waves) fields curve inside a medium whether massless or massive. We have found that the squared interval of a harmonic oscillator is related to medium properties in a quantum mechanical manner. Moreover, the ground state energy of the harmonic oscillator in 1+1 dimensions vanishes. The mass of the oscillator in 3+1 dimensions is found to be quantized.

5 Acknowlegements

I would like to thank Dr. I. B. Tomsah for reading the manuscript and for interesting discussions.

References

[1] Bjorken, J. D., and Drell, S. D., *Relativistic quantum mechanics,* McGraw-Hill, (1964).

[2] Aldaya, V., Bisquert, J. , Guerrero, J. and Navarro-Salas, J., *Group-theoretical construction of the quantum relativistic harmonic oscillator,* Rep. Math. Phys. 37, 387 (1996).

[3] Dirac, P. A. M., *Unitary representations of the Lorentz group,* Proc. Roy. Soc. (London) A.183, 284 (1945).

[4] Yukawa, H., *Structure and Mass Spectrum of Elementary Particles. II. Oscillator Model,* Phys. Rev. 91, 416 (1953).

[5] Kim, Y. S. and Noz, M. E., emphTheory and Applications of the Poincare Group, Reidel, Dordrecht (1986).

[6] Feynman, R. P., Kislinger, M. and Ravndal, F., *Current Matrix Elements from a Relativistic Quark Model,* Phys. Rev. D3, 2706 (1971).

[7] Wen-Chao, Q., *Bound states of the Klein-Gordon and Dirac equations for scalar and vector harmonic oscillator potentials,* Chin. Phys. 11, 757, (2002).

[8] Arbab, A. I., *The complex quantum harmonic oscillator model,* EPL 98, 30008 (2012).

[9] Korbel, P., *On Interpretation of special relativity: a complement to covariant harmonic oscillator picture,* http://arxiv.org/abs/hep-th/0503092.

[10] Aldaya, V., Bisquert, J. , and Navarro-Salas, J., *The quantum relativistic harmonic oscillator: generalized Hermite polynomials,* Phys. Lett. A156, 381 (1991).

[11] Hughston, L. P., *The relativistic oscillator,* Proc. R. Soc. Lond. A.382, 459 (1982).

[12] Landau, L., *Diamagnetismus der Metalle*, Z. Phys.64, 629 (1930).

[13] Trecia Markes, C. and Swamy, N. V. J., *A relativistic model of a charged oscillator in a magnetic field and its application,* Il Nuovo Cimento B.69, 177 (1982).

HADRONIC JOURNAL 45, 383 - 398 (2022)
DOI 10.29083/HJ.45.04.2022/SC383

NEUTRINO EXCHANGING POTENTIAL WITH BESSEL FUNCTION OF LOW ORDER

Bibek Koirala[1,2], Saddam Husain Dhobi[1,2,3], Prakash Subedi[1,2], Milan Gurung[4]
[1]Department of Physics, Patan Multiple Campus, Tribhuvan University, Lalitpur-44700, Nepal
[2]Innovative Ghar Nepal, Laitpur-44700, Nepal
[3]Robotics Academy of Nepal, Lalitpur-44700, Nepal
[4]Central Department of Physics, Tribhuvan University Kirtipur, 44618, Nepal
koiralabibek456@gmail.com / saddam@ran.edu.np

Received August 21, 2022
Revised September 8, 2022

Abstract

In this paper work, we study the nature of neutrino potential exchange with the Bessel function of lower order $n = 0$ and $n = 1$. To study the potential exchange author used theoretical method to develop the relation to study the nature of potential exchange. By developing the different equations, we study the exchange potential of neutrino by changing the masses of particles $m(\nu_e) \leq 7eV, m(\nu_\mu) \leq 0.27MeV, m(\nu_\tau) \leq 31eV$ respectively through the Bessel function. For the Bessel function (J_0) of neutrino potential exchange has greater value in the mass of $m(\nu_\mu) \leq 0.27MeV$ and Bessel function (J_1) is greater in $m(\nu_e) \leq 7eV$ and $m(\nu_\tau) \leq 31eV$ respectively. But in equation (17) and (18), the J_0 shows a minimum value of neutrino potential function with increasing the exchange distance.

Keywords: Neutrino, Neutrino Potential Exchange, Bessel Function, Neutrino Masses

Copyright © 2022 by Hadronic Press, Inc., Palm Harbor, FL 34684, USA

1. Introduction

Neutrino flavor oscillations are now a scientific fact, and research based solely on Mikheyev–Smirnov–Wolfenstein (MSW) effects has been modified in recent years by the realization that neutrinos' refractive effects on themselves due to the neutrino self-interaction potential are crucial. In the context of early universe evolution, solar and atmospheric neutrino anomalies, and core-collapse supernovae, their behavior in a vacuum, in matter, and through neutrino self-interactions has been explored (SN). When neutrino self-interactions become more important than matter potential in astronomical settings. This indicates systems with a large density of neutrinos, and in fact, supernova neutrinos are the focus of the majority of the work on neutrino self-interaction dominance. When contrasted to the initial composition deep inside the exploding star, collective effects such as synchronized and bipolar oscillations affect the flavor content of the expelled neutrinos [1].

The discovery of the phenomenon of neutrino oscillations, which has revealed neutrino features beyond the Standard Model, has been a major accomplishment in basic particle physics in recent decades. However, a complete knowledge of the many elements of neutrino oscillations is still a long way off. The theoretical underpinning of the neutrino oscillation phenomena is explained in this study, with emphasis on paradigmatic models. The many techniques and detectors used to study neutrinos from diverse sources are then reviewed, starting with the pioneering ones and progressing to the current and future detectors. The physics results are ultimately provided, following the same study path that this long odyssey has traversed. The unsolved challenges in this subject are explored, as well as the prospects for their resolution in the near future. Neutrino research has led to some of the most significant advances in particle physics in recent decades. Despite this, the properties of neutrinos are still far from being fully understood. The discovery of the oscillation phenomena threw the Standard Model of elementary particles into disarray, especially because it provided direct proof of a nonzero neutrino mass. Pontecorvo proposed the hypothesis of neutrino oscillations in 1957, before any scientific evidence of the phenomenon.

Many questions remain unanswered after decades of experimental and theoretical research, including the interpretation of this phenomenon and its correlated aspects, oscillation parameters, neutrino masses, mass hierarchy, CP violation in the leptonic sector, and the possibility of a fourth, sterile

neutrino. The widely used MSW model for interpreting solar neutrino oscillations has been validated for oscillations in vacuum and matter, but not for the vacuum-matter transition zone. As proposed by several hypotheses beyond the Standard Model, such as nonstandard neutrino interactions and the probable presence of a very light sterile neutrino, the structure of this transition could be modified in a meaningful way. As a result, more and more refined experimental studies of the transition zone are needed. Several experiments are currently collecting data on neutrino oscillations, while a few others are in the planning or construction stages. These studies use a variety of techniques, such as neutrino flavor disappearance and appearance, short and long source-to-detector baselines, and measuring neutrinos and/or antineutrinos from a variety of sources, including solar, atmospheric, accelerator, geo-, and reactor (anti)neutrinos. Neutrinos interact with matter only weakly, allowing them to provide nearly undistorted information about their source to the observer. By researching solar neutrinos and geoneutrinos, for example, we can learn not only about the character of neutrinos but also about the interiors of the Sun and the Earth [2].

Pauli, who viewed neutrinos as components of the nucleus, had the first idea of their existence in 1930. In certain nuclear decays, (anti)neutrinos are formed in connection with rays, according to Fermi's 1933 theory. Wick predicted the presence of electron capture based on this theory in 1934, and the nuclear recoil observed by Allen in 1942 with $^{7}Be + e \rightarrow \nu + {}^{7}Li$ provided evidence of the neutrino. Davis, following a method suggested by Pontecorvo in 1948, made the first effort to detect the final states created by neutrino interactions in 1955. Reines and Cowan used a reaction outlined by Bethe and Peierls in 1934 to make the first successful measurement in 1956.

The e and μ capture rates, according to Pontecorvo, are the same. In 1948, Puppi proposed the existence of a new neutrino that corresponded to the muon. Lederman, Schwartz, and Steinberger demonstrated the difference between the νμ and νe in 1962. Since 1974, evidence of the lepton, a third form of lepton after e and μ, has been obtained. The corresponding tau neutrino was discovered in 2000 by the DONUT experiment, but the number of neutrinos involved in weak interactions, $N_\nu = 3$, has been known since 1990 thanks to LEP observations of the Z width. In 1957, Pontecorvo proposed the concept of neutrino oscillations for the first time.

In 1957, Pontecorvo proposed the concept of neutrino oscillations for the first time. The same author, who devised the present theory of neutrino

transformation in vacuum in 1967, overcame the restrictions of the first idea. The new ingredient is the mixing of distinct neutrino families, which was first introduced in 1962 by Katayama, Matumoto, Tanaka, Yamada, as well as Maki, Nakagawa, and Sakata independently and more broadly. In 1963, Nakagawa, Okonogi, Sakata, and Toyoda proposed a link between neutrino mixing and neutrino mass. Through 1978, Wolfenstein discovered a new effect involving neutrinos propagating in ordinary matter, which is now known as the matter effect; Mikheyev and Smirnov explained its physical meaning and applicability in 1986. The evidence of oscillations accumulated over many years by the monitoring of solar and atmospheric neutrinos. The Nobel committee recognized the crucial significance of the Sudbury Neutrino Observatory and Super-Kamiokande discoveries as proof of oscillations in 2015, and the number of experiments that contributed significantly to this discovery is fairly big [3].

In the case of massless neutrinos and four-fermion contact interactions, the exchange of a pair of neutrinos between two objects separated by r results in a long-range effective potential proportional to $1/r^5$. The authors look at how this well-known form of neutrino-mediated potentials might change if the distance r is small enough, equivalent to a big enough momentum transfer to invalidate the contact interactions. The authors investigate two scenarios for incorporating a t-channel or an s-channel mediator to open up touch interactions. As long as the external particles are non-relativistic, the authors construct a basic formula that may be used to define the potential in all regimes. The potential drops as $1/r^5$ near the long-range limit in both circumstances, as expected. The t-channel potential exhibits Coulomb-like behavior (i.e. proportional to 1/r) in the short-range limit, but the s-channel potential exhibits $1/r^4$ and $1/r^2$ behaviors [4]. There is no compelling direct evidence for large neutrinos to date, and the current top bounds for ν_e, ν_μ, and ν_τ [6].

$$m(\nu_e) \leq 7eV, m(\nu_\mu) \leq 0.27MeV, m(\nu_\tau) \leq 31eV \qquad (1)$$

$G_F = 1.16639 \times 10^{-5}\, GeV^{-2}\, (\hbar c)^3$ is the Fermi decay constant. Subsequently Feinberg, Sucher, and Au (FSA) recalculated $V_{ee}^{(2)}(r)$ in the framework of the Standard Model and obtained

$$V_{ee}^{(2)}(r) = G_F^2 \left(2\sin^2\theta_W + \frac{1}{2}\right)^2 \left(\frac{1}{4\pi^3 r^5}\right) \qquad (2)$$

where θ_W is the weak mixing angle, with $\sin^2\theta_W = 0.2319(5)$. The result in eq. (2) has been rederived recently by Hsu and Sikivie using a different formalism from that of FS. Numerically, $V_{ee}^{(2)}(r) = 3 \times 10^{-82} r^{-5}$ eV where r is in meters, from which one can see that the interaction energy of two electrons arising from neutrino-exchange is smaller than their mutual gravitational interaction for $r \geq r_0 = 5 \times 10^{-8} m$. However, for $r \leq r_0$ the electroweak interaction arising from $\gamma -$ and Z^0-exchange would dominate, and hence there appears to be no diatnce scale over which $V_{ee}^{(2)}$ leads to detectable effects. The magentiude of corresponding force $\vec{F}_{12}(r) = -\vec{\nabla} V^{(2)}(r)$ [5].

Neutrinos are unique particles in many respects. For starters, they are several orders of magnitude lighter than all other fermions, and no direct measurement has discovered evidence for a non-zero neutrino mass: for all recorded neutrinos, one has measured (within errors) pc = E. Neutrinos are also neutral; they are unaffected by strong interactions and interact relatively weakly, if at all. For example, neutrinos produced in nuclear reactors with energy $E_\nu \sim 1$MeV have a cross section of order $\sigma \sim 10^{-44}$ cm^2, which corresponds to a probability of $\sim 10^{-18}$ in a solid detector with a thickness of one meter, or a probability of $\sim 10^{-11}$ inside the Earthtraveling along a trajectory that passes through its center. Neutrinos can couple with a Z^0 boson and change their 4- momentum without maintaining their identity (neutral current interactions), or they can couple with a $W^\pm$ boson and "transform" into one of the charged leptons $e^\pm$, $\mu^\pm$ or $\tau^\pm$.

The interaction of a W boson, a neutrino, and a charged lepton, for example, results in events like a charged lepton changing into a neutrino with the emission of a (virtual) W boson, or a W boson producing a neutrino charged lepton pair. The concept of neutrino flavor can be defined thanks to charged current processes. The type (mass) of the charged lepton connected to the same charged current vertex determines the flavor of a neutrino. For example, one would write [6] in the decay of a (virtual) W^- or W^+ [6]:

$$W^+ \rightarrow \ell^+ + \nu_\ell, W^- \rightarrow \ell^- + \bar{\nu}_\ell \qquad (3)$$

where the neutrino's label $\ell = e, \mu, \tau$, corresponds to the charged lepton's mass (or kind). The contrast between ν and l, as well as the neutrino's ℓ name, has a very basic and straightforward experimental rationale. A "ν_e" defined according to the convention of equation (1), interacting close to its origination

point can only produce e^-, while a ν_e can only produce e^+, a ν_μ only a μ^-, can only produce a, and so on for the other neutrino kinds. A significant experiment, for example, proved that neutrinos formed in a pair with a μ^+ near their creation point can only arise in the following sequence of processes:

$$\pi^+ \rightarrow \mu^+ + v_\mu, \qquad v_\mu + p \rightarrow \mu^- + \text{hadrons}, \qquad (4)$$

The earliest evidence of neutrinos was discovered in the 1920s while studying nuclear beta decay. Beta decay is a type of radioactivity in which a heavy primary nucleus (A,Z) decays into a lighter secondary nucleus with the same mass number but a one-unit charge difference, an electron (or positron), and nothing else observable:

$$(A, Z) \rightarrow (A, Z \pm 1) + e^{\pm} + \text{nothing else visible} \qquad (5)$$

The decay of a free neutron into a proton and an electron with a lifespan of about 15 minutes is an example of this process (886.7 sec). The decay of pions and muons produces muon neutrinos and anti-neutrinos:

$$\pi^+ \rightarrow \mu^+ + v_\mu, \qquad \mu^- \rightarrow e^+ + v_e + \bar{v}_\mu \qquad (6)$$

When the decay $\pi^{\pm} \rightarrow \mu^{\pm} + \nu$ was discovered it was natural to ask the question if the undected particles produced in the decay were identical with the neutrinos produced in β decay. The ν_τ is associated to the third charged lepton, the τ^- discovered in 1975 at Stanford. Tau neutrinos and anti-neutrinos are expected to be produced in $\tau^{\pm}$ decays.

$$\tau^- \rightarrow v_\tau + W^- \text{or } (v_\tau + e^- + \bar{v}_e) \text{ or } \left(v_\tau + \mu^- + \bar{v}_\mu\right) \text{ or } (v_\tau + [\bar{u}s']) \qquad (7)$$

2. Methodology

The three flavors of neutrinos, ν_e, ν_μ, ν_τ complete the zoo of elementary particles of the Standard Model. Every neutrino is the partner of a charged lepton (electron, muon, tau), connected to it by the weak interaction:

$$\mathcal{L} = \sum_{\alpha=e,\mu,\tau} \left[\bar{v}_\alpha i\eth \nu_\alpha + \frac{g}{\sqrt{2}} \left(\bar{v}_{\alpha,L} \gamma^\mu e_{\alpha,L} W_\mu^+ + h.c \right) + \frac{g}{2cos\theta_w} \bar{v}_{\alpha,L} \gamma^\mu v_{\alpha,L} Z_\mu \right] - \sum_{\alpha,\beta=e,\mu,\tau} \left[m_{\alpha\beta} \bar{v}_{\alpha,L} v_{\beta,R} + h.c \right] \quad (8)$$

Here, g is the weak coupling constant and θ_w is the Weinberg angle. Note that only left-handed neutrinos couple to the weak gauge bosons $W^\pm$ and Z. $m_{\alpha\beta}$ is non zero when $\alpha = \beta$. This means that the flavor eigenstates or interaction eigenstates $\nu_\alpha(\alpha = e, \mu, \tau)$ do not have a definite mass. The mass matrix m can be diagonalized according to

$$m = U m_D V^\dagger \quad (9)$$

where m_D = diag(m_1, m_2, m_3) is a diagonal matrix and U, V are unitary matrices. We define the neutrino mass eigenstates according to

$$v_{j,L} = \sum_\alpha U_{\alpha j}^* v_{\alpha,L} \, , v_{j,R} = \sum_\alpha V_{\alpha j}^* v_{\alpha,R} \quad (10)$$

In terms of the mass eigenstates, the Lagrangian of above equation can be written as [7],

$$\mathcal{L} = \sum_{j=1,2,3} \left[\bar{v}_j i\eth \nu_j + \frac{g}{\sqrt{2}} \left(\bar{v}_{j,L} U_{\alpha j}^* \gamma^\mu e_{\alpha,L} W_\mu^+ + h.c \right) + \frac{g}{2cos\theta_w} \bar{v}_{j,L} \gamma^\mu v_{j,L} Z_\mu \right] - \sum_{j=1,2,3} \left[m_j \bar{v}_{j,L} v_{j,R} + h.c \right] \quad (11)$$

The idea of a long-range force arising from the exchange of virtual neutrinos has been known since the 1930s, but it may have acquired wider notice because to Feynman's attempt to explain gravity using virtual neutrino

exchange. A massless virtual neutrino-antineutrino pair is exchanged between two electrons separated by a distance (r),

$$V_{v,\bar{v}}(r) = \frac{G_F^2}{4\pi^3 r^5} \tag{12}$$

where G_F is the Fermi constant with $\hbar = c = 1$. They later recalculated the result using the Standard Model neutral current interaction, obtaining [32],

$$V_{v,\bar{v}}(r) = \frac{G_F^2}{4\pi^3 r^5}\left(2\sin^2\theta_W + \frac{1}{2}\right)^2 \tag{13}$$

The Weinberg angle is denoted by θ_W. Fischbach then applied the multibody formalism to neutron stars, claiming that unless neutrinos have a finite mass, neutrino interactions result in a catastrophic addition to the star's self-energy. To derive Fischbach's finding in a more compact form, dispersion methods were applied to the massive neutrino computation,

$$V_{v,\bar{v}}(r) = \frac{G_F^2 m_v^3}{4\pi^3 r^2} J(2m_v r) \tag{14}$$

The two-neutrino exchange potential with lepton and nucleon is given [8] as,

$$V_{v,\bar{v}}(r) = \frac{G_F^2 g_{V,1}^f g_{V,2}^f m_v^3}{4\pi^3 r^2} J(2m_v r) \tag{15}$$

Now for Lepton-neutrino the two-neutrino potential exchange from equation (15) can be obtained as

$$V_{v,\bar{v}}(r) = \frac{G_F^2\left(\frac{1}{4} + 2\sin^2\theta_W + 4\sin^4\theta_W\right) m_v^3}{4\pi^3 r^2} J(2m_v r) \tag{16}$$

Here $g_V^f = \frac{1}{2} + 2\sin^2\theta_W$ for lepton exchange. For massless neutrino $m_v \to 0$, but we are consider massive neutrino therefore $m_v \neq 0$, the Bessel function $J(2m_v r)$, first order $n = 0$ and $n = 1$ is given in equation (17) and (18) respectively [9].

$$J_0(2m_v r) = 1 - m_v^2 r^2 + \frac{m_v^4 r^4}{4} \tag{17}$$

$$J_1(2m_v r) = m_v r - \frac{m_v^3 r^3}{2} + \frac{m_v^5 r^5}{12} \tag{18}$$

Therefore, potential of equation (16) for n=0 and n=1 become,

$$V_{v,\bar{v}}^{L0}(r) = \frac{G_F^2\left(\frac{1}{4} + 2\sin^2\theta_W + 4\sin^4\theta_W\right)}{4\pi^3}\left(\frac{m_v^3}{r^2} - m_v^5 + \frac{m_v^7 r^2}{4}\right) \quad (19)$$

$$V_{v,\bar{v}}^{L1}(r) = \frac{G_F^2\left(\frac{1}{4} + 2\sin^2\theta_W + 4\sin^4\theta_W\right)}{4\pi^3}\left(\frac{m_v^4}{r} - \frac{m_v^6 r}{2} + \frac{m_v^8 r^3}{12}\right) \quad (20)$$

Now for Nucleon-neutrino the two-neutrino potential exchange from equation (15) can be obtained for:

Only Neutron,

$$V_{v,\bar{v}}(r) = \frac{G_F^2 m_v^3}{16\pi^3 r^2} J(2m_v r) \quad (21)$$

Here $g_V^f = -\frac{1}{2}$ for Neutron exchange neutrino. For Bessel function $n = 0$ and $n = 1$ equation (21) become,

$$V_{v,\bar{v}}^{N0}(r) = \frac{G_F^2}{16\pi^3}\left(\frac{m_v^3}{r^2} - m_v^5 + \frac{m_v^7 r^2}{4}\right) \quad (22)$$

$$V_{v,\bar{v}}^{N1}(r) = \frac{G_F^2}{16\pi^3}\left(\frac{m_v^4}{r} - \frac{m_v^6 r}{2} + \frac{m_v^8 r^3}{12}\right) \quad (23)$$

Only Proton

$$V_{v,\bar{v}}^{P}(r) = \frac{G_F^2\left(\frac{1}{4} - 2\sin^2\theta_W + 4\sin^4\theta_W\right)m_v^3}{4\pi^3 r^2} J(2m_v r) \quad (24)$$

Here $g_V^f = \frac{1}{2} - 2\sin^2\theta_W$ for proton exchange neutrino. For Bessel function $n = 0$ and $n = 1$ equation (24) become,

$$V_{v,\bar{v}}^{P0}(r) = \frac{G_F^2\left(\frac{1}{4} - 2\sin^2\theta_W + 4\sin^4\theta_W\right)}{4\pi^3}\left(\frac{m_v^3}{r^2} - m_v^5 + \frac{m_v^7 r^2}{4}\right) \quad (25)$$

$$V_{v,\bar{v}}^{P1}(r) = \frac{G_F^2\left(\frac{1}{4} - 2\sin^2\theta_W + 4\sin^4\theta_W\right)}{4\pi^3}\left(\frac{m_v^4}{r} - \frac{m_v^6 r}{2} + \frac{m_v^8 r^3}{12}\right) \quad (26)$$

For Neutron and Proton

$$V_{v,\bar{v}}^{NP}(r) = \frac{-G_F^2\left(\frac{1}{2} - 2\sin^2\theta_W\right)m_v^3}{8\pi^3 r^2} J(2m_v r) \tag{27}$$

For Bessel function $n = 0$ and $n = 1$ equation (27) become,

$$V_{v,\bar{v}}^{NP0}(r) = \frac{-G_F^2\left(\frac{1}{2} - 2\sin^2\theta_W\right)}{8\pi^3}\left(\frac{m_v^3}{r^2} - m_v^5 + \frac{m_v^7 r^2}{4}\right) \tag{28}$$

$$V_{v,\bar{v}}^{NP1}(r) = \frac{-G_F^2\left(\frac{1}{2} - 2\sin^2\theta_W\right)}{8\pi^3}\left(\frac{m_v^4}{r} - \frac{m_v^6 r}{2} + \frac{m_v^8 r^3}{12}\right) \tag{29}$$

3. Result and Discussion

3.1 Lepton Neutrino potential exchange with low order Bessel function

The observation and nature of neutrino potential is based on $\sin^2\theta_W = 0.2319(5)$, $r \geq r_0 = 5 \times 10^{-8} m$, $m(\nu_\mu) \leq 0.27 MeV$, and $G_F = 1.16639 \times 10^{-5}\, GeV^{-2}\,(\hbar c)^3$ is the Fermi decay constant. The developed equation (19) and (20) is interaction of neutrino with Bessel function $n = 0\ (J_0)$ and $n = 1\ (J_1)$ respectively.

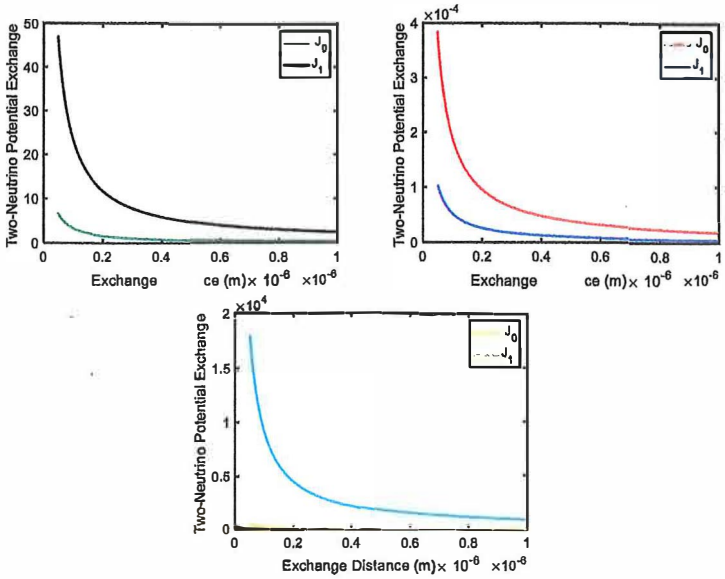

Figure 1: Interaction of neutrino during exchange with distance

The above figure 1, shows the interaction of neutrino potential exchange according to the exchange distance in m. For the Bessel function J_0 and J_1 neutrino potential show same nature with distance that is neutrino potential is decreases by increasing the distance. For J_0 neutrino potential is observed maximum 9 at distance of 0.04×10^{-6}m after that value is gradually decreases with increasing the distance. The form 0.64×10^{-6}m neutrino potential shows consistency up to 1m. For J_1 the neutrino potential is observed maximum 48 at 0.04×10^{-6}m distance. For J_1 the neutrino potential decreases with increasing up to 0.4×10^{-6}m and after slowly decreases with increasing the distance. The neutrino potential is observed high for J_1 in compare to the J_0. In second plot, for J_1 neutrino potential is observed maximum 1 at the distance of 0.04×10^{-6}m and the decreases with increasing the distance up to 0.06 at 1×10^{-6}m distance. For J_0 neutrino potential is observed maximum 3.9×10^{-4} at distance of 0.05m and decreases with increasing the distance up to 1m. For J_0 neutrino potential greater in compare to J_1. In the third figure, for J_0 neutrino potential is observed maximum 0.1×10^{4} at 0.08×10^{-6}m after that its value gradually decreases up to zero at the distance from 0.2×10^{-6}m to 1×10^{-6}m. For J_1 neutrino potential is observed maximum 1.8×10^{4} at the distance of 0.06m and gradually decreases up to $0.1\times 10^{4}$with increasing the distance. On comparing the neutrino potential with Bessel function it is observed that neutrino potential for J_1 has maximum value in compare to J_0.

3.2 Neutron Neutrino potential exchange with low order Bessel function

The observation and nature of neutrino potential is based on $\sin^2\theta_W = 0.2319(5)$, $r \geq r_0 = 5\times 10^{-8}m$, $m(\nu_e) \leq 7eV, m(\nu_\mu) \leq 0.27MeV, m(\nu_\tau) \leq 31eV$, and $G_F = 1.16639\times 10^{-5}\ GeV^{-2}\ (\hbar c)^3$ is the Fermi decay constant. The developed equation (22) and (23) is interaction of neutrino with Bessel function $n = 0\ (J_0)$ and $n = 1\ (J_1)$ respectively.

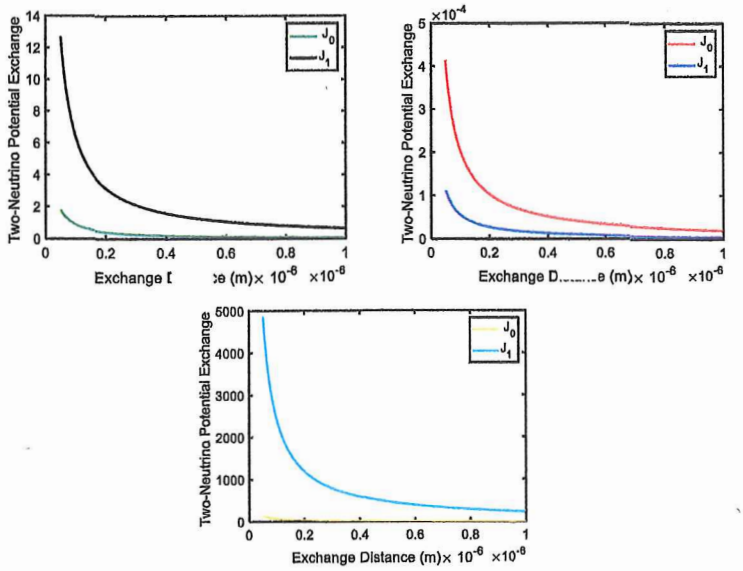

Figure 2: Interaction of neutrino during exchange with distance

The above figure 2, shows the interaction of neutrino potential exchange according to the exchange distance in m. For the Bessel function J_0 and J_1 neutrino potential of exchange has same nature that is neutrino potential is decreases by increasing the distance. At the distance 0.64×10^{-6}m, the neutrino potential becomes almost zero and shows consistency up to 1×10^{-6}m. For J_1 neutrino potential is observed maximum 13 at 0.04×10^{-6}m distance. For J_1 the neutrino potential gradually decreases up to 0.5 at distance of 1×10^{-6}m. For J_1 neutrino potential is observed high in compare to J_0. In second plot, for the Bessel function of J_1 neutrino potential is observed 1 at the distance of 0.04×10^{-6}m. For J_1 neutrino potential is gradually decreases with increasing the distance up to 0.05 at 1×10^{-6}m distance. For the J_0 the neutrino potential is observed maximum 4.2×10^{-4} at distance of 0.06×10^{-6}m. For J_0 the neutrino potential decreases with increasing the distance up to 1×10^{-6}m. For J_0 neutrino potential is greater in compared to J_1. In the third figure, for the J_0 neutrino potential is observed maximum 100 at 0.06×10^{-6}m after that its value gradually decreases up to zero at the distance from 0.2×10^{-6}m to 1×10^{-6}m. For the J_1 neutrino potential is observed maximum 3900 at the distance of 0.06×10^{-6} and after than gradually decreases up to 200 with increasing the distance. On comparing the neutrino potential with Bessel function it is observed that neutrino potential for J_1 has maximum value in compare to J_0.

3.3 Proton-Neutrino potential exchange with low order Bessel function

The observation and nature of neutrino potential is based of $\sin^2\theta_W = 0.2319(5), r \geq r_0 = 5 \times 10^{-8} m, m(\nu_e) \leq 7eV, m(\nu_\mu) \leq 0.27$ MeV, $m(\nu_\tau) \leq 31eV$, and $G_F = 1.16639 \times 10^{-5}\, GeV^{-2}\, (\hbar c)^3$ is the Fermi decay constant. The developed equation (25) and (26) is interaction of neutrino with Bessel function $n = 0\ (J_0)$ and $n = 1\ (J_1)$ respectively.

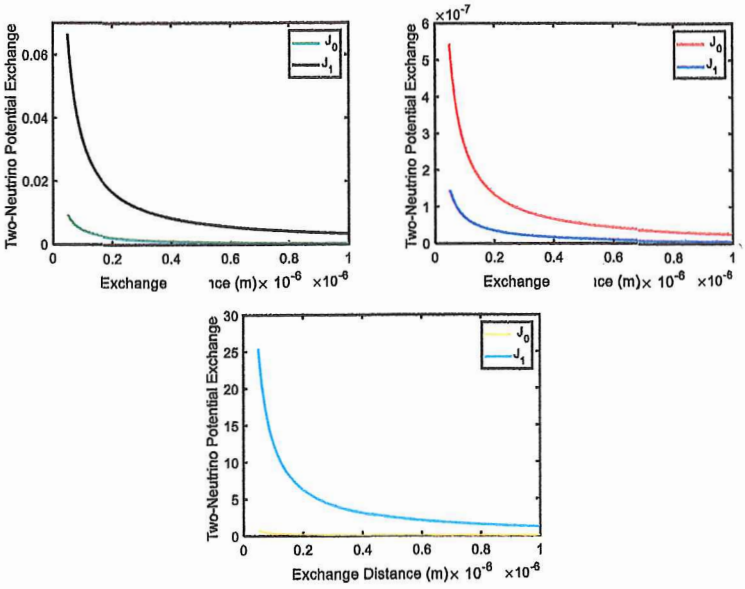

Figure 3: Interaction of neutrino during exchange with distance

The above figure 3, shows the interaction of neutrino potential exchange according to the exchange distance in m. For J_0 and J_1 neutrino potential exchange has same nature. The neutrino potential is decreases by increasing the distance. At the distance 0.64×10^{-6}m, the neutrino potential becomes almost zero and shows consistency up to 1×10^{-6}m. For J_1 neutrino potential is observed maximum 0.076 at 0.06×10^{-6}m distance. For J_1 the potential is gradually decreases up to 0.006 at distance of 1×10^{-6}m. For J_1 function neutrino potential is high in compared to the J_0 . In second plot, for J_1 neutrino potential exchange is observed maximum 1.5×10^{-7} at the distance of 0.04×10^{-6}m. For J_1 the potential is gradually decreases with increasing the distance up to 0.3 at 1×10^{-6}m distance. For J_0, maximum value of neutrino potential is observed 5.5×10^{-7} at distance of 0.06×10^{-6}m. For J_0 the potential gradually decreases with increasing the distance up to 1×10^{-6}m. For J_0 the neutrino potential is greater in compared to J_1. In the third figure, for J_0 the potential is observed maximum 0.1 at 0.06×10^{-6}m after that its

value gradually decreases up to zero at the distance from 0.2×10^{-6}m to 1×10^{-6}m. For J_1 neutrino potential exchange is observed maximum 26 at the distance of 0.04×10^{-6}m. After potential is gradually decreases up to 2 at the distance of 1×10^{-6}m and the potential for J_1 has maximum in compare to J_0.

3.4 Neutron-Proton-Neutrino potential exchange with low order Bessel function

The observation and nature of neutrino potential is based of on $\sin^2\theta_W = 0.2319(5), r \geq r_0 = 5\times 10^{-8}m, m(\nu_e) \leq 7eV, m(\nu_\mu) \leq 0.27MeV, m(\nu_\tau) \leq 31eV$ and $G_F = 1.16639\times 10^{-5}\ GeV^{-2}\ (\hbar c)^3$ is the Fermi decay constant. The developed equation (28) and (29) is interaction of neutrino with Bessel function $n = 0\ (J_0)$ and $n = 1\ (J_1)$ respectively.

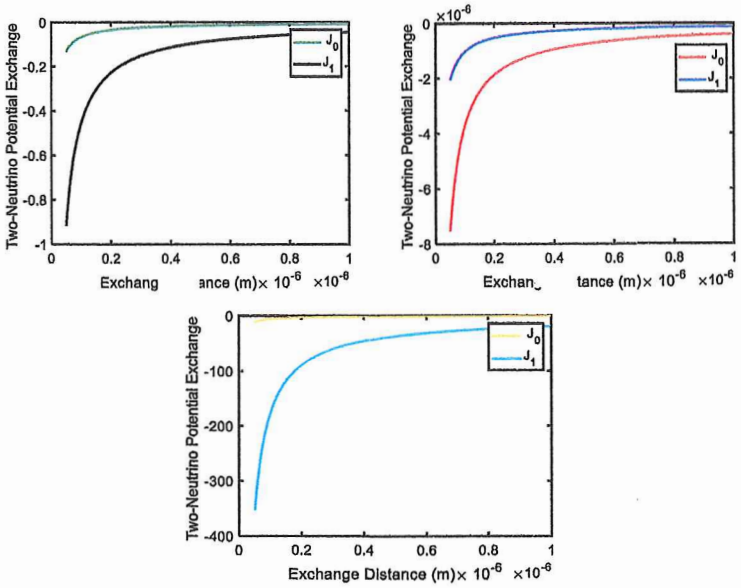

Figure 4: Interaction of neutrino during exchange with distance

The above figure 4, shows the interaction of neutrino potential exchange according to the exchange distance in m. For J_0 and J_1 neutrino potential exchange has same nature. The neutrino potential is increases by increasing the distance. At the distance 0.64×10^{-6}m, the neutrino potential becomes almost zero and shows consistency up to 1×10^{-6}m. For J_1 neutrino potential is observed minimum of –0.86 at 0.0410^{-6}m distance. For J_1 potential gradually increases up to -0.04 at distance of 1×10^{-6}m. The potential at for J_1function has low value in compared to the J_0 Bessel function. In second

plot, for the Bessel function J_1 has minimum value of neutrino potential exchange of -2× 10^{-6} at the distance of 0.04× 10^{-6}m. For J_1 the potential gradually increases with increasing the distance up to 0.1 × 10^{-6} at 1m distance. For J_0 has minimum value of neutrino potential -7.8× 10^{-6} at distance of 0.0610^{-6}m. The neutrino potential for J_0 has a low value in compare to J_1. In the third figure, for the J_0 has a minimum potential -10 at 0.0610^{-6}m after that its value gradually decreases up to zero at the distance from 0.210^{-6}m to 110^{-6}m. For, J_1 potential is minimum -350 at the distance of 0.06× 10^{-6}m. For, the Bessel function J_1 potential is minimum in compared to J_0.

4. Conclusion

For the Bessel function $n = 0$ (J_0) and $n = 1(J_1)$ the neutrino potential exchange with the exchange distance is analysed. For, the Bessel function $n = 0$ (J_0) neutrino potential exchange in mass of $m(\nu_\mu) \leq 0.27MeV$ is observed has high and for the Bessel function $n = 1$ (J_1) neutrino potential exchange in the masses of $m(\nu_e) \leq 7eV$ and $m(\nu_\tau) \leq 31eV$ is observed high. The neutrino potential exchange value of the both function J_0 and J_1 are decreasing with increase in distance. From the equation (17) and (18), the interaction of the neutrino with Bessel function J_0 and J_1 shows a high interaction potential exchange. The potetnial is found greater in the masses of $m(\nu_e) \leq 7eV$ and $m(\nu_\tau) \leq 31eV$ for J_0 in compared to the J_1.

Acknowledgment

We would like to thanks all the faculties' member of Department of Physics, Tribhuvan University, Nepal; Innovative Ghar Nepal and Robotics Academy of Nepal for their support during this work.

References

[1] J. D. Uribe, E. A. Becerra-Vergara, and J. A. Rueda, *Universe*. **7**(1) (2021).

[2] G. Bellini, L. Ludhova, G. Ranucci, and F. L. Villante, *Advances in High Energy Physics.* 2014 (2014).

[3] G. Fantini, A. Gallo Rosso, F. Vissani, and V. Zema, The Formalism Of Neutrino Oscillations: An Introduction, *Gran Sasso Science Institute*, (2020).

[4] X. J. Xu and B. Yu, *JHEP.* 2 (2022).

[5] E. Fischbach, Long-Range Forces and Neutrino Mass, Lecture Note, (2022).

[6] P. Lipari, Introduction to Neutrino Physics, CERN Note, (2022).

[7] J. Kopp, Theoretical Neutrino Physics, Lecture Notes, (2019).

[8] F. Ferrer, J. A. Grifols, and M. Nowakowski, Long range forces induced by neutrinos at finite temperature, arXiv (2022).

[9] R. Mathpal, Mathematical Physics Unit – 2, Presentation, (2022).

HADRONIC JOURNAL 45, 399 - 421 (2022)
DOI 10.29083/HJ.45.04.2022/SC399

NEW THERMODYNAMICS: HOW MANKIND'S USE OF ENERGY INFLUENCES CLIMATE CHANGE

Kent Mayhew
68 Pineglen Cres.
Ottawa, Ontario, Canada K2G 0G8
kent.mayhew@gmail.com

Received November 3, 2022

Abstract

Radiative heat transfer is currently thought of only in terms of photons as EM waves interacting with a molecule's lopsided charge distributions. This and infrared spectrometry have rendered the claim that both oxygen and nitrogen are transparent to infrared radiation. This has emboldened the greenhouse effect. Photons acting as particles hence transferring their momentum/energy onto gases is discussed. This phenomenon has been witnessed (but not acknowledged) in various experiments. Importantly, this changes how one models climate change.

As shown by their heat capacities, all polyatomic gases absorb heat. This includes O_2 and N_2 which constitute 99% of our atmosphere. Our whole atmosphere becomes both Earth's thermal blanket, and the heat sink for human activities. It will be shown that man's energy use does explain what has been witnessed in climate change. Namely, when compared to our Sun's energy that reaches Earth's surface, man's energy use results in a minimum of 0.6 °C temperature increase in the lower troposphere.

Keywords: Earth's thermal blanket, global warming, radiative heat transfer, net-zero-effect

Copyright © 2022 by Hadronic Press, Inc., Palm Harbor, FL 34684, USA

1 Introduction

Starting with the 19th century industrial revolution, mankind's activities have resulted in climate change. This is indicated by an inarguable, modest yet startling increase to our lower troposphere's mean temperature [1],[2]. The overwhelming belief is that this is a result of the emission of greenhouse gases by mankind's technology. For this anomalous temperature increase [1], there exists other plausible explanations both known and unknown [2].

Most of our Sun's visible light (energy) passes through our atmosphere striking Earth's surface. Once absorbed, it is transformed into longer wavelengths, i.e., infrared energy. Once radiated back into our atmosphere, this radiation is then incorrectly thought to be backscattered by greenhouse gases. Greenhouse gases are claimed to be specialized in their unique capability of absorbing and then radially radiating (backscattering), infrared photons. This accepted explanation involves photons behaving as waves, interacting with the greenhouse gas' lopsided charge distributions.

Accordingly, backscattering involves a portion of Earth's radiated heat being redirected back towards the Earth. This is backscattering resulting in more energy remaining in the atmosphere. This alters Earth's "radiative forcing", which is the difference between the amount of energy that enters our Earth's atmosphere versus the amount that escapes into outer space. Greenhouse gases holding our energy in our atmosphere, supposedly warm our climate (lower troposphere), in what is known as the "greenhouse effect" [3]-[5].

This author has challenged the greenhouse effect, with the understanding that our atmosphere as a whole forms Earth's thermal blanket [6]-[8]. The notion of our atmosphere being Earth's thermal blanket was originally proposed by Joseph Fourier (1768-1830) of the Fourier series fame. Fourier correctly postulated that our Sun's visible light (luminous heat) passes through our atmosphere thus reaching Earth's surface. It is then transformed into "non-luminous heat," which could not readily pass back through our atmosphere.

An issue lay in the operation of infrared spectrometers. Specifically, the spectrometer is evacuated, then the residing blackbody spectrum (defined by the Stefan-Boltzmann equation) is measured. The gas in question is then placed into the spectrometer and once thermal equilibrium is attained, measurements are made. The resulting output spectrum is then obtained by subtracting the background blackbody spectrum. Unfortunately, this subtraction assumes that the blackbody spectrum is not associated with the gas' energetics.

The subtraction of the background spectrum is nothing short of the subtraction of the gas' thermal signature [6]-[8]. Specifically, when in thermal equilibrium, it is the subtraction of the interaction of the gas molecules with their surrounding photons (acting as particles). Photons acting as particles, involve the photon's momentum/energy being passed onto the gas molecules. In equilibrium polyatomic gases adsorb, and radiate thermal radiation [9]. Therefore, the background spectrum must be associated with a gas' thermal signature.

This is what this author refers to as the "infrared spectrometry blunder" (ISB). The blunder is not realizing that blackbody radiation is associated with the gas' thermal signature. This results in the incorrect association of infrared spectrometry with all of matter's thermal energy. Spectrometry identifies gases based upon the photons acting as EM waves [9] interacting with a gas' lopsided charge distribution. Fig. 1 shows our Sun's irradiance vs wavelength, with the absorption by different molecules (H_20, CO_2 and O_3) interacting with photons of specific wavelengths acting as waves.

Infrared photons acting as waves does not fully describe heat transfer. Infrared photons acting as particles provides clarity, i.e., "thermal photons" [9] being photons whose momentum/energy is absorbed by matter (both condensed and gaseous). This results in that matter's infinitesimal temperature increase. This occurs over ranges of photon frequencies with most thermal photons belonging to the infrared spectrum.

Strangely, infrared radiation emanating from matter is referred to as thermal radiation, yet the sciences remain obscure to any notion of thermal photons. If matter only radiated infrared photons without absorbing any, then the notion of thermal equilibrium becomes illusionary. Clearly, it is not.

Such oversights explain scientific misunderstandings, including the erroneous claim that nitrogen (N_2) and oxygen (O_2) are transparent to infrared radiation. This occurs even though their heat capacities inform us that they absorb thermal energy in a fashion similar to all polyatomic gases. Note that this author previously incorrectly stated that N_2 and O_2 are "opaque" to infrared photons, when better terminology would have been "transparent" [9].

Testing the incorrect assertion that certain gases are transparent (or even opaque) to the infrared photons, Allmendinger [10] placed styrofoam tubes filled with various gases in the sunlight. He clearly showed that all atmospheric gases absorb thermal energy based upon their temperature increases. Furthermore, Allmendinger shone lights with strong infrared components into such tubes,

showing that all tested gases experience gas-dependent temperature increases [10],[11].

Gases do absorb a photon's momentum as thermal energy in the process of radiative heat transfer. This is based in part upon Allmendinger's findings that larger gaseous atoms/molecules attained higher limiting temperatures than smaller atoms/molecules. Obviously, atoms/molecules have a size dependent infrared absorption cross-section [9]. This author agrees with Allmendinger that his work proves that the greenhouse effect is an illogical science. Note Allmendinger believes that albedo changes are the primary cause for climate change, something I consider to be secondary.

There is little experimental evidence that actually proves the greenhouse effect. "If one googles "greenhouse gas experiment" one will find numerous researchers who have shone directional infrared light upon both CO_2 and air with some interesting results" [12-16]. "Although not overly scientific, they demonstrate the following accepted premise. Greenhouse gases are molecules with a lopsided charge distribution, e.g., carbon dioxide (CO_2), water vapour (H_2O), methane (CH_4) etc. Hence, EM waves of specific frequencies can excite the greenhouse gas molecules due to interactions with the lopsided charge distribution. Such interactions are often defined in terms of Maxwell's equations. [9]

In such greenhouse gas experiments both the air and CO_2 heat up, with the heating of the CO_2 always at a slightly higher rate with a somewhat higher final/limiting temperature, i.e., in" [16] "similar lights with strong infrared component heat a vessel filled with air heated from 23.4 C to 31.6 C, while a similar vessel filled with CO_2 heated from 23.4 C to 36.1 C. [9]

What is problematic in such greenhouse gas experiments is the fact that the air is 99% homonuclear nitrogen (N_2) and oxygen (O_2), both of which are claimed to be opaque" (transparent) "to infrared radiation. Therefore, if scientifically accepted, the minute concentration of CO_2 in air (i.e., 0.04%) is supposedly enough to heat air at a rate that is approximately 65% of that for pure CO_2. [based upon (31.6-24.3)/(36.1-24.3)=0.645]. To this author such an explanation is ridiculous. Although it demonstrates that infrared radiation can heat a gas, the science is lacking.

Consider the following rudimentary analysis. The fact that air heats at nearly ⅔ the rate of carbon dioxide points to the likelihood that the average scattering cross-section of predominantly diatomic air is ⅔ that of triatomic carbon dioxide.

In a different experiment, Seim and Olsen [17] conclude that CO_2 and air behave in a similar manner when it comes to backscattering. Like Allmendinger's experiments, this challenges the logic behind the greenhouse effect. Seim and Olsen [18] unwittingly show that profound differences exist between kinematic and radiative heat transfer, which fits with this author's assertions [9].

Infrared spectrums measured by satellites are claimed to be proof of the greenhouse effect [19]. There is no argument that so-called greenhouse gases (e.g., CO_2) will be witnessed in spectrums obtained in satellites. Understandably, satellite based infrared spectrums will show the presence of greenhouse gases in our atmosphere, i.e., the subtraction of the thermal (Stefan-Boltzmann) part of an infrared spectrum, enables one to identify what gases are present based upon their lopsided charge distributions. If this was not done, then the output spectrum would be dominated by the thermal Stefan-Boltzmann spectrum rendering it impossible to determine any uniqueness associated with various surrounding gases.

David Talbot points out that: "Geological records show that in the past 400,000 years, atmospheric concentrations of carbon dioxide, average Earth temperature, and sea levels have risen and fallen roughly in tandem, in 100,000-year cycles paced by slight oscillations in Earth's orbit" [20].

CO_2 as the driver of climate change must be debated. Those with vested interests claim that plots of carbon dioxide vs temperature (on geologic time scales) prove that the greenhouse effect is real. Based upon Antarctic ice core samples the rise in atmospheric CO_2 (aCO_2) seems to lag the rises in surface air temperatures (SAT) [21]. The solubility of CO_2 is much greater than that of either N_2 or O_2 i.e., 22 times. If the climate warms, then more CO_2 should come out of solution from our oceans than O_2. This would explain the lag. Note that inherent obstacles in ice core analysis exist [21]. Even so, this questions the accepted science.

Others have concluded that the greenhouse effect is poor science [22]-[25], with most claiming that global warming is not anthropogenic. A conclusion that differs from this author's, i.e., global warming is anthropogenic but is not due to the greenhouse effect [6]-[8]. So-called greenhouse gases tend to be triatomic or larger molecules, thus on a per molecule basis they will backscatter more thermal energy than diatomic gases. This is confirmed by gas' heat capacities where gas molecules with more atoms absorb more heat than gas molecules consisting of fewer atoms [26],[27]. For example, all triatomic gases have higher heat

capacities than diatomic gases. The fact that a polyatomic gas' heat capacity is more closely related to the molecule's size (number of atoms) rather than its charge distribution (lopsided or otherwise) confirms that something is amiss in the sciences.

Certainly, the emission of greenhouse gases will both thicken our Earth's thermal blanket, and increase any backscattering. Importantly, adding CO_2 to our atmosphere contributes to ocean acidification [28],[29]. Thus, emissions of CO_2 must be curtailed.

Our whole atmosphere is Earth's thermal blanket. Our Sun's irradiance impacts the blanket's exterior. Conversely, man's energy use occurs on that blanket's interior where climate change is witnessed, i.e., our lower troposphere. The implication is that one of the anthropogenic associations with global warming is man's energy use degrading into thermal energy (heat) [6]-[9]. Other components exist such as changes to Earth's albedo, i.e., due to our cement jungles. Some consider that the pollution contributes to climate change [30]. Even if pollutants do not directly influence our atmosphere's temperatures, however they do affect our ecosystems [31].

2 Biological Evidence of Thermal Photons

Reptiles that see in the infrared don't see long distances. Intuitively, this alienates any claim that infrared atmosphere's gases are transparent to the infrared. The same can be said of night vision goggles. The closer one's infrared vision is to the visible spectrum the further one can see. This implies a wavelength/frequency dependence, where longer infrared wavelengths provide poorer distance vision.

The reason is that the adsorption and radiation of thermal (infrared) photons by our atmosphere's gases causes distortions, hence lessens one's ability to see. Reptiles that hunt small mammals (e.g., snakes) have evolved to be able to see a mammal's radiated heat over short distances thus improving their ability to hunt.

3 Gaseous Experimental Systems

The witnessed variations in our atmosphere's temperature profile informs us that gases do adsorb our Sun's thermal energy [32]. Since homonuclear diatomic N_2 and O_2 are not transparent (or opaque) to thermal radiation, then one must reconsider atmospheric physics because our atmosphere is 78% N_2 and 21% O_2.

As has been previously discussed [9], consider a box containing diatomic gases, as illustrated in Fig.2. As an enclosed space, the box is filled with

blackbody radiation emanating from its walls. At room temperature (e.g., T = 300K) this blackbody spectrum's peak (as defined by Wein's law) is in the infrared. Blackbody radiation can be explained in terms of inelastic collisions of the wall's molecules [6],[9]. When in thermal equilibrium the gas molecules absorb the photon's impulses, while simultaneously emitting radiation due to inelastic molecular collisions (both intermolecular and intramolecular).

The system's walls impose their kinematics upon the enclosed diatomic gas molecules [26],[27]. Moreover, such walls absorb and/or reflect photons thus giving the illusion of the systematic elastic collisions, even though the reality is that the collisions are inelastic. [6],[9],[28],[33],[34].

The total energy associated with the system's thermal photons generally is infinitesimal when compared to the total energy associated with the gas molecule's kinematic energies (translational, rotational plus vibrational). A gas molecule's speed is infinitesimal in comparison to the speed of light. Accordingly, it is a grandiose mistake to ignore a system's blackbody/thermal radiation when contemplating heat transfer.

4 Heating Atmospheric Gases

Fig. 3 and Fig. 4 illustrate homonuclear atmospheric gases above the Earth's surface. Unlike gases inside of an experimental apparatus, there are not six structured walls that impose their kinematics upon gas molecules that interact with them.

Fig. 3 further shows that visible light tends to pass through the atmosphere. Conversely infrared/thermal photons as illustrated in Fig. 4 tend to be absorbed by the atmosphere's gases. Such radiative heat transfer is primarily due to the photon's momentum transfer (photons acting as particles) but may also include energy transfer due to photons behaving as EM waves. This applies to all infrared photons including those originating from our Sun and/or from Earth's surface.

Atmosphere's gases exchange energy by:

- Absorption and emission of photons.
- Intermolecular collisions.
- Collisions with Earth's surface.
- Collisions with other gas molecules.

In thermal equilibrium, the total energy emitted equals the total energy absorbed. This, holds even if the radiative and adsorption spectrums (power at each frequency) are not identical. The expectation becomes that increases in our

atmosphere's polyatomic gas' vibrational energy will lead to increases in both their kinematic and radiative energy transfers. In the open system atmosphere, thermal equilibrium in the context of gases in an experimental closed system rarely exists.

As traditionally described: Our Sun's visible radiation that passes through our atmosphere is either absorbed (as illustrated in Fig. 3) or reflected by Earth's surface. The reflected light gives surfaces their color. The absorbed light eventually will be radiated by the Earth's surface, as infrared photons back into our atmosphere. Such infrared photons generally are backscattered adding to the lower troposphere's temperature.

As Earth's thermal blanket, our atmosphere regulates our temperatures. Without our atmosphere, Earth's temperatures would resemble the moon, where the bright side (T = 400 K), is dramatically different than the dark side (T= 40 to 90 K). The impacts of our Earth's diurnal nature warrant additional consideration.

5 Stefan-Boltzmann Equation

Stefan's law describes the intensity (I) of a blackbody spectrum:

$$I = \sigma T^4 \qquad 1$$

where "σ" is a constant and "T" is the temperature.

Eqn. 1 is obtained by first taking the energy density [$u(\nu)$] at a particular frequency (ν):

$$u(\nu) = \left(\frac{2\pi h\nu^3}{c}\right)(1/e^{h\nu/kT} - 1) \qquad 2$$

Then integrating across all frequencies (0 to infinity) to get total intensity. This gives a blackbody spectrum as defined by:

$$\int_0^\infty u(\nu)d\nu = \int_0^\infty \left(\frac{2\pi h\nu^3}{c^2}\right)(1/e^{h\nu/kT} - 1)d\nu \qquad 3$$

Eqn. 3 is calculated using change of variable: $x = h\nu/kT$ and then using: $\int_0^\infty (x^3 dx)/(e^x - 1) = \pi^4/15$. One then obtains that: $\sigma = 2\pi^5 k^4/15c^2h^3$.

Calculating the energy associated within a particular range of frequencies other than from 0 to infinity, is not readily doable. Therefore, the following analysis is based upon simple geometry.

6 Anthropogenic Component of Global Warming

All of mankind's energy use eventually degrades into thermal energy and thus adds to Earth's lower atmosphere's temperature. The second law [35] is not required to explain such things.

According to the US Department of Energy (2015): The Sun's energy incident upon the Earth and its surrounding atmosphere is 430 quintillion joules per hour (4.30×10^{20} J/hr). While the amount of energy that man uses in a year is 410 quintillion joules. The amount of heat generated by man per hour becomes:

(4.10×10^{20})(J/hr) 24(hr/day)/365 (day/yr) = 4.68×10^{16} J/hr

The ratio of man's energy use to the energy from our Sun becomes:

$4.68 \times 10^{16} / 4.30 \times 10^{20} = 1.09 \times 10^{-4}$

This certainly causes one to pause when contemplating man's energy use contributing to climate change.

7 Issue of Perspective

Fig. 5 shows a standard perspective for our Sun's spectrum, i.e., cut off at λ = 3,000 nm. The implication being that the UV, visible and near infrared parts respectively constitute 5%, 43% and 52% of our Sun's energy outputs.

Fig. 5 does not include all the infrared wavelengths, i.e., wavelengths that one associates with heat. Accordingly, Fig. 5's appearance confuses one into thinking that the majority of our Sun's insolation resides in the near infrared and visible range. Added to this, is the confusion one often experiences when jumping scales, e.g., from nm to μm to mm.

If one is concerned with the thermal phenomena, then our Sun's spectrum must be extended throughout the infrared, to at least the microwave part of the EM spectrum as illustrated in Fig. 6. In which case our Sun's insolation becomes a constant slowly decreasing asymptotic function (approx. linear), rather than a traditional blackbody curve, e.g., Fig. 5.

What becomes apparent is the girth of our Sun's spectrum in the infrared is immense, e.g., infrared wavelength range: 700 nm $< \lambda <$ 100,000 nm. Fig. 6 becomes a more complete sketch for considering our Sun's thermal spectrum.

For clarity the near infrared is taken to consist of: 700 nm < λ < 3,000 nm. The thermal infrared is taken to consist of: 3,000 nm < λ < 8,000 nm. While the far infrared is: 8,000 nm < λ < 100,000 nm.

If the Sun's irradiance is considered as asymptote starting in the thermal infrared and ending in the microwave (3,000 nm to 100,000 nm), then the area under the spectrum's curve could be approximated as a straight line parallel to the wavelength axis with a spectral irradiance approximated by 0.075 ($W/m^3/nm$).

Therefore, the thermal infrared energy density (energy per unit volume) approximates:

$(0.075)(8{,}000\text{-}3{,}000) = 375\ W/m^3$

And the far (long) infrared energy density approximates:

$(0.075)(100{,}000\text{-}8{,}000) = 6{,}900\ W/m^3$

In order to attain a more complete understanding, similar geometric principles will now be applied to the ultraviolet, visible and near infrared spectrums. As shown in Fig. 6, for the Sun's spectrum from UV through to the long infrared spectrum, one obtains the following Table 1, giving rough approximations for the energy per unit volume for the various parts of our Sun's spectrum.

Table 1	Energy Density per Spectrum		
Spectrum	Area under graph (W/m^3)	Ratio	%
Ultra violet	½[(370-170) 0.8] = 80	80/8887.5	0.09%
Visible light	(740-370) 1.85 = 684.5	648.5/8887.5	7.7%
Near infrared	½(3,000-740).75 = 848	848/8887.5	9.5%
Thermal infrared	(0.075)(8,000-3,000) = 375	375/8887.5	4.2%
Long infrared	(0.075)(100,000-8,000)= 6,900	6,900/8887.5	77.6%

Ostensibly Table 1 indicates that our Sun's energy, associated with both the thermal and far infrared, may actually be several times the energy that is associated with the near infrared into the visible light.

How much of our Sun's insolation is attributable to visible light? It approximates:

$$684.5\ (W/m^3)/8887.5\ (W/m^3) = 0.077$$

Only 7.7% of our Sun's radiation is actually in the visible spectrum. This, challenges the 43% assumption based upon Fig. 5.

8 Our Atmosphere and Infrared Photons

Much of the Sun's infrared energy is absorbed by gases (and other particles) in the upper atmosphere. This explains why Earth's thermosphere has exceptionally high measured temperatures, i.e., upwards of 2600 degrees °C. Conversely, temperatures measured in the mesosphere ($-2.5 < T < -90$ °C) and stratosphere ($-15 < T < -51$ °C) tend to be sub-zero. In part this has to do with the differences between temperatures measured in radiation dominated open systems and those where the gas' kinematic energies dominate [32].

Obviously, most of the Sun's infrared energy doesn't propagate through the thermosphere into the mesosphere. The reason the stratosphere is warmer than the mesosphere is that heat travels into the stratosphere from the Earth's surface and/or its troposphere [32].

This all fits with this author's assertion that infrared photons (acting as particles) tend to be absorbed and radially radiated by most all atmosphere gases (including O_2 and N_2). Furthermore, it fits with what is known about infrared radiation.

Most of our Sun's visible light passes through our atmosphere and is either reflected or absorbed by earth's surfaces. Absorbed energy is transformed into heat. Approximately 29% of the Sun's incident radiation is reflected back out into space, i.e., Earth's albedo is 2.9.

Approximately 7.7% of the Sun's energy makes it to Earth's surface as visible light, while 29% is reflected back into space. Thus, the percentage of our Sun's visible light that is transformed into heat, eventually being absorbed by our lower troposphere becomes:

$$(1.0 - 0.29) \times 7.7\% = 5.5\%.$$

Therefore, of the Sun's 430 quintillion J/hr, the Sun's energy that becomes heat in the lower troposphere approximates:

$$0.055 \times 4.30 \times 10^{20} = 2.37 \times 10^{19} \text{ J/ hr}$$

The amount of heat generated by man per hour is determined to be: 4.68×10^{16} J/hr. The ratio of man's energy to our Sun's heat energy entering in our troposphere approximates:

$$4.68 \times 10^{16} / 2.37 \times 10^{19} = 1.97 \times 10^{-3}$$

The average Earth temperature is 288 K [36]. Assume a linear functionality between the atmosphere's thermal energy density and its temperature. Then, the approximate measured temperature increase attributable to man's activities becomes:

$$1.97 \times 10^{-3} \times 288 = 0.57 \text{ K} = 0.57 \text{ °C} \approx 0.6 \text{ °C}$$

The approximate 0.6 °C fits with the scale of what has been witnessed in climate change. In 2019 a BBC produced show on the application of statistical analysis to climate change titled, "Climate Change by Numbers" showed with over 95% certainty, that since 1880 Earth has experienced a 0.85 °C temperature increase attributed to human activities." [37]. Note that this author previously incorrectly discussed the possibility of climate change being due to man's energy use with a rough value of 2 degrees [8].

9 Analysis Accuracy

This analysis is founded upon assumptions, e.g.:

1) Our atmosphere is fully transparent to visible light, i.e., 100% of visible light passes through the atmosphere.
2) The Sun's blackbody spectrum stops at the microwave. It probably extends (how far) into the microwave.
3) The Sun's blackbody thermal energy through the infrared spectrum was approximated as rectangular vs triangular.

1) and 2) will cause 0.6 °C to increase, while 3) should cause it to decrease. Since visible light is scattered by our atmosphere 1) is not true, i.e., our skies are blue due to scattering of visible light. If only 70% of our Sun's visible light makes it to Earth's surfaces, then the expected temperature increase due to man's activities should approximate 0.8 °C.

This requires the acceptance of this author's claims concerning the erroneous sciences. One could counter that this is indirect proof of those claims.

Certainly, more exacting analysis is required. Such analysis can only be properly accomplished once the sciences are rewritten. This includes how thermal photons of various frequencies interact with atmospheric gases (Thomas Allmendinger type experiments) and atmosphere physics.

10 Modeling

Climate change models must include man's energy use.

Issues with current modelling do exist. Consider NASA's published "Earth's Energy Budget" [36]. As helpful as it appears, it is at best a guess. Displayed aspects are inferred, based upon the currently embraced, questionable science. For example, one applies Wein's law and infers a blackbody spectrum similar to Fig. 1, when Fig. 6 provides a better reality.

Consider a satellite measuring the heat radiating into and out of the Earth, e.g., CERES instrumentation that forms the basis of NASA's publication [35]. The incoming solar radiation can be accurately measured (e.g., 340.2 W/m^2), and so too the outgoing infrared radiation (e.g., 239.9 W/m^2) [38]. As accurate as such thermosphere located satellite data may be, one wonders if rewriting the science changes anything. For example, realizing that most of our Sun's radiation (e.g., infrared) is absorbed by the thermosphere alters one's atmospheric measurement when compared to those made in outer space.

More troublesome is analyzing the energy spectrums at other locations. If thermal photons are continually absorbed and radiated by atmospheric polyatomic gases, then one could not possibly know the true origins of the photons, e.g., backscattering distorts measurements. Since most visible photons pass through the atmosphere this could make most measured blackbody spectrums to appear valid.

11 Water Vapours, Clouds and Contrails

How problematic is the modelling of water vapour [39]? Water vapour makes up 0.3% of our atmosphere but unlike other gases its distribution is far from uniform e.g., as high as 4% in the tropics and as low as 0% in the polar regions. In accepted models water vapour forms the largest percentage of the atmosphere's so-called greenhouse gases, i.e., as much as 95%.

Again, this lacks the realization that all atmospheric polyatomic gases absorb infrared photons. There is no arguing that on a per molecule basis, triatomic

water will interact with more infrared photons than smaller diatomic gases that dominate our atmosphere.

Water plays a more significant role when it forms real surfaces. Nighttime clouds do elevate our atmosphere's local temperature. This occurs as the clouds' water vapors, droplets and ice crystals absorb and then radially radiate the infrared photons/radiation emanating from Earth's surface. The clouds' molecules also experience intermolecular inelastic collisions with other atmospheric gas molecules, exchanging kinematic energies, i.e., translational, rotational, and vibrational energies.

Conversely, daytime clouds and contrails [38], [40] cool the lower troposphere by reflecting and/or backscattering significant portions of our Sun's daytime insolation. Therefore, contrails in the daytime also reflect our Sun's insolation back towards space. Conversely, like clouds, contrails in the night sky help hold heat near Earth's surface.

One cannot simply make any one assertion with any real certainty based upon current models nor the accepted science.

12 Heat Sinks: Atmosphere and Oceans

Earth's atmosphere is the heat sink for mankind's energy use. Just as our atmosphere is mankind's heat sink, our oceans are our atmosphere's heat sink. Therefore, man's activities indirectly affect our ocean's temperatures. Furthermore, ocean currents are huge conveyor belts, storing heat in their depths.

Due to the ocean's storage of heat, there must be a time delay between the heating of our atmosphere and what is witnessed as climate change. A delay measured in years to decades. Accordingly, what one witnesses today is due to cumulative effects from our past. Thermal effects from today's causations will be witnessed both today and in the future. If energy use is decreased, then a time delay will be required before our planet actually reaps the benefits.

13 Net-Zero-Effect

Wind turbines transform our atmosphere's kinetic energy into electricity. This can be thought of as the removal of energy from our atmosphere. Thus, theoretically wind turbines enable man's activities to be a "net-zero-effect" upon our atmosphere's energy budget. Even energy lost in generation is returned back into the atmosphere. Other renewable energy sources, e.g., solar and wave power also have the potential of being net-zero-effect power sources.

Most processes, e.g., burning of fossil fuels are not net-zero-effect energy production, as they add energy into our over heated lower troposphere. This includes nuclear power. Furthermore, steam generation involves both an elevation of temperatures and lost work. Lost work heats our atmosphere [33],[41]-[44]. There are also the unwanted by-products.

14 Moving Forward

Recent theories predict that our climate may witness a temperature increase of as much as 1.5 °C, by 2030 [45]. This Malthusian prediction is based upon the incorrect greenhouse effect rather than man's energy use. If the situation is truly dire, then we may have one of those "situations with a high perceived threat and a low perceived ability to react" that "often lead to denial of the threat, rather than eliciting a response" [46].

"Environmental decision makers and practitioners need and deserve high-quality environmental evidence for effective decision making" [47]. They also need a new foundation based upon common sense science.

Designers, entrepreneurs, and engineers are investigating solutions to reduce man's impact on our environment. For example, Sheehan and Welsh have created an epicatalysis thermal diode (ETD) coupled to a thermoelectric converter (TEC). It "utilizes the phenomenon of epicatalysis to establish a stationary temperature" thus enabling the device to harvest the surrounding ambient thermal energy [48],[49]. Another example is Elon Musk's Hyperloop, which involves a system of sealed tubes in which pods travel at high speeds with little or no air resistance nor friction [50]. Less unsightly and wildlife-friendly wind turbines also could provide the better solution, e.g., tulip turbines.

15 Feedback Effects

Think of glaciations often associated with the Pleistocene. They started with a couple of degrees drop in temperature, which lead to increased ice cap sizes. thus, increasing the reflection of our Sun's visible energy and changing Earth's albedo. This contributed to the lowering of Earth's mean temperature. Note that glaciations are considered to involve temperature decreases of near 5 degrees.

Just as feedback effects apply to glaciation, they apply to climate change. Melting of the ice caps lowers Earth's albedo, which means that more of our Sun's visible light will be absorbed as heat by the Earth, hence our troposphere will be warmed even more. Furthermore, increased temperature can be

associated with elevation in the number of forest fires. And the list goes on. This brings to light the precarious balances here on Earth.

Rising temperatures increase the water vapor content of our atmosphere. This in turn causes higher retention of thermal energy by our atmosphere.

Although calculated for a sense of scale, the approximated 0.6 °C temperature (or more) increase that can now be attributed to mankind's energy use may not seem to be that much. Unfortunately, it only tells part of the story.

Conclusions

Whether or not one believes, our cognitive biases concerning anthropogenic induced climate change tends to be fully entrenched. Accepting that climate change is real and that the science behind the greenhouse effect is misguided, one is left with man's contribution to global warming being due to alterations of Earth's albedo, pollution, and as discussed here, mankind's energy use.

Accepted science realizes that all matter radiates photons as thermal radiation. But it fails to understand that matter must absorb photons, if thermal equilibrium is a reality. This void, can in part be attributed to the infrared spectrometry blunder, becoming one of the reasons that the sciences failed to realize the wave-particular duality of photons in radiative heat transfer.

Photons that are absorbed as heat are, what this author calls "thermal photons". Such photons have frequency dependence (ranges) that needs investigation. Remaining oblivious to thermal photons has led thermodynamics to incorrectly limit heat transfer to the kinematics of matter. This is nothing short of ignoring the radiative heat transfer that one feels when standing in the sunshine.

Accepting that thermal photons exist and are absorbed by all polyatomic atmospheric gases renders the science behind the greenhouse effect non-sensible. O_2 and N_2 are not transparent to infrared frequencies, as claimed.

Much of our Sun's radiance is in the infrared. This energy tends to be absorbed and then radially radiated by our thermosphere gases, thus helping to explain why the thermosphere's measured temperatures tend to be so outlandishly high.

Temperatures in the mesosphere and stratosphere are lower because most of the Sun's thermal photons have been absorbed, and radially radiated by the atmospheric gases (and particles) in the thermosphere. Thus, backscattering much of our Sun's thermal energy back into outer space.

Our Sun's visible light tends to pass through our atmosphere. When impacting Earth's surface, much is absorbed by the Earth's surfaces. Conversely, about 29% of the Sun's visible photons are reflected by Earth's surface back towards outer space.

The visible light absorbed by Earth's surfaces is transformed into heat. This heat eventually radiates as infrared photons (heat). These infrared photons then behave as thermal photons, being absorbed by most of our atmospheric gases, i.e., heating the lower troposphere. Some of this absorbed energy is backscattered (radiative forcing), i.e., directed back towards Earth's surface.

Hence, our atmosphere as a whole is Earth's thermal blanket. This new understanding alters how one views anthropogenic climate change. Based upon new realizations mankind's total energy use was compared to our Sun's visible light that passes through our atmosphere heating our lower troposphere, where climate change is witnessed.

Our Sun's total energy output remains massive in comparison to mankind's energy use. However, only a percentage (rough analysis 5.5%) of this energy actually makes it to Earth's surface, thus heating the lower troposphere, where climate change occurs. Of note; Earth's thermal blanket explains why temperatures on Earth are so radically different to those on the moon.

Although based upon new insights and approximations, it has been shown that man's energy use should result in a lower troposphere temperature increase of 0.6 °C, but this author believes 0.6 °C to be on the low side. A more realistic value may be 0.8 °C, or more. This needs to be further investigated. Due to all the permutations, any full analysis will not be a simple task.

Just as our atmosphere is the heat sink for all our activities, the oceans are our atmosphere's heat sink. There must be a time delay between causation and effect when it comes to global warming. Accordingly, what we do today, will be witnessed in the future.

Accepting global warming is real. Then, not only must our energy production be clean, it should also approach a "net-zero-effect" which means renewable energy with an emphasis upon extraction from our biosphere before use. Specifically, energy should be extracted from our lower troposphere before use, and once used it naturally returns back into our troposphere. Net-zero-effect energy is our best way forward if one wants to slow down climate change, irrelevant of its root cause.

Figures

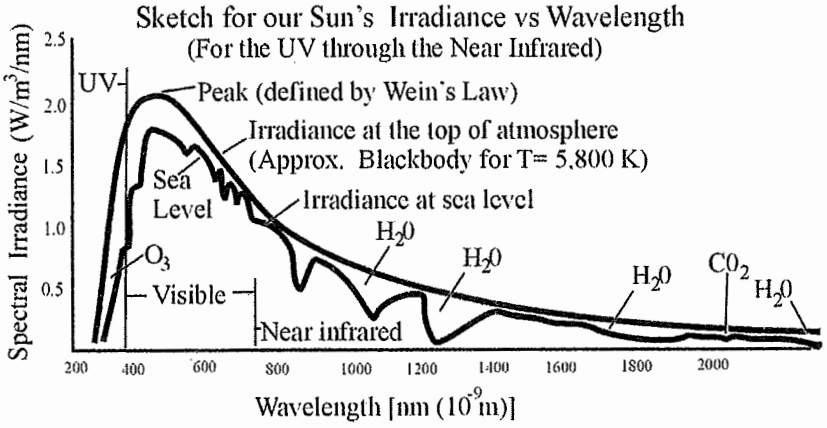

Fig. 1: Sketch of our Sun's irradiance as is traditionally depicted with the accepted absorptions of O3, H2O and CO2. Note that the absorptions are predominately based upon infrared spectrometry, that being photons interacting as EM waves with lopsided molecular charge distributions.

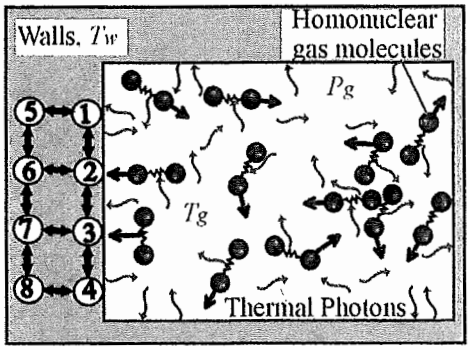

Fig. 2: Shows a homonuclear gas at temperature (Tg), intermixed with thermal photons in a fully enclosed system.

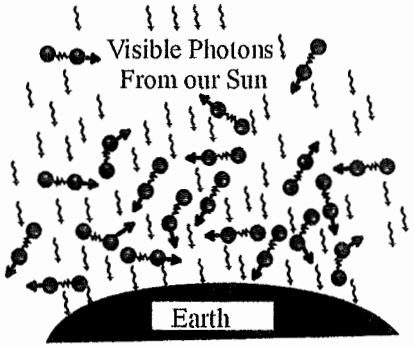

Fig. 3: Shows visible photons passing through the Earth's atmosphere and being absorbed by Earth's surface. Note that some visible photons are also reflected by Earth's surface and then pass back out through the Earth's atmosphere

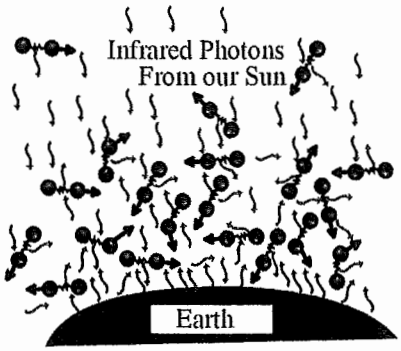

Fig. 4: Shows homonuclear gases above Earth's surface adsorbing and then radially radiating infrared (thermal) photons. Also shown are infrared (thermal) photons radiating from the Earth's surface whose momentum is absorbed by the overlying Earth's atmosphere.

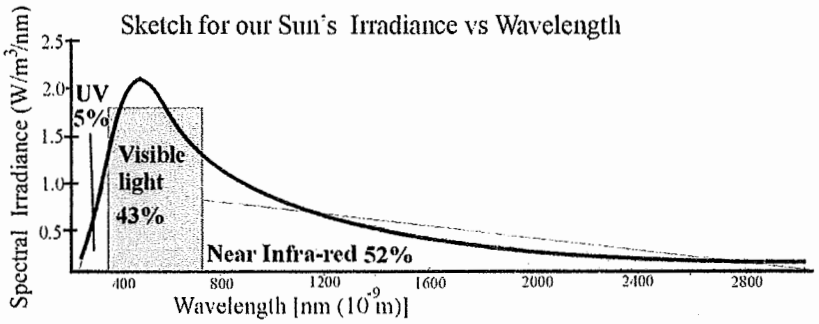

Fig. 5: Sketch of our Sun's irradiance curve, showing the traditionally accepted percentages for UV, visible and near infrared spectrum, which fails to consider the full infrared spectrum.

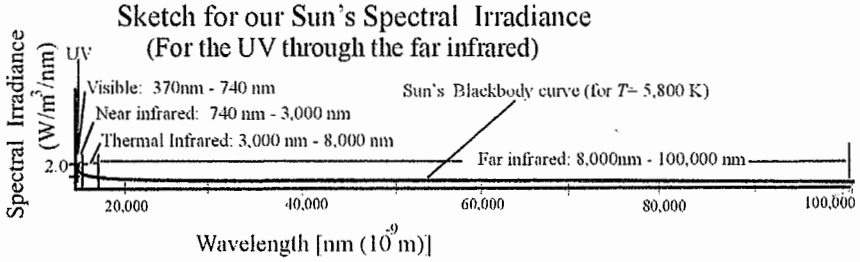

Fig. 6: Sketch of our Sun's irradiance when extended through the far infrared. Infrared being those wavelengths most often associated with heat.

Acknowledgements

I would like to thank Lloyd and Gail Mayhew for their assistance in putting this paper together.

References

[1] Cheshmezangi, Z. "The analysis of Global Warming Patterns from 1970 to 2010", Atm. and Clim. Sci Vol 10, 3, (2020)

[2] Andronova, N.G. and Schlesinger, M.E. "Causes of Temperature Changes during the 19th and 20th Centuries". Geophy. Res. Lett., 27, (2000) 2137-2140.

[3] Darkwah, W., Odum B., Addae, M., Koomson, A., Kwakye, D., Ewurabena, A., Asenso, ,Buanya, B.,"Greenhouse effect: Greenhouse gases and their Impact on Global warming" J. Sci. Res. and Rep. 17(6), (2017) pg 1-9

[4] Mitchell, John F. B. (1989). "The "Greenhouse" effect and Climate Change". Rev. of Geophy. 27 (1):115-139.

[5] Claussen, E.; Cochran, V.A.; Davis, D.P., eds. (2001). "Global Climate Data". Climate Change: Science, Strategies, & Solutions. University of Michigan

[6] Mayhew K.W, "New Thermodynamics: Untangling Entropy's Web, Includes treatise on Global Warming" (2020) https://www.amazon.ca/New-Thermodynamics-Untangling-Entropys-Treatise/dp/B087SGS55J

[7] Mayhew, K.W., "New Thermodynamics: Rethinking the Science of Climate Change", EJERS, Vol. 5, 5, (2020) pg 569-564

[8] Mayhew, K.W., "New Thermodynamics: Global Warming and Man's Activities", EJERS, Vol. 4, 7, (2019), pg 58-62

[9] Mayhew, K.W., "New Thermodynamics: Wave-Particle Duality in Radiative Heat Transfer" Hadronic Journal, Vol 44 (3), 2021

[10] Allmendinger, T. "Thermal Behaviour of Gases Under the Influence of Infrared Radiation" Int. J of Phys. Sci. Vol 11 (15) pg 183- 205 2016

[11] Allmendinger, T. "Thermal Radiation of the Atmosphere and Its Role in the So-called Greenhouse Effect" Atm. And Cli Sci. Vol 8, 2 (2018)

[12] https://www.youtube.com/watch?v=kwtt51gvaJQ , Sept., 2021

[13] https://www.youtube.com/watch?v=vFajQNg9yUY , Sept., 2021

[14]https://aliceinmethodologyland.com/2021/01/23/the-greenhouse-effect-in-a-jar-edible-modeling-activity-and-dramatization-with-young-learners/, Sept., 2021

[15]https://www.motherjones.com/environment/2016/05/ greenhouse-effect-video-prove-global-warming/ , Sept 2021

[16] https://www.youtube.com/watch?v=Ge0jhYDcazY , Sept., 2021

[17] Seim, T.O. and Olsen B.T "The influence of IR Adsorption and Backscattering Radiation from CO2 on air temperature during Heating in a simulated Earth/Atmosphere Experiment" Atm and Clim, Sci. vol 10 no 2 (2020)

[18] Seim, T.O. and Olsen B.T. "Unexpected relationships between thermal and radiative transfer" Atm. and clim. Sci. vol 10 no 4 (2020)

[19] Harries, John Edward, Brindley, H.E.,Sagoo, Pretty, Bantges Richard "Increases in greenhouse forcing inferred from the outgoing longwave radiation spectra of the Earth in 1970 and 1997" Lett to Nature vol 410 pg 355-357, 2001

[20] https://www.integrityresearchinstitute.org/climatechart.pdf
[21] Liu, Z., Huzng, S. Jin, Z, ."Breakpoint lead-lag analysis of the last deglacial climate change and atmospheric CO2 concentration on global and hemispheric scales" Quaternary International V. 490 2018 pg 50-59
[22] Dengler, J.,"Physics of the Green House Effect" http://klima-fakten.net/?page_id=1245&unapproved=345&moderation-hash=1f603c25efb89516b71ac4c7a12809 d8&lang=en#comment-345
[23] Nikolov, N., and Zeller, K., "New Insights on the Physical Nature of the Atmospheric Greenhouse Effect Deduced from an Empirical Temperature Model" Environ Pollutt Climate Change 2017 1,
[24] Volokin, Den and ReLlez, Lark, "On the average temperature of airless spherical bodies and magnitude of Earth's atmospheric thermal effect" Springer Plus 2014 3:723
[25] Holmes, R.I., "On apparent relationship between total solar irradiance and atmospheric temperature at 1 bar" Earth Sci 2019: 8, 60 346-351
[26] Mayhew, K.W., "A New Perspective for Kinetic Theory and Heat Capacity", Prog. in Phys., Vol. 13 (4) 2017 pg 166-173
[27] Mayhew, K.W. "Kinetic Theory: Flatlining of Polyatomic Gases", Prog. in Phys., Vol. 14 (2) 2018 pg 75-79
[28]https://www.epa.gov/ocean-acidification/understanding-science-ocean-and-coastal-acidification Sept., 2021
[29]https://www.nrcan.gc.ca/sites/www.nrcan.gc.ca/files/energy/Climate-change/pdf/CCCR-Chapter7-ChangesInOceansSurroundingCanada.pdf Sept., 2021
[30] Knippertz, P., Evans, M., Field, P. et al. "The possible role of local air pollution in climate change in West Africa." Nature Clim Change 5, 815–822 (2015).
[31] Bytnerowicz, A., Omasa, K., Paoletti, E., "Integrated effects of air pollution and climate change on forests: A Northern Hemisphere Perspective" Envir. Poll. 147 (2007) Pg 438-445
[32] Mayhew, K.W., "New Thermodynamics: Questioning Temperature in Open Systems, e.g., in Atmospheric Physics" Hadronic journal 44, 431-444 (2021)
[33] Mayhew, K.W., "New Thermodynamics: Inelastic Collisions, Lost Work, And Gaseous Inefficiency", Hadronic Journal, 44, (1) 67-97 (2021)
[34] Mayhew, K.W., "New thermodynamics: Illusions of Elastic Collisions in the Sciences", EJERS, Vol. 5, 1, (2020), pg 87-9
[35] Mayhew, K.W. "New Thermodynamics: The Second Law Buried by Illusions" Hadronic Journal 45, 97-116 (2022)
[36] https://www.encyclopedie-environnement.org/en/climate/ average-temperature-earth/ Aug. 2022
[37] https://www.bbc.co.uk/programmes/p02jsdrk Aug. 2022
[38]https://earthobservatory.nasa.gov/features/EnergyBalance#:~:text=The%20Earth's%20climate%20is%20a,joule%20of%20energy%20every%20second).
[39]https://iopscience.iop.org/article/10.1088/1748-9326/aae018/meta
[40] Burkhardt, U., Karcher, B., "Global radiative forcing from contrail cirrus" Nature Clim Change 1 54-58 (2011)
[41] Mayhew, K.W., "Second law and lost work", Phys. Essays **28**, vol 1,152 (2015)

[42] Mayhew, K.W., "New Thermodynamics: Inefficiency of a Piston-Cylinder", EJERS Vol 5, 2, (2020) pg 187-191
[43] Mayhew, K.W., "Resolving Problematic Thermodynamics", Hadronic Journal, vol 41, 3, (2018) pg 259-272
[44] Mayhew, K.W., "New Thermodynamics: Reversibility and Free Energy", Hadronic Journal, Vol 43, 1, 2020 pg. 51-60
[45] Xu, Y., Ramanathan, V. and Victor, D.G. "Global Warming will Happen Faster than We Think", Nature, 564, (2018) pg 30-32.
[46] Jeanson A.L, et.al. "Twenty actions for a "good Anthropocene"-perspectives from early-career conservation professionals". Env. Rev. Vol 28,1, (2020) pg 99-108
[47] Cooke, S. J. et al, "On "success" in applied environmental research – what is it, how can it be achieved, and how does one know when it has been achieved" . Env. Rev. Vol 28,4, (2020) pg 357-372
[48] Sheehan, D., Welsh, T.M. "Epicatalytic thermal diode: Harvesting ambient thermal energy", Sustainable Energy Technologies and Assessments 31 (2019) 355-368
[49] Sheehan, D., "Maxwell Zombies: Conjuring the Thermodynamic Undead" Am. Sci. 106 (2018) pg 234-241
[50] https://en.wikipedia.org/wiki/Hyperloop Nov., 25, 2020

HADRONIC JOURNAL 45, 423 - 430 (2022)
DOI 10.29083/HJ.45.04.2022/SC423

ON THE INDUCTION OF A LOW-ENERGY NUCLEAR REACTION IN A SUPERSONIC PLASMA VORTEX

Igor Bayak
Belarus, 230025, Grodno Av.
Kosmonavtov 4V 45
bayak@tut.by

Received November 4, 2022

Abstract

The device of a vortex plasma thruster is proposed, in which the collective accelerator mechanism of nuclear fusion reaction is used. It is shown that in the approximation of three nuclei, the threshold value of the potential energy spent on overcoming the Coulomb barrier is several orders of magnitude less than the threshold value of the kinetic energy of paired collisions of nuclei. This paper also presents a generator of electrical energy and a generator of artificial ball lightning, which use the phenomenon of induction of cold fusion in a supersonic plasma vortex.

Copyright © 2022 by Hadronic Press, Inc., Palm Harbor, FL 34684, USA

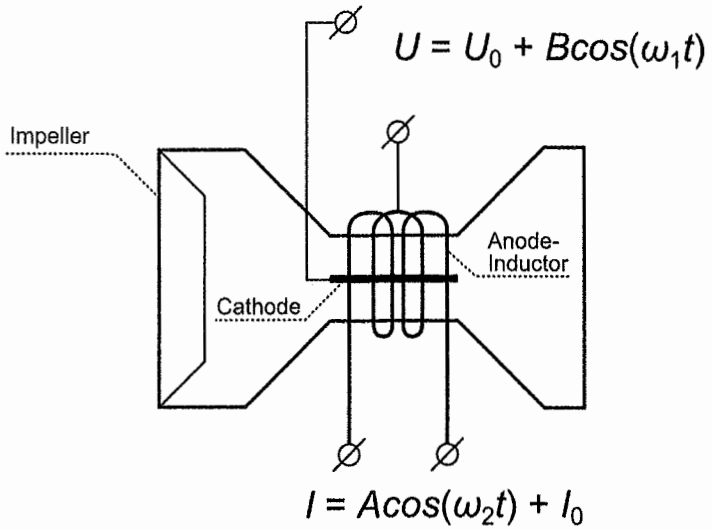

Figure 1: Schematic diagram of a vortex plasma thruster

The proposed device for discussion relates to the physics of plasma thrusters [1]. At the same time, it differs significantly from cylindrical Hall thrusters [2] and from wall-less Hall thrusters [3], but at the same time it has similarities with them. The main element of a vortex plasma thruster is a conical funnel, in which a gas vortex is formed with the help of an impeller, flying at supersonic speed into a cylindrical chamber of a high-frequency inductor, where it turns into a rotating plasma cylinder with a double electric layer structure.In alternating-constant crossed fields (radial electric and axial magnetic), the plasma rotates as a whole under the action of these fields, and the diameter of the double electric layer of the cylindrical plasma shell is compressed with the frequency of oscillations of the electric field ω_1. In addition, in the alternating radial electric field of the coaxial electrodes of the cylinder, an alternating radial plasma current arises, inducing an alternating azimuthal own magnetic field of the plasma, under the action of which (by virtue of Ampere's law) the plasma together with its double electric layer oscillates with a frequency of ω_1 in the axial direction. At the same time, ion-sound waves are spontaneously formed in the plasma cylinder of the double electric layer due to the nonequilibrium of

the plasma caused by its rotation, and when the oscillation frequency of the variable part of the electric field coincides with the oscillation frequency of one of the modes of the standing ion-sound wave, the oscillation amplitude of the ion density of the wave resonantly increases. In addition, the shock wave created by the supersonic plasma flow compresses the plasma cylinder with a ring of shock density of the double electric layer passing through it. It is also expected that the collective-accelerator mechanism of extremely compressed plasma oscillations will create conditions for launching a cold nuclear fusion reaction. In this case, at the outlet of the funnel, we will get not only a faster, but also a hotter gas vortex, which can be returned to the input of the impeller (turbine) with the help of a pipe branch, turning the jet engine into a motor-generator of thermal and electrical energy. In turn, if we remove the exhaust funnel in our scheme, tightly closing the chamber to the right of the solenoid, then instead of a jet engine, we will get a device (figure 2) that generates an artificial tornado and ball lightning. Note, at the same time, that between the incoming and outgoing flows there is a ball lightning, which is a double electric layer of plasma rotating and oscillating in the cylindrical part of the vessel, and low-energy nuclear reactions are excited on its surface.

Let us now supplement our verbal description with the necessary formulas. Similar to how it is done when deriving a barometric formula [4], from the force balance equation, we obtain the formula for the dependence of the pressure P of the main (background) flow of a rotating plasma on the distance r to the cylinder axis

$$P = P_0 \exp\left(\frac{-MU^2}{RTB^2r^2}\right)$$

where P_0 is the pressure on the chamber wall, U is the voltage between the anode and the cathode, M is the molar mass, B is the magnetic field induction, T is the plasma temperature, R is the universal gas constant, and $P_0 = \rho\frac{\omega^2 r_0^2}{2}$, where ρ is the density of the gas medium, ω is the angular velocity of rotation of the plasma, and r_0 is the radius of the cylindrical chamber. At the same time, the pressure of the external electric field gradient $\nabla E \approx \frac{U}{r^2}$ on the double electric layer of the cylindrical plasma shell

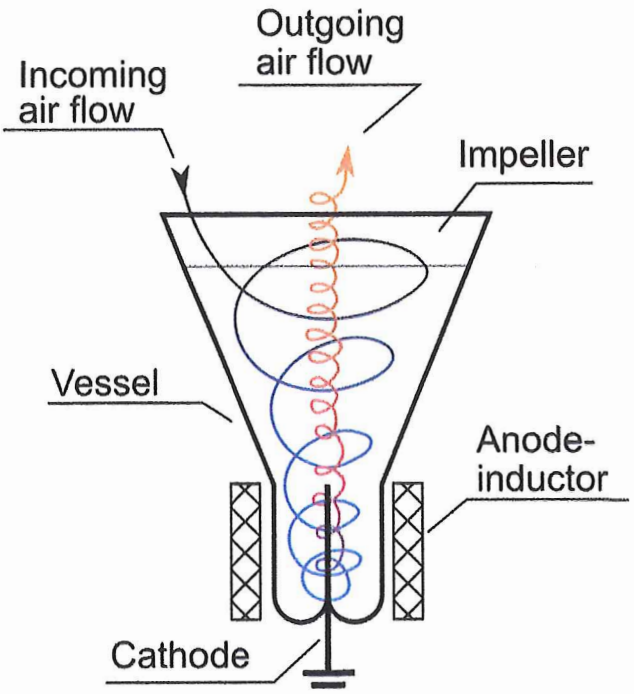

Figure 2: Schematic diagram of the ball lightning generator

having radius r, initial concentration n_0 and width D is equal to

$$P' = \frac{r_0 n_0 U D^2}{r^3}$$

On the other hand, the pressure of the centrifugal force on the double layer of the cylindrical plasma shell rotating with the tangential velocity v_τ, which consists of the drift velocity $\frac{U}{rB}$ and the velocity of the aerodynamic twisting of the gas, is equal to

$$P'' = \frac{n_0 r_0 M v_\tau^2 D}{r^2}$$

In turn, the radius of the double layer of the plasma flow can be calculated from the equality $P' = P''$

$$r = \frac{UD}{Mv_\tau^2}$$

and the compression ratio of the cylindrical shell of the double plasma layer

$$\frac{r_0}{r} = \frac{r_0 M v_\tau^2}{UD}$$

Thus, the density and concentration of the cylinder of the double electric layer having a radius of r significantly exceeds the density and concentration of the main (background) plasma at a distance of r from the axis of the cylindrical chamber, and therefore the greatest density of the probability of nuclear fusion is localized in the cylindrical shell of the double plasma layer. In other words, a thin dense shell of a double layer of plasma rotates in a rarefied region of the plasma, and the overcoming of the Coulomb barrier of nuclear fusion reactions occurs mainly due to the collective interaction of nuclei assembled together in the ring of the double layer, and not due to paired collisions, as is the case in high-temperature plasma. Indeed, let the average distance between pairs of neighboring nuclei having a charge q and imaginatively connected in a chain along a circle of radius r be s. Then, in the approximation of three nuclei, the radial force pushing each nucleus of the chain outside the circle by two neighboring nuclei is equal to

$$F_r \approx 2\frac{q^2}{s^2} \cdot \frac{s}{r} = \frac{2q^2}{sr}$$

and the tangential force acting on a nucleus that, relative to neighboring nuclei, has a deviation from the average value of Δs, that is, shifted by a distance of Δs, is equal to

$$F_\tau \approx \frac{q^2}{(s+\Delta s)^2} - \frac{q^2}{(s-\Delta s)^2} \approx \frac{4q^2 \Delta s}{s^3}$$

Imaginary chains of nuclei lie on the positively charged surface of the double layer (or rather, they move chaotically in the thickness of this surface), which is why density waves will propagate along the ring of the double layer, and in

the case of resonance with the frequency of forced oscillations of the external electric field, there should be a significant increase in the amplitude of the displacement Δs, and consequently a significant decrease in the distance of convergence of the nucleus $s - \Delta s$, which is responsible for overcoming the Coulomb barrier in nuclear synthesis reactions. Finally, we calculate, in the approximation of three nuclei, the threshold value of the potential energy that must be expended to overcome the Coulomb barrier by the average nucleus, equal to $b = s - \Delta s$

$$U = \frac{2q^2(s-b)^2}{s^3}$$

Then, since the concentration of ions n of the double plasma layer and the average distance between the ions s are related by the formula $n = \frac{1}{s^3}$, we finally have

$$U = 2nq^2(n^{-\frac{1}{3}} - b)^2$$

and, for example, at $b = 10^{-13}\,cm$, $n = 10^{18}\,cm^{-3}$, we get a threshold value of the proton potential energy $U \approx 0.3\,eV$, which is several orders of magnitude less than the threshold value of the kinetic energy of paired collisions approximately equal to $1\,MeV$.

In conclusion, we recognize that our theoretical conclusions require more detailed mathematical modeling and experimental verification. Moreover, if the purpose of the experiment is to study the dependence of the dynamic properties of the plasma vortex on the pressure in the vessel, then the schematic diagram of the installation can also be changed (Figure 3). On the other hand, it should be recognized that the presented mathematical calculations are quite sufficient to initiate R & D. We also draw your attention to the fact that the analysis of the operation of the vortex plasma engine device is based on classical physical concepts, but taking into account a new view of the mechanism of collective interaction of nuclei in the reaction of the so-called cold nuclear fusion.

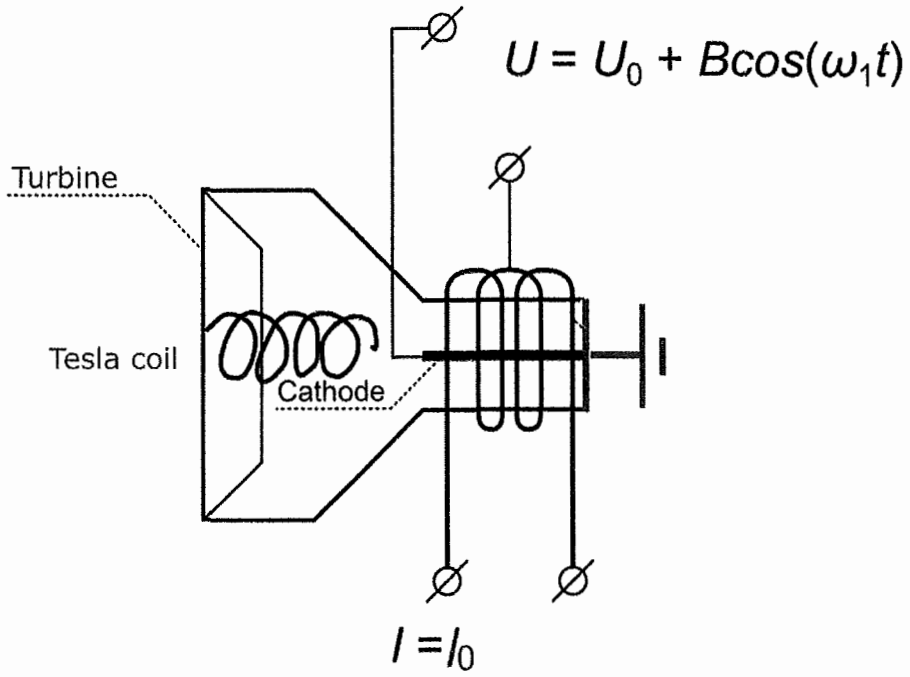

Figure 3: Schematic diagram of a plasma vortex generator initiated in a closed vessel using a Tesla coil

Declarations

Data availability

Data sharing not applicable to this article as no datasets were generated or analysed during the current study.

Funding and/or Conflicts of interests/Competing interests

No funds, grants, or other support was received. The author have no relevant financial or non-financial interests to disclose.

References

[1] Dan M. Goebel, Ira Katz. Fundamentals of Electric Propulsion: Ion and Hall Thrusters. John Wiley & Sons (2008)

[2] Artem Smirnov, Yegeny Raitses, and Nathaniel J. Fisch. Experimental and theoretical studies of cylindrical Hall thrusters. Physics of Plasmas 14, 057106 (2007)

[3] Jacob Simmonds, Yevgeny Raitses. Ion acceleration in a wall-less Hall thruster. Journal of Applied Physics 130, 093302 (2021)

[4] Berberan-Santos, Bodunov, and Pogliani. On the barometric formula. Am. J. Phys., Vol. 65, No. 5, May 1997

HADRONIC JOURNAL 45, 431 - 441 (2022)
DOI 10.29083/HJ.45.04.2022/SC431

ANALYSIS OF THE ORIGIN, STRUCTURE AND PROPAGATION OF TRANSVERSE ELECTROMAGNETIC WAVES USING BIPOLARS

Farzad Haghmoradi-Kermanshahi
Electrical Engineering Department
Faculty of Engineering, Razi University
Kermanshah 67149, Iran
f.haghmoradi@yahoo.com

Received October 18, 2022
Revised November 13, 2022

Abstract

An electromagnetic wave is a transverse wave composed of electric and magnetic fields perpendicular to each other and simultaneously to the direction in which the wave is traveling. These waves, regardless of frequency and wavelength, travel at the speed of light $c \approx 3\times10^{8} m/s$ in vacuum. This paper uses the bipolars chain to study how these waves are formed and move in space. Also using bipolars Faraday's law and Lenz's law of induction, for which no explanation has been offered until now, will be examined.

Keywords: Bipolars; Electromagnetic waves; Faraday's law; Lenz's law.

Copyright © 2022 by Hadronic Press, Inc., Palm Harbor, FL 34684, USA

1. Introduction

The universe is filled with bipolars. Being filled does not mean with a substance like ether, but it means a continuous and rigid structure which surrounds the entire universe. In other words, space has a solid, continuous and incompressible structure. According to Ref [1], since space transmits waves and forces, it is absurd to assume that it is empty, whereas it must be a solid and incompressible medium. And the fundamental reality of fields acting at a distance can only be interpreted under the assumption that space is a universal medium.

It is proposed, electromagnetic waves are composed of bipolars [2] which are connected in a chain and produce sinusoidal waves. These waves travel at the speed of light in space and are propagated in a direction perpendicular to both electric and magnetic fields. Consider an electromagnetic wave emitted in the positive direction of the x axis in a way that the resulting electric and magnetic fields oscillate along the y and z axes, respectively (Fig.1a). Then the electric and magnetic fields can be written as sinusoidal functions of position x and time t [3]:

$$E = E_m \sin(kx - \omega t) \tag{1}$$

$$B = B_m \sin(kx - \omega t) \tag{2}$$

in which E_m and B_m are the amplitude of fields and, ω and k are the angular frequency and angular wave number of the wave, respectively.

The rigidity of space has caused particles such as electrons to be characterized by the oscillation of a point of space, resulting in the propagation of electromagnetic waves in a certain condition [4].

Figure 1b shows a stationary particle with negative charge in which only one of the electric field lines generated by it is represented as a bipolars chain (The charged particle is surrounded by a large number of bipolars and here for convenience, only one string of them is shown). As the particle oscillates along y axis, the bipolars chain starts to oscillate sinusoidally and travels in the positive direction of the x axis [2] (Fig. 1c).

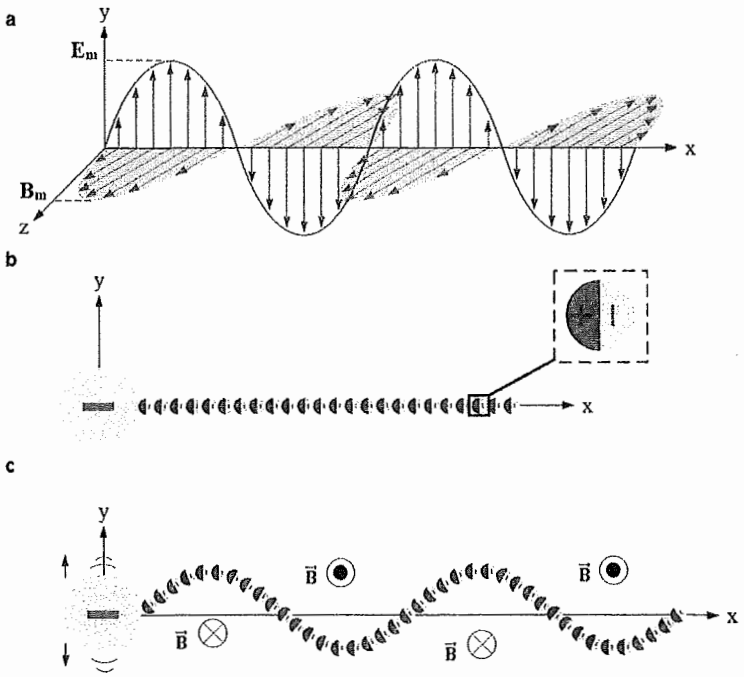

Fig.1: (a) A snapshot of the resultant electric and magnetic fields of an electromagnetic wave traveling in the positive direction of an x axis. (b) Formation of bipolars chain around a stationary particle with negative charge. (c) A snapshot of formed bipolars chain around an oscillating particle with negative charge.

2. Electromagnetic wave

Figure 2 depicts two metal plates located at a certain distance from each other and connected to an alternating voltage generator in a way that a sinusoidal electric field with amplitude E_m and angular frequency ω is produced between these plates.

Now, if a negatively charged particle is released in a space between the plates, it begins to oscillate vertically. (It is assumed that the angular frequency ω is large in a way that the oscillation amplitude of the particle becomes smaller than the distance between the two plates and accordingly, the particle strikes neither the upper nor the lower plates).

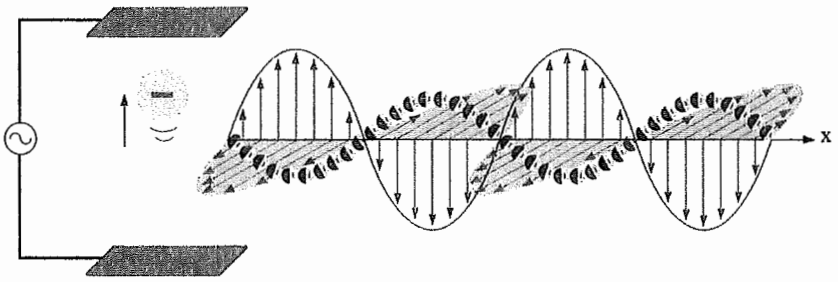

Fig.2: A negatively charged particle oscillating through an alternating electric field produced between two plates and the resultant electromagnetic wave.

Substituting Newton's second law [5] into the equation $E = F/q$ yields [6]:

$$\begin{cases} F = ma \\ F = qE \end{cases} \rightarrow a = \frac{qE}{m} \tag{3}$$

where a is the acceleration of a charged particle.

By substituting $x = 0$ into Eq. (1), the electric field related to a charged particle oscillating along the y axis will be given as

$$E(0,t) = E_m \sin(-\omega t) \tag{4}$$

The acceleration of a charged particle is obtained from Eqs. (3) and (4) as

$$a = \frac{qE_m}{m} \sin(-\omega t) \tag{5}$$

The equation of the particle oscillation is

$$y = y_m \sin(\omega t) \tag{6}$$

in which y_m is the amplitude of particle oscillation and the amplitude of the bipolars chain oscillation simultaneously.

By taking the second derivative of y with respect to time, the acceleration of the particle is obtained:

$$y' = y_m \omega \cos(\omega t) \tag{7}$$

$$y'' = a = -y_m \omega^2 \sin(\omega t) \tag{8}$$

Equating Eqs.(5) and (8) yields:

$$\left| y_m \omega^2 \right| \sin(\omega t) = \frac{|q| E_m}{m} \sin(\omega t) \rightarrow y_m = \frac{|q|}{m\omega^2} E_m \tag{9}$$

where the values of m and q for an electron equal:

$$q = e = -1.602176634\times10^{-19}\ \text{C} \tag{10}$$

$$m = m_e = 9.1093837015\times10^{-31}\ \text{kg} \tag{11}$$

According to Fig. 3a, the equation of motion of bipolars chain for a negatively charged particle is:

$$y(x,t) = -y_m \sin(kx - \omega t) \tag{12}$$

Substituting Eq. (9) into Eq. (12) gives:

$$y(x,t) = -\frac{|q|}{m\omega^2} E_m \sin(kx - \omega t) \tag{13}$$

and from Eqs. (1) and (13)

$$y(x,t) = -\frac{|q|}{m\omega^2} E(x,t) \tag{14}$$

In mathematics, the curvature [7] is defined by:

$$K = \frac{|y''(x)|}{\left[1+y'^2(x)\right]^{3/2}} \tag{15}$$

Here, it is expressed as:

$$K(x,t) = \frac{\left|\partial^2 y(x,t)/\partial x^2\right|}{\left[1+(\partial y(x,t)/\partial x)^2\right]^{3/2}} \tag{16}$$

The first and second derivatives of Eq. (13) with respect to x are

$$\frac{\partial y(x,t)}{\partial x} = -\frac{k|q|}{m\omega^2} E_m \cos(kx - \omega t) \tag{17}$$

$$\frac{\partial^2 y(x,t)}{\partial x^2} = \frac{k^2|q|}{m\omega^2} E_m \sin(kx - \omega t) \tag{18}$$

Substituting Eqs. (17) and (18) into Eq. (16) leads to

$$K(x,t)=\frac{\frac{k^2|q|}{m\omega^2}E_m\left|\sin(kx-\omega t)\right|}{\left[1+\frac{k^2|q|^2}{m^2\omega^4}E_m{}^2\cos^2(kx-\omega t)\right]^{3/2}} \tag{19}$$

Substituting $\omega/k=c$ [8] into Eq. (19) results in

$$K(x,t)=\frac{\frac{|q|}{mc^2}E_m\left|\sin(kx-\omega t)\right|}{\left[1+\frac{|q|^2}{m^2c^2\omega^2}E_m{}^2\cos^2(kx-\omega t)\right]^{3/2}} \tag{20}$$

The expression $F(x,t)$ can be defined as

$$F(x,t)=\left[1+[\frac{|q|}{mc\omega}E_m\cos(kx-\omega t)]^2\right]^{3/2} \tag{21}$$

so, Eq. (20) can be written as

$$K(x,t)=\frac{|q|}{mc^2}E_m\left|\sin(kx-\omega t)\right|/F(x,t) \tag{22}$$

The generated magnetic field is directly proportional to the degree of curvature of bipolars chain:

$$|B|\propto K \tag{23}$$

B can be related to K with

$$|B(x,t)|=A(x,t)\cdot K(x,t) \tag{24}$$

where the term $A(x,t)$ will be obtained by substituting Eqs.(2) and (22) into Eq. (24)

$$B_m\left|\sin(kx-\omega t)\right|=A(x,t)\cdot\frac{|q|}{mc^2}E_m\frac{\left|\sin(kx-\omega t)\right|}{F(x,t)}$$

$$\rightarrow A(x,t)=F(x,t)\cdot\frac{mc^2}{|q|}\cdot\frac{B_m}{E_m} \tag{25}$$

Substituting $E_m/B_m=c$ [3] into Eq. (25) gives

$$A(x,t) = F(x,t) \cdot \frac{mc}{|q|} \tag{26}$$

Figure 3b depicts a snapshot of the bipolars chain formed by an oscillating particle with positive charge as well as its corresponding electric and magnetic fields.

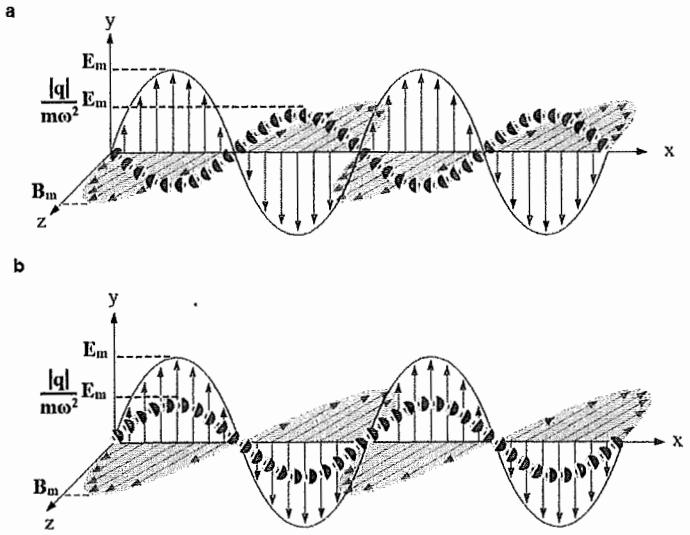

Fig.3: A snapshot of the resultant electromagnetic wave due to a sinusoidal bipolars chain produced by an oscillating particle with: (a) negative charge (b) positive charge.

3. Faraday's law and Lenz's law of induction

According to Faraday's law, a current is induced by changing the amount of magnetic field passing through a loop (Fig. 4a) and in accordance with Lenz's law, this induced current has a direction such that the magnetic field due to the current opposes the change in the magnetic flux which induces the current [9].

For instance, if the N pole of a magnet approaches a loop, the induced current take a direction which causes the loop to become an imaginary magnet in a way that its north pole will be formed against the N pole of the real magnet and prevents it from approaching (Fig. 4b).

In the same way, pulling this real magnet away from the loop (the N pole is toward the loop) creates an imaginary magnet with the S pole against the N pole of the real magnet and prevents it to move further apart (Fig. 4c).

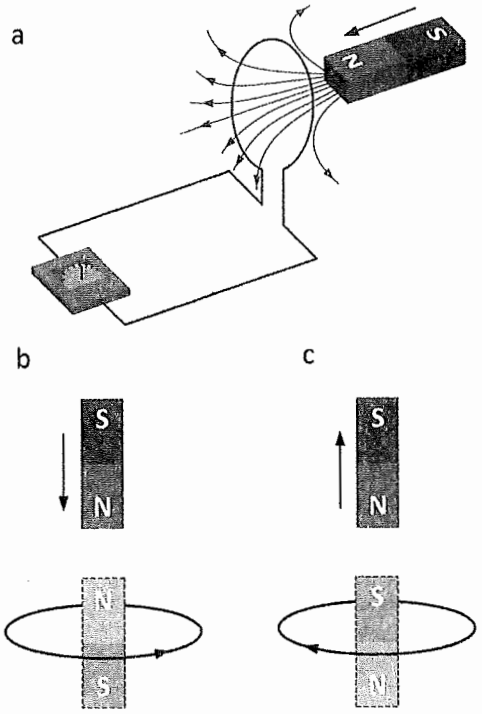

Fig.4: (a) An induced current is registered by the ammeter as a result of a relative motion between the loop and the bar magnet. (b) The movement of the N pole of a magnet toward a loop. (c) The movement of the N pole of a magnet away from a loop.

Using bipolars, Faraday' law and Lenz's law can be examined.

Figure 5a shows a magnet with facing end of N pole, moving toward a copper ring. In this case, the magnetic field passing through the ring begins to increase. This increment is due to the fact that a number of magnetic field lines generated by the magnet are dragged from the outside to the inside of the copper ring (Fig. 5b).

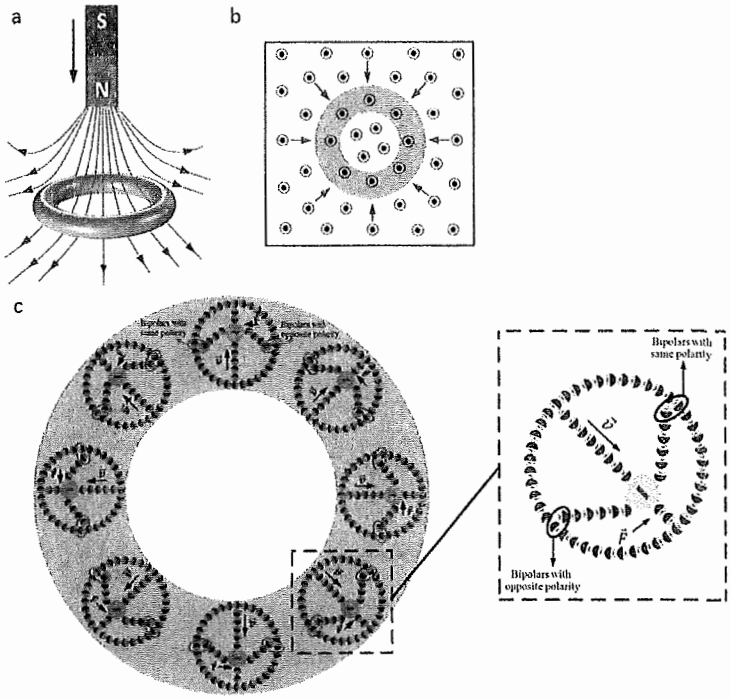

Fig.5: (a) The movement of the N pole of a magnet toward a copper ring. (b) The motion of the magnetic field lines from the outside to the inside of a copper ring. (c) The mechanism why a clockwise current is generated in a copper ring due to the motion of magnetic field lines through using bipolars.

As is known, in copper, the electric charges are carried by electrons [10]. Dragging the magnetic field lines from the outside to the inside of the copper ring is exactly the same as electrons moving from the inner diameter of the ring to the outer one in the presence of fixed field lines.

In this case, according to Ref [2], the bipolars arranged by the magnetic field with the opposite polarity as the ones oriented by electrons, exert a force on free electrons to deflect toward bipolars with the same polarity.

As depicted in Fig. 5c, all free electrons start to move counterclockwise along the copper ring. In other words, a clockwise current is induced in the ring in a way that the N pole of the resulting imaginary magnet will be located against the N pole of the real magnet, preventing it from approaching the ring.

As the real magnet moves away from the copper ring (Fig. 6a), the magnetic field lines are dragged from the inside to the outside of the ring (Fig. 6b). It is exactly the same as free electrons in the copper move from the outer diameter of the ring to the inner one in the presence of fixed field lines. In this case, free electrons flow clockwise through the ring and a counterclockwise electric current is generated (Fig. 6c). Eventually, the resulting S pole of the imaginary magnet is placed facing the retreating N pole of the real magnet and prevents it from moving away from the ring.

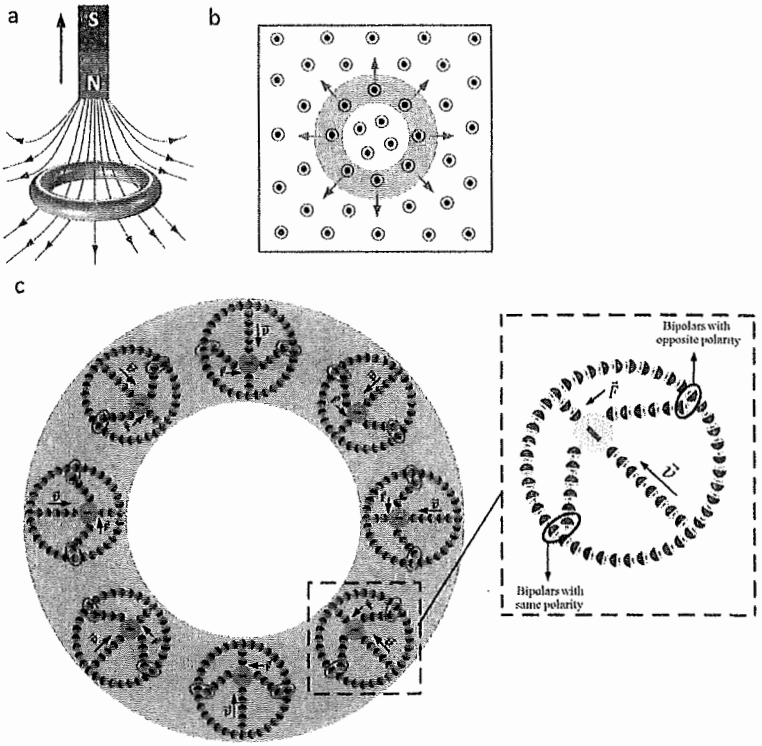

Fig.6: (a) The movement of the N pole of a magnet away from a copper ring. (b) The motion of the magnetic field lines from the inside to the outside of a copper ring. (c) The mechanism why a counterclockwise current is generated in a copper ring due to the motion of magnetic field lines through using bipolars.

4. Conclusion

The formation and propagation of electromagnetic waves have been presented through using bipolars. Also, the substantiation of Faraday's law and Lenz's law of induction, which has remained inherently unknown up to know, were plausibly demonstrated. In future, phenomena such as the double-slit experiment and the wave-particle duality of electrons can be scrutinized by bipolars.

References

[1] R. M. Santilli, *"Perche' lo spazio e' rigido" ("Why space is rigid")*, IL Pungolo Verde, Campobasso, Italy (1956)

[2] Haghmoradi-Kermanshahi, F.,The basic theory of bipolars existence and their role in the examination of electric and magnetic fields. *Physics Essays*, Volume 34, Number 3, September 2021, pp. 315-321(7).

[3] Halliday, D., Resnick, R. & Walker, J. *Fundamentals of Physics*. 10th ed, **2,** Ch.33, pp 975-979 (John Wiley & Sons Inc, New York, 2014).

[4] Review of Sir R. M. Santilli studies on the aether in I. Gandzha and J. Kadeisvili, *New Sciences for a New Era:Mathematical, Physical and Chemical Discoveries of Ruggero Maria Santilli,* Sankata Printing Press, Nepal (2011)

[5] Yong, H. D., Freedman, R. A. & Ford, A. L. *Sears and Zemansky's University Physics: With Modern Physics.* 13th ed, **1,** Ch.4, 115 (Pearson Education Inc, Addison-Wesley, San Francisco, 2012).

[6] Halliday, D., Resnick, R. & Walker, J. *Fundamentals of Physics*. 10th ed, **2,** Ch.22, pp 630-632 (John Wiley & Sons Inc, New York, 2014).

[7] George B. Thomas Jr., Maurice D. Weir, Joel R. Hass, *Thomas' Calculus Early Transcendentals.*13th ed, Ch.13, pp 772-778 (Pearson Education Inc, Boston, 2014).

[8] Yong, H. D., Freedman, R. A. & Ford, A. L. *Sears and Zemansky's University Physics: With Modern Physics.* 13th ed, **1,** Ch.15, 479 (Pearson Education Inc, Addison-Wesley, San Francisco, 2012).

[9] Halliday, D., Resnick, R. & Walker, J. *Fundamentals of Physics*. 10th ed, **2,** Ch.30, pp 864-871 (John Wiley & Sons Inc, New York, 2014).

[10] Fischer-Cripps, A. C. *The Electronics Companion.* Ch. 1, 13 (CRC Press, London, 2004).

HADRONIC JOURNAL 45, 443 - 453 (2022)
DOI 10.29083/HJ.45.04.2022/SC443

PROBING THE ELECTROMAGNETIC STRUCTURE OF NUCLEONS

M Y Hussein
Department of Physics
University of Bahrain
P.O. Box 32038
Kingdom of Bahrain
And
Search Center, Shaikh Ebrahim Bin Mohammed Al Khalifa
Center for Culture and Research
P.O. Box 13725
Muharraq, Kingdom of Bahrain

Received July 13, 2022

Abstract

We present an improved study of the nucleon charge structure by studying its electromagnetic form factors and charge radii, based upon the relativistic view of Lorentz contraction idea for the nucleon and in association with the momentum distribution of the quarks in the nucleon within the framework of quark-parton model. The mean square charge radii of nucleons were also investigated. The behavior of the electromagnetic chare form factors is predicted.

Copyright © 2022 by Hadronic Press, Inc., Palm Harbor, FL 34684, USA

1. Introduction

The understanding of nucleon structure is one of the central problems of hadronic physics [1]. The complex structure of hadrons can be described by a convenient way in terms of form factors. The electromagnetic form factors of the proton and neutron are considering as fundamental properties of the nucleon, and gave a critical test ground for models based on Quantum Chromodynamics (QCD). A detailed knowledge of these form factors is essential to our understanding of the electromagnetic response functions of nuclei. Measurements of the electric and magnetic form factors, F_E and F_G, as function of the four-momentum transfer q^2provide experimental information relating to the nucleon structure.

The (elastic or inelastic) electron-hadron scattering is the traditional way to determine the form factors, and it allows a direct comparison with the theory. The experimental determination of the proton form factor has been carried out by directing high energy electron beams at a hydrogen target, and making precision measurements of the momentum and angle of scattered electrons by means of magnetic spectrometers. The first experiments demonstrating the deviation of the scattering from the expected for point particles and thus measuring the form factors were carried out by Hofstadter and his calibrators in 1961, at Stanford, and have since been extended in numerous laboratories [1]. Recent measurements at the Jefferson Laboratory essentially improved the experimental data concerning the elastic form factors of protons and deuterons up to relatively large values of momentum transfer [2,3,4]. A large body of precise data obtained primarily from elastic scattering of electrons by protons and deuterons now exists for these form factors. Recent data for large space-like momentum transfer are in remarkable agreement with the prediction for q^2 as small as $5(GeV)^2$ [5]. The study of the internal structure of light hadrons can be carried on with a high intensity electron machine and a large program is under way to measure the form factors of the nucleon resonance [6,7,8]

Nucleon's charge structure has been a subject of extensive investigation for the past years [9]. There have been numerous attempts aiming at a plausible explanation of the charge structure and form factor using a

variety of techniques including, for instance, the empirical charge distributions [10] on one hand and the quark-parton models on the other [11], which besides being the easiest to understand has had tremendous success to its credit.

2. Electromagnetic Structure of Nucleons Within QPM

The present investigation is an attempt to understand and account the electricmagnetic form factors for the proton and neutron within the general prescriptions of quark-parton model (QPM). Our consideration is based on the hypothesis that the proton has a disc-like appearance due to the influence of Lorentz contraction when the energy of the incident beams is in the high-energy region. In view of this geometrical picture with finite but small disc thickness, it is essential to consider not only the transverse distribution functions, h_i (x,b), but also a longitudinal spatial distribution, g_i (y,z), with a suitable cut off $z_0 = 0.017\,fm$.

In the QPM, the nucleon can be described by the mean number densities of quarks, $f_i(x), f_i(y)$

$$f_i(x) = \int h_i(x,b)db \qquad (1)$$

$$f_i(y) = \int g_i(y,z)dz \qquad (2)$$

Where x is the fractional longitudinal momentum, y is the fractional transverse momentum, and according to the conservation of momentum $x^2 + y^2 = 1$.

The disc's plane is described by the transverse coordinate b, and the longitudinal, z. The corresponding distribution functions of partons in the

transverse and longitudinal coordinates and momentum are: $h_i(x,b)$, $g_i(y,z)$, respectively, given as

$$h_i(x,b) = \left(\pi A(x)\right)^{-1} f_i(x) e^{\frac{-b^2}{A(x)}} \tag{3}$$

$$g_i(y,z) = \left(z_0\left(1 - \frac{z_0^2}{3B(y)}\right)\right)^{-1} f_i(y)\left(1 - \frac{z^2}{B(y)}\right) \tag{4}$$

where A(x) and B(y) are decreasing functions: $A(x) = e^{-\beta x}, B(y) = e^{-\beta y}$, and z_0 is the thickness of the disc (the cut-off in the longitudinal direction, z). hence, the mean square charge radius is given by

$$\langle r^2 \rangle = \int dx\, dy\, \delta(x^2 + y^2 - 1) \sum_i e_i \int d^3 r \rho_i(x, b\,; y, z) r^2 \tag{5}$$

e_i represents the charge of the quark of flavor u, d, or s. $d^3 r = d^2 b dz, r^2 = z^2 + b^2$, and ρ_i is the total distribution function for the longitudinal and transverse momentum,

$$\rho_i(x, b\,; y, z) = h_i(x, b) g_i(y, z) \tag{6}$$

using the definition in (6) and substituting (3) and (4) into (5),

$$\langle r^2 \rangle = \int dx \int dy\, \delta(x^2 + y^2 - 1) \sum_i e_i \int \int d^2 b dz (z^2 + b^2)$$

$$\left(\pi A(x)\right)^{-1} f_i(x) e^{\frac{-b^2}{A(x)}} \left(z_0\left(1 - \frac{z_0^2}{3B(y)}\right)\right)^{-1} f_i(y)\left(1 - \frac{z^2}{B(y)}\right) \tag{7}$$

evaluating the integral (7) over *dz* with limits [0, z_0= 0.017 fm] gives

$$\langle r^2\rangle = \int dx \int dy\ \delta(x^2+y^2 - 1)(\pi A(x))^{-1}\left(z_0\left(1-\frac{z_0^2}{3B(y)}\right)\right)^{-1}$$
$$\sum_i e_i f_i(x) f_i(y) \int d^2b\, d\, e^{\frac{-b^2}{A(x)}}\left(b^2 z_0 - \frac{z_0^2 b^2}{3B(y)} + \frac{z_0^3}{3} - \frac{z_0^5}{5B(y)}\right) \tag{8}$$

integrating over d^2b, where $d^2b=b\ db$

$$\int_0^{2\pi}\int_0^{\infty} e^{\frac{-b^2}{A(x)}}\left(b^2 z_0 - \frac{z_0^2 b^2}{3B(y)} + \frac{z_0^3}{3} - \frac{z_0^5}{5B(y)}\right) b\,db$$
$$= \pi A(x)\left[A(x) z_0 - \frac{z_0^2 A(x)}{3B(y)} + \frac{z_0^3}{3} - \frac{z_0^5}{5B(y)}\right] \tag{9}$$

then substitute the result in (8),

$$\langle r^2\rangle = \int dx \int dy\ \delta(x^2+y^2-1)\left(\frac{3B(y)}{z_0(3B(y)-z_0^2)}\right)$$
$$\sum_i e_i f_i(x) f_i(y)\left[A(x) z_0 - \frac{z_0^2 A(x)}{3B(y)} + \frac{z_0^3}{3} - \frac{z_0^5}{5B(y)}\right] \tag{10}$$

after simplifying, $\langle r^2\rangle$ becomes

$$\langle r^2\rangle = \int dx \int dy\ \delta(x^2+y^2-1)\sum_i e_i f_i(x) f_i(y)\left[A(x) + \frac{5z_0^2 B(y) - 3z_0^4}{5(3B(y)-z_0^2)}\right] \tag{11}$$

then integrating over dy, using the two properties of Dirac delta function

$$\delta(\varepsilon^2 - a^2) = \frac{1}{2a}(\delta(\varepsilon - a) + \delta(\epsilon + a)) \tag{12}$$

$$\int f(\varepsilon)\,\delta(\varepsilon)\,d\varepsilon = f(\varepsilon) \tag{13}$$

implies

$$\int dy\ \delta(x^2 + y^2 - 1) f(y) = \frac{f(\sqrt{1-x^2})}{2\sqrt{1-x^2}} \tag{14}$$

such that $y = \sqrt{1-x^2}$, finally, the mean-square charge radius takes the form

$$\langle r_p^2 \rangle = \int_0^1 dx \left[A(x) + \frac{5z_0^2 B(\sqrt{1-x^2}) - 3z_0^4}{5(3B(\sqrt{1-x^2}) - z_0^2)} \right] \frac{Q_p(x)}{2\sqrt{1-x^2}} \tag{15}$$

$$\langle r_n^2 \rangle = \int_0^1 dx \left[A(x) + \frac{5z_0^2 B(\sqrt{1-x^2}) - 3z_0^4}{5(3B(\sqrt{1-x^2}) - z_0^2)} \right] \frac{Q_n(x)}{2\sqrt{1-x^2}} \tag{16}$$

where N refers to the nucleon type (proton p, or neutron n), $Q_N(x) = \sum_i e_i\, f_i(x) f_i(\sqrt{1-x^2})$ is the total quark density function, given as:

$$Q_p(x) = \frac{2}{3} u_v(x) u_v\left(\sqrt{1-x^2}\right) - \frac{1}{3} d_v(x) d_v\left(\sqrt{1-x^2}\right)$$

$$Q_n(x) = \frac{2}{3} d_v(x) d_v(\sqrt{1-x^2}) - \frac{1}{3} u_v(x) u_v(\sqrt{1-x^2}) \tag{17}$$

The electromagnetic charge form factor for the nucleon can be extracted from taking the Fourier transform of the QPDF (6) as was mentioned previously, recalling the definition of form factor with changing variables:

$$F_i(q, x, y) = \int d^3 r \rho_i(x, b\,; y, z) e^{iq \cdot r} \tag{18}$$

$$= \int\int d^2b\, dz\, h_i(x,b) g_i(y,z) e^{iq\cdot r}$$

$$= \int dz\, g_i(y,z) e^{iqzx} \int d^2b\, h_i(x,b) e^{iqby}$$

$$= G_i(q,x,y) H_i(q,x,y)$$

The charge form factor is

$$F(q) = \int dx \int dy\ \delta(x^2+y^2-1) \sum_i e_i F_i(q,x,y) \tag{19}$$

evaluating $G_i(q,x,y)$ and $H_i(q,x,y)$ using (3) and (4):

$$G_i(q,x,y) = \int_0^{z_0} \left(z_0 \left(1 - \frac{z_0^2}{3B(y)} \right) \right)^{-1} f_i(y) \left(1 - \frac{z^2}{B(y)} \right) e^{iqzx} dz$$

$$= \left(z_0 \left(1 - \frac{z_0^2}{3B(y)} \right) \right)^{-1} f_i(y) e^{i\frac{qxz_0}{2}} (P + iS)$$

$$= \left(z_0 \left(1 - \frac{z_0^2}{3B(y)} \right) \right)^{-1} f_i(y) (P^2 + S^2)^{1/2} \tag{20}$$

P and S are shorthand for

$$P = \left[\frac{-z_0^2}{qxB(y)} + \frac{2}{qx} + \frac{4}{q^3x^3B(y)} \right] \sin\frac{qxz_0}{2} - \frac{2z_0}{q^2x^2B(y)} \cos\frac{qxz_0}{2} \tag{21}$$

$$S = \frac{-2z_0}{q^2x^2B(y)} \sin\frac{qxz_0}{2} + \frac{z_0^2}{qxB(y)} \cos\frac{qxz_0}{2} \tag{22}$$

$$H_i(q,x,y) = \int_0^{2\pi} \int_0^{\infty} \left(\pi A(x) \right)^{-1} f_i(x) e^{-b^2/A(x)} e^{iqby}\, b db d\varphi$$

$$= f_i(x) e^{-q^2y^2A(x)/4} \tag{23}$$

Thus,

$$F_n(q) = \int dx \int dy\ \delta(x^2+y^2-1)\left(z_0\left(1-\frac{z_0^2}{3B(y)}\right)\right)^{-1}$$

$$(P^2+S^2)^{1/2}e^{-q^2y^2A(x)/4}\sum_i e_i f_i(x)f_i(y)$$

$$= \int_0^1 \left(\frac{3B\left(\sqrt{1-x^2}\right)}{z_0\left(3B\left(\sqrt{1-x^2}\right)-z_0^2\right)}\right)(P^2$$

$$+S^2)^{1/2}e^{-\frac{1}{4}q^2(1-x^2)A(x)}\frac{Q_n(x)}{2\sqrt{1-x^2}} \qquad (24)$$

$$F_p(q) = \int dx \int dy\ \delta(x^2+y^2-1)\left(z_0\left(1-\frac{z_0^2}{3B(y)}\right)\right)^{-1}$$

$$(P^2+S^2)^{1/2}e^{-q^2y^2A(x)/4}\sum_i e_i f_i(x)f_i(y)$$

$$= \int_0^1 \left(\frac{3B\left(\sqrt{1-x^2}\right)}{z_0\left(3B\left(\sqrt{1-x^2}\right)-z_0^2\right)}\right)(P^2+S^2)^{1/2}e^{-\frac{1}{4}q^2(1-x^2)A(x)}\frac{Q_p(x)}{2\sqrt{1-x^2}}$$

(25)

3. Results

By choosing an appropriate value for β we can reproduce the current signs and values for both $\langle r_n^2\rangle$ and $\langle r_p^2\rangle$ as shown in Tables (1). In our calculations, we use the structure functions from MRST [12]

TABLE 1 Results reproduce the current signs and values for both $\langle r_n^2\rangle$ and $\langle r_p^2\rangle$

A) With $\langle r_p^2\rangle$ fixed at 0.707 fm²

Parton Distribution	β	$\langle r_n^2 \rangle$ in fm^2
MRS T	14.15	-0.378
CTEQ	9.13	-0.376

B) Independent $\langle r_p^2 \rangle$

Parton Distribution	β	$\langle r_n^2 \rangle$ in fm^2
MRST	12.72	-0.120
CTEQ	7.70	-0.120

Because u_v is significantly larger than d_v in x-space, and considering equation (10), the calculation of $\langle r^2 \rangle$ is dominated by u_v such that equation (10) can be well approximated by

$$L_p(x) \cong \frac{2}{3} u_v(x) u_v(y) \tag{11a}$$

$$L_n(x) \cong -\frac{1}{3} u_v(x) u_v(y) \tag{11b}$$

This clearly shows that

$\langle r_p^2 \rangle$)0, while $\langle r_n^2 \rangle$ ⟨0

In fact, for the same β one obtains a factor of -0.15 for the ratio in equation (5). Thus even with the arbitrariness of choosing β the signs of $\langle r^2 \rangle$ are well understood in this treatment which suggest that the u-quark is the dominating factor in the nucleon charge distribution.

The uncertainty associated with the choice of parton distribution function do not affect our conclusions as we have used different sets and obtained similar results. In fact usually a limited shift in β is all it took to reproduce the same results with a different set of parton distribution functions.

Calculations are also performed for the proton and the neutron form factors as function of q^2 are shown in table and table. From these results, it is immediately yield the results are in remarkable agreement with both the theoretical equation and the experimental measurements available. Calculations are performed for the proton form factors as a function of the momentum transfer q^2. In our calculations, we use the structure functions from MRST [12]

TABLE 2 Proton charge form factor $Gp(q^2)$, theoretical results at fixed β (=-7.3415).

q^2 $(GeV)^2$	$G_{Theory}(q^2)$	$G(q^2)=(1+q^2/0.71)^{-2}$	Experiment
1	0. 1264	0.1723	0.180
2	0. 0592	0.0686	0.068
3	0.0544	0.0366	-
4	0.0317	0.0227	0.02
5	0.0315	0.0155	-
6	0.0365	0.0112	-
7	0.0417	0.0084	-
8	0.0307	0.0066	-

TABLE 3 Neutron charge form factor

q^2 $(GeV)^2$	$G_{Theory}(q^2)$	$G(q^2)=-\frac{a\mu_n\tau}{1+b\tau}\left(1+\frac{q^2}{0.71}\right)^{-2}$
1	0.03236	0.038
2	0.01606	0.021
3	0.01463	0.013
4	0.0096	0.009

4. **Conclusion**

We have used a simple model of the nucleon in connection with the quark-parton model and the current information on parton distributions to re-establish both the value and the sign of the nucleon charge radii. It seems that the up quark is dominating the calculations of the root mean square charge radii. Equations (15) and

(16) shows clearly why positive sign appear in mean square charge radius for the proton and why negative sign appear for the neutron. The major uncertainty in this work is the fact that the parton distributions. We note that the calculations are found to be ideally suited in accounting for the observed data on the charge form factors

References

1). Yu. A. Alexandrov, Neutron News 5, 20 (1994); Phys. Rev. C49, 2297 (1994).
R. Pohl, A. Antognini, F. Nez, F. D. Amaro, F. Biraben,
et al., Nature 466 (2010) 213–216.
doi:10.1038/nature09250.

2) V. G. Nikolenko and A.B Popov, Z. Phys, A 341, 465 (1992). S. Dubnicka, A. Dubnickova, P. Weisenpacher, J. Phys. G29 (2003) 405–430.arXiv:hep-ph/0208051, doi:10.1088/0954-3899/29/2/316.
J. C. Bernauer, Ph.D. thesis, Institut f¨ur Kernphysik Johannes Gutenberg-Universit¨at Mainz (2010).
3) Yu. A. Alexandrov, Z. Phys, A 344, 219 (1992); Nucl. Inst. And Meth. In Phys. Res. A284, 134-136 (1989). X. Zhan, K. Allada, D. Armstrong, J. Arrington, W. Bertozzi,et al., Phys.Lett. B705 (2011) 59–64. arXiv:1102.0318, doi: 10.1016/j.physletb.2011.10.002.
4) S. Kopecki, J. V. Harvey, N. Nill, P. Riebs and J. Schmidynayer, in Baryon 92 International conference on the structure of Baryons and related meson (Yale Univ. New Haven (1992)).
5) Yu. A. Alexandrov, Report No JINR E3-92-384 (1994).
6) Yu. A. Alexandrov, Fundamental Properties of the neutron (Oxford 1992)
7) H. Leeb and C.Teichtmeister, Phys. Rev, C48, 1719 (1993)
8) L. Foldy, Rev. Mod. Phys.,30, 371 (1958)
9) Y. Tzeng and S. Hsiao, Nuovo Cimento, 106A, 573 (1993)
10) L. M. Sehgal, Phys, Lett., 53B, 106 (1974)
11) A. Neigawa and D. Kiang, Phys. Rev., D14,3235 (1976),
D. Parashar and R.S. Kaushal, Phys. Rev. D13, 2684 (1976)
12) A. D. Martin, W. J. stirling , R. Thorne and and G. Watt , Eur.Phys.J. C64, 653 (2009)

HADRONIC JOURNAL 45, 455 - 468 (2022)
DOI 10.29083/HJ.45.04.2022/SC455

STUDIES ON THE NONLINEARITY OF WAVE-PARTICLE DUALITY

Yi-Fang Chang
Department of Physics
Yunnan University
Kunming, 650091, China
yifangch@sina.com

Received November 20, 2022
Revised December 13, 2022

Abstract

First, photoelectric effect and Compton scattering show photons as particles, and interference and diffraction of particles show particles as waves, therefore, duality exists probably only under interactions. Its test is that duality not exists when there are not interactions. Next, some nonlinear quantum equations and wave equations have soliton solutions, which correspond to particles. This is mathematical description of wave-particle duality, and whose condition is also interactions and nonlinearity. Third, based on the soliton-chaos double solutions of nonlinear equations, we propose the field-particle duality, and field (wave)-quantum-chaos ternary. Further, if we develop mathematical form, more multiplicity will be obtained. Finally, in the quantum entangled states, velocities of different phases obey possibly general Lorentz transformation (GLT).

Key words: wave-particle duality, interaction, nonlinear equation, field, soliton, chaos, entangled state.

Copyright © 2022 by Hadronic Press, Inc., Palm Harbor, FL 34684, USA

I. Reconsider of Duality

It is known that sound wave and water wave are the propagation ways of sound and water. Light wave and electromagnetic wave are propagations of field and its change on photon. Macroscopic wave is a way of motion, and general wave is a propagation way with field change. But, invariant static electric field and gravitational field cannot form wave.

Young discovered wave interference of light by double-slit experiment. Wave seems to must existence of interactions. Interference and diffraction all are interactions between waves each other. The "existence" of electromagnetic wave-particle duality depends on physical conditions as well as on the frequency of light [1]. Moreover, there has interaction with slits. Coherence already is interactions. The scale of diffraction screen must be suitable with wave-length.

In quantum mechanics wave-particle duality is that every particle or quantum entity may be partly described in terms not only of particles, but also of waves. It has been verified not only for elementary particles, but also for compound particles like atoms and even molecules. Because the extremely short wavelengths of macroscopic particles, wave nature usually cannot be detected. Generally, wave-particle duality seems to be clear without saying. But, so far its meaning or interpretation has not been satisfactorily resolved. Bohr proposed duality as one aspect of the concept of complementarity.

Photoelectric effect and Compton scattering are shown photons as particles. Interference and diffraction of particles show particles as waves. Photoelectric effect and electro-optic effect all are interactions between photons and electrons. These are all interactions, so duality exists probably only under interactions and nonlinearity. Of cause, there have linear waves in Nature.

In quantum mechanics a particle with energy E and momentum $\boldsymbol{p}$ can be associated with a wave by the relations [2]:

$$E=h\nu,\ \boldsymbol{p}=h\boldsymbol{k}. \qquad (1)$$

De Broglie proposed that each electron orbit in an atom is actually a circular standing wave. From the wave function physicists derive fundamental equations of wave in quantum mechanics: non-relativistic Schrödinger equation, relativistic Klein-Gordon (KG) equation and Dirac equations, etc. Quantum mechanics unifies the wave-particle duality into a single consistent theory, which is extremely successful. Microscopic waves correspond to bosons, photons and gravitons, and QED and quantum field theory.

Duality is that any particles all possess wave nature, and it is directly represented by Feynman path integral as a global description in quantum mechanics. Davisson, Germer and Thomson observed diffraction of electrons [3,4], then diffractions of protons, neutrons, atoms, molecules and C_{60} [5] are observed. In 2003, the Vienna group found interference fringes for a

fluorinated buckyball composed of 108 atoms. Single-photon interference exists over large distances [6]. Single electron has wave character. Both are able to belong in interaction of single particle and slits.

Particles act like waves include many aspects: Free particles have generally forms of wave packet. The tunnel effect reflects wave, and corresponds to transmission wave. The stationary wave of quantum equations corresponds to stationary state in Bohr atom model, in which electron interactions with nucleus. In quantum mechanics, probability wave, coherent superposition of wave, the partial wave method and resonance in scattering theory, etc., all show wave nature of particles.

New double-slit experiments show wave-particle duality. Double-slit interference of light is result of interaction between two beams of light. Moreover, there has interaction between light and slit, but it may be neglected. Diffraction is related to interaction between wave and diffraction screen. Recently Couder, *et al.* showed single-particle diffraction and interference at a macroscopic scale, which use macroscopic oil droplets on a vibrating surface as a model of wave-particle duality—localized droplet creates periodical waves around and interaction with them leads to quantum-like phenomena: interference in double-slit experiment [7], unpredictable tunneling of a classical wave-particle association [8], orbit quantization[9].

In the formalism of quantum mechanics, any particles are encoded in their wave function, which evolves according to Schrödinger equation. Propagation of waves leads to wave-like phenomena such as interference and diffraction. Following development is quantum field theory.

De Broglie proposed a pilot wave construct to explain the observed wave-particle duality, which is nonlocality [10]. Then it is extended by Bohm. In these cases interactions derive the pilot wave and the quantum potential. Moreover, Hugh Everett, et al., proposed the many-worlds interpretation (MWI).

Based on the complete special relativity which includes the generalized Lorentz transformation (GLT) in the spacelike interval, we searched contradiction between the uncertainty principle in quantum mechanics and strict classification of the timelike-spacelike intervals in special relativity. Further, we proposed new interpretation of the duality in the double-slit experiment that is the particle-wave duality corresponds to the timelike and spacelike intervals, respectively [11]. Such the duality is mutually exclusive and complementary. Moreover, we derived the new LT and GLT for very small space and time, and researched possible unification of quantum theory and complete special relativity [11].

2. Mathematical Description and Possible Condition of Wave-Particle Duality

It is known that the nonlinear Schrödinger equation

$$\phi_{xx} + i\phi_t + k|\phi|^2\phi = 0, \quad (2)$$

has a soliton solution [12]:

$$\phi_s = \phi_0 \sec h[\sqrt{\frac{k}{2}}\phi_0(x - u_e t)]\exp[i(\frac{u_e}{2})(x - u_c t)]. \quad (3)$$

The nonlinear Schrödinger equation describes Langmuir waves in plasmas, the self-trapping phenomena of nonlinear optics, etc.

The nonlinear Dirac equation is

$$\gamma_\mu \partial_\mu \psi + m\psi - l_0^2 \psi(\psi^+\psi) = 0. \quad (4)$$

Its solution of the probability density $\rho = \psi^+\psi = \overline{\psi}\gamma_4\psi$ is

$$\rho = \frac{1}{2 - \exp(-l_0^2\eta + c)}. \quad (5)$$

This is analogous to a soliton [13].

The cubic Klein-Gordon equation is:

$$\partial_\mu^2\varphi - m^2\varphi + a\varphi^3 = 0. \quad (6)$$

Its simplest soliton solution with a kink shape is:

$$\varphi = \sqrt{\frac{2}{a}} m \sec h(m\eta + C_0). \quad (7)$$

The sine-Gordon equation is:

$$\phi_{xx} - \phi_{tt} = \frac{1}{2}\pi\lambda^2 \sin(2\pi\phi). \quad (8)$$

It describes propagation of a crystal dislocation, a unitary theory of particles, propagation of magnetic flux on a Josephson line, etc [12]. Its soliton solution is:

$$\phi = \frac{2}{\pi} tg^{-1}[\exp(\pm\pi\lambda \frac{x - ut}{\sqrt{1 - u^2}})]. \quad (9)$$

The nonlinear Born-Infeld equation [14] as nonlinear Maxwell equation and nonlinear electromagnetic field is

$$(1 - \varphi_t^2)\varphi_{xx} + 2\varphi_x\varphi_t\varphi_{xt} - (1 + \varphi_x^2)\varphi_{tt} = 0. \quad (10)$$

It has soliton solution [12]. From the nonlinear electromagnetic soliton model we explained the magic ball lightning [15]. The Korteweg-de Vries (KdV) equation is:

$$\psi_t + \sigma\psi\psi_x + \psi_{xxx} = 0. \quad (11)$$

Its soliton solution is [12]:

$$\psi = \frac{3u}{\sigma} \sec h^2(\frac{\sqrt{u}}{2}\eta). \quad (12)$$

KdV equation describes magnetohydrodynamic waves and ion-acoustic waves in plasma, the anharmonic lattice, longitudinal dispersive waves in elastic rods, etc [12]. Moreover, the modified KdV equation, which used to describe Alfen waves in a collisionless plasma, etc., and the Boussinesq equation have also soliton [12].

In a word, since soliton corresponds mathematically to particle, nonlinear equations in quantum mechanics and some nonlinear waves have soliton solutions, which are the most direct mathematical descriptions of wave-particle duality. Its condition is interactions and nonlinearity. Probably, different interactions are namely different particles. Generally, some cases hold also in macrostructures, it will derive the extensive quantum theory [16-19].

Probably interaction and nonlinearity are necessary conditions of duality. Its test is that duality not exists when there are not interactions. For any single particle, for example, electron, proton, etc., its mass and life and decay modes are not reflect wave nature, and are all determined, in which the magnetic moment of electron agrees exactly with QED. D'Ariano and Yuen discussed impossibility of measuring the wave function of a single quantum system [20], but, may measure the Wigner function as ensemble [21], in which for quasi-classical state $W(x,y)\geq 0$, as idea coherent state of harmonic oscillator.

Nonlinearity may be a nonlinear equation or be one pair of equations. Both cases exist only: Single particle, and interactions between particles or particle and other object. The later may show wave. They are respectively geometrical optics or wave optics, and are also difference of Newton and Huygens. Such wave optics describes interference and diffraction, and all has interaction.

Interactions of macroscopic objects have rules, and correspond to classical mechanics. Interactions of microscopic particles and wave have probability, and correspond to quantum mechanics. Further, if interactions of macrostructures have also probability, they will correspond to the extensive quantum theory, for example, in solar evolution [16,17], etc.

Single particle passes through slits, their interactions possess probability, and general interactions possess probability, which shows probability of quantum mechanics. Linear wave cannot form particle and duality. This corresponds possibly to difference of single slit and double-slit experiments.

In field, wave and particle, there are not interactions, so are not duality. For high energy and small space-time, interactions may be neglected. Weak interactions derive decay, and have probability. In a word, equations of field, wave and particle have interactions, such duality may appear.

Usual microscopic duality exists necessarily. The explanation of interaction and nonlinearity may be applied to macrostructures, and corresponds to the extensive quantum theory [17-19].

General gravitational interactions are very weak, which exhibits hard particle and duality. But, the gravitational wave based on the nonlinear equations of general relativity for the strong gravitational field should be nonlinear wave. Gravitational field equations of general relativity are nonlinear:

$$R_{ik}=\frac{\partial\Gamma^{l}_{ik}}{\partial x^{l}}-\frac{\partial\Gamma^{l}_{il}}{\partial x^{k}}+\Gamma^{l}_{ik}\Gamma^{m}_{lm}-\Gamma^{m}_{il}\Gamma^{l}_{km}=kT_{ik}+\frac{1}{2}Rg_{ik}=kT_{ik}{}^{*}, \quad (13)$$

here $$\Gamma^{i}_{kl}=\frac{1}{2}g^{im}(\frac{\partial g_{mk}}{\partial x^{l}}+\frac{\partial g_{ml}}{\partial x^{k}}-\frac{\partial g_{kl}}{\partial x^{m}}). \quad (14)$$

From this some solutions of the equations are discussed quantitatively [22]. For example, if in gravitational equations the cosmic term $\Lambda g^{\mu\nu}$ exists, the simplified equations are:

$$g^{\mu\nu}\frac{\partial^{2}g^{\mu\nu}}{\partial x_{\mu}\partial x_{\nu}}+\Lambda g^{\mu\nu}=\frac{1}{2}\frac{\partial g^{\mu\nu}}{\partial x_{\mu}}\frac{\partial g^{\mu\nu}}{\partial x_{\nu}}. \quad (15)$$

Assume that $g^{\mu\nu}\equiv$g, and let $\eta=\frac{x+y+z-ut}{\sqrt{1-u^{2}}}$, it will be very simple nonlinear ordinary differential equation:

$$gg''+\Lambda g=(g')^{2}/2. \quad (16)$$

Its solution is:

$$g=\exp\{-2[arc\Phi(-\sqrt{\Lambda/\pi}\eta+C)]^{2}\}. \quad (17)$$

Here $\Phi(x)$ is probability integral. This solution is like soliton.

New observed gravitational waves are tests of general relativity, and proved they are nonlinear waves. Generally assume that velocity of gravitational wave is also the speed of light. We proposed that the two velocities should be different *i.e.* the velocity of the gravitational wave will deviate from the velocity of light, at least since light deflects while the gravitational wave propagates along a straight line in a strong gravitational field, like an electromagnetic wave in an electromagnetic field [22]. Detectors observed association with the γ-ray burst (GRB) 1.7s after GW170817 [23]. This is very small value, but, it proved clearly both velocities of gravitational wave and electromagnetic wave are different [22], and is inevitable result of general relativity. We calculated gravitational redshift and the deflection of light for a binary neutron star (BNS), delay time is 0.1792s [24].

Further, we proposed three predictions of gravitational waves: their observations must be nonlinear waves; velocity of gravitational wave should be slightly higher than the velocity of light; gravitational waves in black holes may emit and be observed [25].

3. Wave-Particle Duality Extends to Field-Particle Duality and Field-Quantum-Chaos Ternary

The fundamental characteristics of soliton and chaos in nonlinear equation are completely different. We proved that some nonlinear equations have double solutions with soliton and chaos [26]. All nonlinear equations with a soliton solution may derive chaos. While only some equations with a chaos solution have a soliton. The conditions of the two solutions are different.

For Eq.(2) we may derive a difference equation:

$$X_{n+1} = 1 - \frac{H}{2} X_n^2 . \qquad (18)$$

It is a known equation, which has the chaos solution, and its parameter determined the bifurcation-chaos is $\mu = H/2$. Eq. (4) corresponds to difference equation:

$$X_{n+1} = 1 - \frac{1}{4} l_0^4 X_n^2 . \qquad (19)$$

It has the chaos solution and the parameter $\mu = l_0^4 / 4$. Eq. (7) may become

$$\frac{d\varphi}{d\eta} = m\varphi(1 - \frac{a}{2m^2}\varphi^2)^{1/2} . \qquad (20)$$

It has the chaos solution. By a substitution $\psi = 3u[1-(u/4)(-x)^2]/\sigma$ for KdV equation (11), the difference equation is

$$X_{n+1} = 1 - \frac{1}{4} u X_n^2 . \qquad (21)$$

In a $0 \le u \le 8$ region, the values of bifurcation-chaos are *u=3,5,..., 5.6046207...*

Conversely, the simplest difference equation with the chaos solution is

$$X_{n+1} = 1 - \mu X_n^2 . \qquad (22)$$

It may correspond to a differential equation of first order

$$x' = 1 - \mu x^2 , \qquad (23)$$

and a partial differential equation of second order

$$\phi_{xx} - \phi_{tt} + a\phi - b\phi^3 = 0 . \qquad (24)$$

It is Eq.(6). When $|x| < 1/\sqrt{\mu}$ for Eq. (22),

$$x = \frac{1}{\sqrt{\mu}} th(\mu\eta + C). \qquad (25)$$

It is namely a soliton solution. A bifurcation-chaos region $2 \geq \mu \geq 0, x \in [-1,1]$ corresponds to $\infty \geq \mu^{-1/2} \geq 1/\sqrt{2} = 0.7071$ ... For single stable solution $0.75 \geq \mu_0 \geq 0$, i.e., $\infty \geq \mu_0^{-1/2} \geq$ 1.154, so the condition on $|x| < \mu^{-1/2}$ is satisfied necessarily in the region, the soliton can exist. While for two-branch region, $1.25 \geq \mu_1 \geq 0.75$, i.e., $1.154 \geq \mu_1^{-1/2} \geq 0.894$; for a region from four-braches to chaos, $1.401152 \geq \mu \geq 1.25$, i.e., $0.894 \geq \mu^{-1/2} \geq 0.845$. Since $|x| \leq 1$, the necessary condition in which the soliton appears is $\mu \leq 1$, it corresponds to the region of single solution and a part of two-branch region. For the rest $|x| < \mu^{-1/2}$ does not hold generally.

The logistic equation

$$\frac{dF}{dt} = F(\alpha E - F) \qquad (26)$$

corresponds to a difference equation

$$X_{n+1} = 1 - \frac{1}{4}\alpha^2 E^2 X_n^2, \qquad (27)$$

whose parameter is $\mu = (\alpha E)^2 / 4$. In the $0 \leq \mu \leq 2$ region, two branches appear for $\alpha E = \sqrt{3}$, four branches appear for $\alpha E = \sqrt{5}$, etc., there is the chaos for $\alpha E = (5.6046207)^{1/2} \approx 2.37$. The equation (27) has the solution

$$F = \frac{\alpha E}{1 + C\exp(-\alpha E t)}. \qquad (28)$$

When $t \geq 0$, Eq. (28) is analogous to a soliton since $F = \alpha E / (1 + C)$ for t=0 and $F = \alpha E$ for $t \to \infty$. It shows that the state will reach to stable at last as time increases continuously.

The difference equation with a chaos solution

$$X_{n+1} = \lambda \sin(\pi X_n), \qquad (29)$$

corresponds to a partial differential equation of second order

$$\phi_{xx} - \phi_{tt} = \frac{1}{2}\pi\lambda^2 \sin(2\pi\phi). \qquad (30)$$

It is namely the sine-Gordon equation (8) with the soliton solution (9).

Further, we discussed some possible meanings of the double solutions. In the mathematical aspect, when some parameters are a certain constant, the soliton is derived; while these parameters vary in a certain region, the

bifurcation-chaos appears. Therefore, the former corresponds to a stable state, and the latter is a changeable process. In the physical aspect, perhaps, the double solutions are two different states. These parameters are the order parameters. These states often depend on the integral constants, the boundary conditions and the initial conditions. This explains again that the solutions of the nonlinear equations depend on the initial values sensitively. It connects the chaos control by a method of parameter-control. When we control the order parameter in the nonlinear system, chaos appear, disappear, synchronize, even a determinational soliton is produced, for different parameteric values. For example, the soliton can be derived in a propagation of shallow water waves, but if the flow rate reaches a certain value, there will form the turbulence. Moreover, the soliton solution corresponds to particle, and the chaos solution corresponds to the field, including the stochastic field. So wave-particle duality develops to field-particle duality. This connects probably the double solution theory of the de Broglie-Bohm nonlinear wave mechanics [10], where the particle is described by the mobile singularity of soliton of the wave equation. In the neurobiological physical aspect, based on the quantum and nonlinear neurobiology [27], we discussed the possible meaning on the soliton-chaos double solutions [28]. The quantized soliton corresponds to the extensive quantum biology and conduction. While chaos corresponds to oscillations of some neurons, and even is related with thinking. Based on the analysis for EEG scientists found that usual brain wave is chaos, which possesses the behavior of the strange attractor with the fractal dimension. Only the brain wave of falling sickness is periodicity. The double solutions may be applied simultaneously to neurobiology, which shows just the nonlinear whole neurobiology [27].

The double solutions show the simultaneous existence on determinism and probabilism quantitatively from an aspect in some nonlinear systems. Unification of field and particle is namely quantum field theory as QED, etc. When some parameters vary in a certain region, the double solutions imply to form the ternary: field (wave)-quantum (particle)-chaos.

Further, based on the Eqs.(27)(28) and their mathematical development we may derive the evolutional model of system (Fig.1), which is completely analogy with the nonlinear theory of economic growth [29].

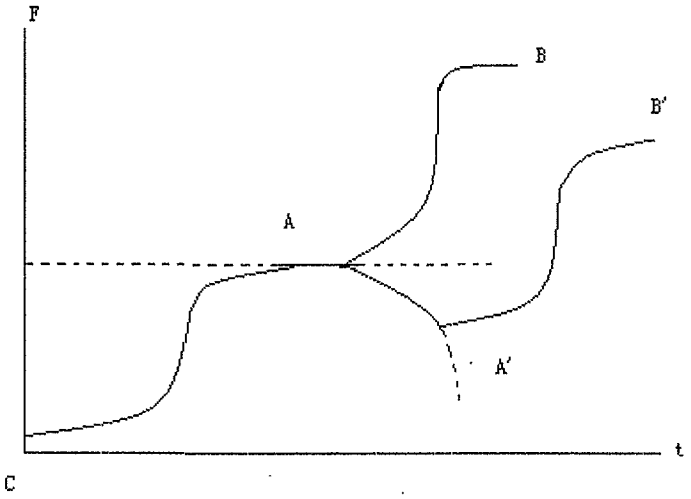

Fig.1 The three laws of evolutional system

In Fig.1 may represent the three laws of evolutional system. CA expresses the limits to growth (maximum $F = \alpha E$) and the first law: takeoff-growth-stagnancy law. AA' expresses the second law: conservation and decay law. It agrees with Lotka-Volterra model, and is two-bifurcation phenomena of nonlinear system. An infinite clone of the same developed mode will derive a disorder competition, and finally reach necessarily to chaos. AB expresses the third law: growth mode transition and new developed period law. It is three developed phases of system, and corresponds to a development of the paradigms in science.

Generally, we develop mathematical form, and obtain more multiplicity.

4. Mathematics of Entangled States

Based on the classification of the timelike and spacelike intervals, one does not add any hypothesis, we necessarily derived the two symmetrical types of topologically separated structures: the v<c Lorentz transformation (LT) and the $\bar{v}$>c general Lorentz transformation (GLT) [13,30]:

$$x_1' = \bar{\gamma}(x_1 - c^2 t/\bar{v}), t' = \bar{\gamma}(t - x_1/\bar{v}), \qquad (31)$$

where $\bar{\gamma} = 1/\sqrt{1-(c/\bar{v})^2}$. LT and GLT are connected by de Broglie relation $v\bar{v} = c^2$, in which v is group velocity and soliton velocity, and $\bar{v}$ is phase velocity. Phase as a state in $\bar{v}$ is a very magic definition.

Based on the Einstein-Podolsky-Rosen (EPR) article [31], Santilli edited *International Teleconference on Einstein's Argument that "Quantum Mechanics Is not a Complete Theory"*, and overviewed historical and recent verifications of the EPR argument and their applications in physics, chemistry

and biology [32]. Santilli studied also the classical determinism predicted by EPR, and many aspects on EPR argument [32].

Further, physicists researched the entanglements. The quantum entangled states have different phases, for example, $|\psi_B>$ and $|\psi_C>$ for

$$\psi_T = \psi_B |2> + \psi_C |3>. \qquad (32)$$

in Which Way (WW) experiments [33-35]; $|\leftrightarrow>$ and $|\updownarrow>$ in quantum teleportation, etc. These phase velocities obey possibly GLT. GLT shows the nonlocality between phases.

Based on the special relativity principle, an invariant speed c_h is necessarily obtained. Therefore, the exact basic principles of the special relativity should be redefined as: I. The special relativity principle, which derives necessarily an invariant speed c_h. II. Suppose that the invariant speed c_h in the theory is the speed of light in the vacuum c [13,30]. If the second principle does not hold, the theory will be still the extensive special relativity, in which the formulations are the same, only c is replaced by the invariant speed $c \to c_h$. Further, LT is unsuitable for photon and neutrino, the photon transformation (PT) is unified for space $x' = r + ct$ and time $t' = t + (r/c)$. It may reasonably overcome some existing difficulties, and cannot restrict that the rest mass of photon and neutrino must be zero. LT, GLT and PT together form a complete structure of the Lorentz group. Moreover, we discussed that if the invariant speed c_h are various invariant velocities, the diversity of space-time will correspond to many worlds [13,30].

The quantum entangled state possesses some new characters, for example, coherency, nonlocality, quantum teleportation, and may probably apply GLT. We proposed that it should be a new fifth interaction. At present, some physicists proposed that their entangled distance is infinite, and even is an action at a distance. I think, it is middle-rang, and neither infinite nor very short. Its strength seems to obey neither the Newtonian long-range gravitational law nor the short-range interaction. It should be middle one. From this five interactions may be exhibited completely in Fig.2 [30].

The quantum entangled state as the new interaction will be a special place at a middle state among the known four interactions, and seems to be fully enlightening meaning. Such the fifth interaction is very mystic, which is called spooky action at a distance by Einstein.

It is a concretization in quantum theory, for interactions between the system and the environment, and for interactions between the observer and the observed phenomenon, in which both difference is very little for the microscopic scale.

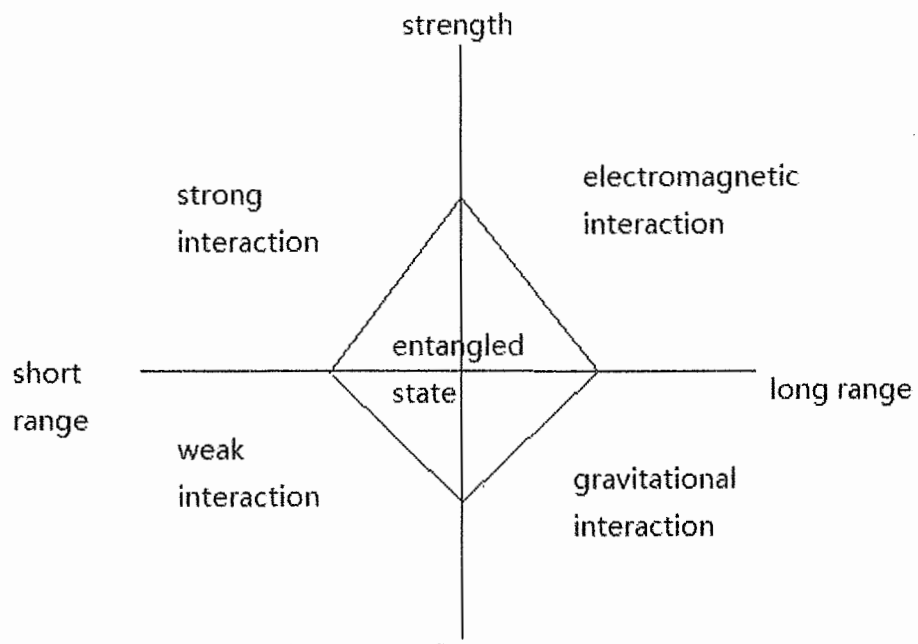

Fig.2 Relation among five interactions

From the EPR prediction [31], the nonlocality and entangled state become the frontline in modern physics. Based on GLT in the complete special relativity, we proposed that the entangled states must obey GLT because of they possess some characters as the spacelike vectors. It changes the phase of the entangled field, whose phase particle (phason) has some characters and corresponding equations. Assume that tachyon is similar to photon and J=1 and m=0 or mass is very small as similar neutrino, and may show the action at a distance. We researched that this field as wave has some characters, and discussed the corresponding quantum communication by a pair of entangled states is generated on both positions, or by preparing and transmitting a pair of entangled instruments, so the quantum communication. Manipulation for one position can pass the same message or information to the other, so we may implement the quantum communication. Further, assume that the entangled field has a similar magnetic theory, which may be a quantum cosmic field, or be the extensive quantum theory, or God or the Buddha-fields, etc. These are all macroscopic fields, which correspond to de Broglie-Bohm nonlinear "hidden variable" theory, but it is microscopic [36].

Based on quantum entanglement, we researched a simple entangled communication scheme, whose key is to establish two mutually entangled particles or devices A and B. We observe and control the information of A position, then can know the corresponding results of the other B. This is not to send directly information each other. It should agree and test GLT [37,38].

In a word, study and application of nonlocality and entangled field have important scientific and social significance [36,38].

References

[1] R. M. Santilli, Overview of historical and recent verifications of the Einstein-Podolsky-Rosen argument and their applications to physics, chemistry and biology. APAV - Accademia Piceno Aprutina dei Velati, Pescara, Italy (2021).
[2] W. Pauli, *Pauli. Lectures on Physics: Vo.5. Wave Mechanics*. Cambridge: The MIT Press. **1973**.
[3] G.J. Davisson and L.H. Germer, *Phys.Rev*. 30(**1927**):705.
[4] G.P. Thomson, *Nature*. 120(**1927**):802.
[5] M. Arndt, et al., *Nature*. 401(**1999**):680.
[6] J.D. Frauson and K.A. Potocki, *Phys.Rev*. A37(**1988**):2511.
[7] Y. Couder and E. Fort, *Phys.Rev.Lett*. 97(**2006**):154101.
[8] A. Eddi, E. Fort, F. Moisy and Y. Couder, *Phys.Rev.Lett*. 102(**2009**):240401.
[9] E. Fort, A. Eddi, A. Boudaoud, J. Moukhtar and Y. Couder, *PNAS*. 107(**2010**): 17515.
[10] L. de Broglie, *Non-linear Wave Mechanics*. Elsevier. **1960**.
[11] Yi-Fang Chang, *International Journal of Physics and Applications*. 4(**2022**):17.
[12] A.C. Scott, F.Y.F. Chu and D.W. Mclaughlin, *Proc.of IEEE*. 61(**1973**):1443.
[13] Yi-Fang Chang, *New Research of Particle Physics and Relativity*. Yunnan Science and Technology Press. **1989**. *Phys.Abst*. 93(**1990**):No1371.
[14] M. Born and L. Infeld, *Proc.Roy.Soc.London*. 144A(**1934**): 425.
[15] Yi-Fang Chang, *International Journal of Modern Applied Physics*. 6(**2016**):1.
[16] Yi-Fang Chang, *Publ.Beijing Astron.Obser*. 16(**1990**):16.
[17] Yi-Fang Chang, *Phys.Essays*. 15(**2002**):133.
[18] Yi-Fang Chang, *NeuroQuantology*. 10(**2012**):183.
[19] Yi-Fang Chang, *International Journal of Modern Mathematical Sciences*. 16 (**2018**):148.
[20] G.M. D'Ariano and H.P. Yuen, *Phys.Rev.Lett*. 76(**1996**):2832.
[21] Ch. Kurtsiefer, T. Pfau and J. Mlynek, *Nature*. 386(**1997**):150.
[22] Yi-Fang Chang, *Apeiron*. 3(**1996**):15.
[23] B. P. Abbott, et al., (LIGO Scientific Collaboration and Virgo Collaboration), *Phys.Rev.Lett*. 119(**2017**):161101.
[24] Yi-Fang Chang, *International Journal of Modern Theoretical Physics*. 7(**2018**):16.
[25] Yi-Fang Chang, *Philosophy Study*. 12(**2022**):181.
[26] Yi-Fang Chang, *International Journal of Modern Mathematical Sciences*. 8(**2013**): 183.

[27] Yi-Fang Chang. *NeuroQuantology*. 10(**2012**): 190.
[28] Yi-Fang Chang. *NeuroQuantology*. 11(**2013**): 56.
[29] Yi-Fang Chang, *International Journal of Modern Social Sciences*. 2(**2013**):20.
[30] Yi-Fang Chang, *International Journal of Modern Theoretical Physics*. 2(**2013**):53.
[31] A. Einstein, B. Podolsky and N. Rosen, *Phys.Rev*. 47(**1935**):777.
[32] R.M. Santilli ed. *International Teleconference on Einstein's Argument that "Quantum Mechanics Is not a Complete Theory"*. Sept.1-5.2020. Hadronic Press. **2021**.
[33] M.O. Scully, B.G. Englert and H. Walther, *Nature*. 351(**1991**):111-116.
[34] B-H. Englert, *Phys.Rev.Lett*. 77(**1997**):2154.
[35] S. Durr, T. Nonn and G. Rampe, *Nature*. 395(**1998**):33.
[36] Yi-Fang Chang, *Algebras, Groups, and Geometries*. 36(**2019-2020**):481.
[37] Yi-Fang Chang, *Asian Journal of Research and Reviews in Physics*. 5(**2021**):34.
[38] Yi-Fang Chang, *Philosophy Study*. 12(**2022**)7:365.

INDEX
HADRONIC JOURNAL, VOLUME 45, 2022

A NEW DESCRIPTION OF THE COMPLEX NEUTRINO PROBLEM IN CONNECTION WITH THE COSMOLOGY, 1

H. Strusny
Hohenschoenhauser Str. 1
10369 Berlin, Germany

INVESTIGATE THE EFFECT OF TEMPERATURE ON QUASIPARTICLE EXPECTATION VALUE AND PAIR CORRELATION FUNCTION FOR SINGLET WAVE IN AN OPEN QUANTUM DISSPATIVE SYSTEM AT NON-EQUILIBRIUM, 59

Nabin Kumar Teemilsina[1,2], Saddam Husain Dhobi[1,2,3], Kishori Yadav[1,2], Bibek Koirala[1,2], Padam Prakash Ghimire[1,2], Dilip Rokka[1,2], Suresh Prasad Gupta[1,2], Jeevan Jyoti Nakarmi[1,2]
[1]Department of Physics, Patan Multiple Campus, Tribhuvan University, Lalitpur-44700, Nepal
[2]Innovative Ghar Nepal, Lalitpur-44700, Nepal
[3]Robotics Academy of Nepal, Lalitpur-44700, Nepal

KEPLER PROBLEM AND PERIHELION IN THE MODEL OF THE DYNAMIC QUANTUM VACUUM, 81

Davide Fiscaletti
SpaceLife Institute, Via Roncaglia, 35 – 61047 San Lorenzo in Campo (PU), Italy
Štefan Čelan
Scientific Research Centre Bistra, Slovenski trg 6, SI-2250 Ptuj, Slovenia
Amrit Šorli
Scientific Research Centre Bistra, Slovenski trg 6, SI-2250 Ptuj, Slovenia

NEW THERMODYNAMICS: THE SECOND LAW BURIED BY ILLUSIONS, 97

Kent Mayhew
68 Pineglen Cres.
Ottawa, Ontario, Canada K2G 0G8

THEORY OF GRAVITATIONAL ENERGY, MOMENTUM AND STRESS, WITH THE PREDICTION OF LONGITUDINAL WAVES, 117

Kenneth Dalton
General Delivery
Bang Saphan Yai 77140
Prachuap Kiri Khan, Thailand

INCONSISTENCIES IN EM THEORY - THE KELVIN POLARIZATION FORCE DENSITY CONTRADICTION, 133
Zoltan Losonc
Independent Researcher
WHAT ARE BLACK HOLES AND DO THEY REALLY EXIST?, 207
Salah A. Mabkhout
Department of Mathematics
Thamar University – Dhamar – Republic of Yemen
PLANCK-SCALE QUANTUM FIELD THEORY-II-EVALUATION OF QED ANALOGUE AMPLITUDES, 235
J. J. Bevelacqua
Bevelacqua Resources
343 Adair Drive
Richland, WA 99352 USA
MASS FORMULA OF HADRONS FOR THREE GENERATION QUARK STANDARD MODEL AND DIFFERENCES ON ELECTROMAGNETIC MASS OF BARYON-MESONS, 253
Yi-Fang Chang
Department of Physics
Yunnan University
Kunming, 650091, China
NEGENTROPIC THERMODYNAMICS I: PROOF OF THE NEGENTROPIC NATURE OF THE TRANSFORMATION OF HEAT INTO WORK, 263
José C. Íñiguez
Retired Instructor of Science and Mathematics
1227 21st Street
Douglas, AZ 85607
NEGENTROPIC THERMODYNAMICS II: AN AUTOPOIETIC, HEAT-ENGINE-CENTERED MODEL FOR RAYLEIGH-BÉNARD CONVECTION, 297
José C. Íñiguez
Retired Instructor of Science and Mathematics
1227 21st Street
Douglas, AZ 85607
HADRONIC CONDUCTIVITY: A NEW FORM OF SUPERCONDUCTIVITY, 333
Alexander O.E. Animalu
Department of Physics and Astronomy
University of Nigeria, Nsukka
Enugu State, Nigeria

ON THE POSSIBILTY OF FUSING HYDROGEN WITH HIGH LEVEL NUCLEAR RADIOACTIVE WASTE VIA COLD NUCLEAR FUSION, 357

U.V.S. Seshavatharam
Honorary faculty, I-SERVE, Survey no-42, Hitech City
Hyderabad-84, Telangana, India
S. Lakshminarayana
Department of Nuclear Physics, Andhra University
Visakhapatnam-03, Andhra Pradesh, India

ON RELATIVISTIC HARMONIC OSCILLATOR, 369

A. I. Arbab
Department of Physics, College of Science, Qassim University
P.O. Box 6644, Buraidah 51452, Saudi Arabia

NEUTRINO EXCHANGING POTENTIAL WITH BESSEL FUNCTION OF LOW ORDER, 383

Bibek Koirala[1,2], Saddam Husain Dhobi[1,2,3], Prakash Subedi[1,2], Milan Gurung[4]
[1]Department of Physics, Patan Multiple Campus, Tribhuvan University, Lalitpur-44700, Nepal
[2]Innovative Ghar Nepal, Laitpur-44700, Nepal
[3]Robotics Academy of Nepal, Lalitpur-44700, Nepal
[4]Central Department of Physics, Tribhuvan University
Kirtipur, 44618, Nepal

NEW THERMODYNAMICS: HOW MANKIND'S USE OF ENERGY INFLUENCES CLIMATE CHANGE, 399

Kent Mayhew
68 Pineglen Cres.
Ottawa, Ontario, Canada K2G 0G8

ON THE INDUCTION OF A LOW-ENERGY NUCLEAR REACTION IN A SUPERSONIC PLASMA VORTEX, 423

Igor Bayak
Belarus, 230025, Grodno Av., Kosmonavtov 4V 45

ANALYSIS OF THE ORIGIN, STRUCTURE AND PROPAGATION OF TRANSVERSE ELECTROMAGNETIC WAVES USING BIPOLARS, 431

Farzad Haghmoradi-Kermanshahi
Electrical Engineering Department
Faculty of Engineering, Razi University
Kermanshah 67149, Iran

PROBING THE ELECTROMAGNETIC STRUCTURE OF NUCLEONS, 443
M Y Hussein
Department of Physics, University of Bahrain
P.O. Box 32038, Kingdom of Bahrain
And
Search Center, Shaikh Ebrahim Bin Mohammed Al Khalifa
Center for Culture and Research, P.O. Box 13725
Muharraq, Kingdom of Bahrain
STUDIES ON THE NONLINEARITY OF WAVE-PARTICLE DUALITY, 445
Yi-Fang Chang
Department of Physics
Yunnan University
Kunming, 650091, China

INDEX VOL 45, 2022.....469